2012-03

Potential Vorticity Streamers as Precursors to Tropical Cyclone Genesis in the Western Pacific

Rozak, Edward J.

Monterey, California. Naval Postgraduate School

NAVAL POSTGRADUATE SCHOOL

MONTEREY, CALIFORNIA

THESIS

POTENTIAL VORTICITY STREAMERS AS PRECURSORS TO TROPICAL CYCLONE GENESIS IN THE WESTERN PACIFIC

by

Edward J. Rozak

March 2012

Thesis Advisor: Richard Moore
Second Reader: Patrick Harr

Approved for public release; distribution is unlimited

THIS PAGE INTENTIONALLY LEFT BLANK

REPORT DOCUMENTATION PAGE			Form Approved OMB No. 0704–0188
Public reporting burden for this collection of information is estimated to average 1 hour per response, including the time for reviewing instruction, searching existing data sources, gathering and maintaining the data needed, and completing and reviewing the collection of information. Send comments regarding this burden estimate or any other aspect of this collection of information, including suggestions for reducing this burden, to Washington headquarters Services, Directorate for Information Operations and Reports, 1215 Jefferson Davis Highway, Suite 1204, Arlington, VA 22202–4302, and to the Office of Management and Budget, Paperwork Reduction Project (0704–0188) WashingtonDC20503.			
1. AGENCY USE ONLY ***(Leave blank)***	**2. REPORT DATE** March 2012	**3. REPORT TYPE AND DATES COVERED** Master's Thesis	
4. TITLE AND SUBTITLE Potential Vorticity Streamers as Precursors to Tropical Cyclone Genesis in the Western Pacific		**5. FUNDING NUMBERS**	
6. AUTHOR(S) Edward J. Rozak			
7. PERFORMING ORGANIZATION NAME(S) AND ADDRESS(ES) Naval PostgraduateSchool Monterey, CA 93943–5000		**8. PERFORMING ORGANIZATION REPORT NUMBER**	
9. SPONSORING /MONITORING AGENCY NAME(S) AND ADDRESS(ES) N/A		**10. SPONSORING/MONITORING AGENCY REPORT NUMBER**	
11. SUPPLEMENTARY NOTES The views expressed in this thesis are those of the author and do not reflect the official policy or position of the Department of Defense or the U.S. Government. IRB Protocol number _____N/A_____.			
12a. DISTRIBUTION / AVAILABILITY STATEMENT Approved for public release; distribution is unlimited		**12b. DISTRIBUTION CODE**	

13. ABSTRACT (maximum 200words)

The term tropical transition (TT) is used to describe the formation of a tropical cyclone from an extratropical precursor. The overarching goal of this thesis is to re-examine TT in the western North Pacific. This is accomplished via the synthesis of a subjective climatology of all tropical cyclones (TCs) from 2002–2008 and a case study analysis of ensemble prediction data for the particularly intriguing event of TS 16W in September of 2008.

The climatological analysis indicated that TT events represented 14% of all TCs during the study period. The maximum frequency of TT events occurred in the late summer / early fall. The resulting storm systems tended to form farther to the north than non-TT events and were found to be relatively weak and short- lived.

The results of the case study analysis lend credence to the earlier finding that the genesis pathway of TS 16W exhibited a two-stage evolution. The first stage involved the forcing of near-continuous deep convection by a tropopause-level potential vorticity (PV) anomaly. The second stage involved the rearrangement of the upper-level PV structure via diabatic processes, resulting in a necessary reduction of vertical wind shear.

14. SUBJECT TERMS Tropical Cyclones, Tropical Transition, Potential Vorticity			**15. NUMBER OF PAGES** 117
			16. PRICE CODE
17. SECURITY CLASSIFICATION OF REPORT Unclassified	**18. SECURITY CLASSIFICATION OF THIS PAGE** Unclassified	**19. SECURITY CLASSIFICATION OF ABSTRACT** Unclassified	**20. LIMITATION OF ABSTRACT** UU

NSN 7540–01–280–5500 Standard Form 298 (Rev. 2–89)
Prescribed by ANSI Std. 239–18

THIS PAGE INTENTIONALLY LEFT BLANK

Approved for public release; distribution is unlimited

POTENTIAL VORTICITY STREAMERS AS PRECURSORS TO TROPICAL CYCLONE GENESIS IN THE WESTERN PACIFIC

Edward J. Rozak
Captain, United States Air Force
B.S., Plymouth State University, 2003

Submitted in partial fulfillment of the
requirements for the degree of

MASTER OF SCIENCE IN METEOROLOGY

from the

NAVAL POSTGRADUATESCHOOL
March 2012

Author: Edward J. Rozak

Approved by: Richard Moore
Thesis Advisor

Patrick Harr
Second Reader

Wendell A. Nuss
Chair, Department of Meteorology

THIS PAGE INTENTIONALLY LEFT BLANK

ABSTRACT

The term tropical transition (TT) is used to describe the formation of a tropical cyclone from an extratropical precursor. The overarching goal of this thesis is to re-examine TT in the western North Pacific. This is accomplished via the synthesis of a subjective climatology of all tropical cyclones (TCs) from 2002–2008 and a case study analysis of ensemble prediction data for the particularly intriguing event of TS 16W in September of 2008.

The climatological analysis indicated that TT events represented 14% of all TCs during the study period. The maximum frequency of TT events occurred in the late summer / early fall. The resulting storm systems tended to form farther to the north than non-TT events and were found to be relatively weak and short- lived.

The results of the case study analysis lend credence to the earlier finding that the genesis pathway of TS 16W exhibited a two-stage evolution. The first stage involved the forcing of near-continuous deep convection by a tropopause-level potential vorticity (PV) anomaly. The second stage involved the rearrangement of the upper-level PV structure via diabatic processes, resulting in a necessary reduction of vertical wind shear.

THIS PAGE INTENTIONALLY LEFT BLANK

TABLE OF CONTENTS

LIST OF FIGURES

THIS PAGE INTENTIONALLY LEFT BLANK

LIST OF TABLES

THIS PAGE INTENTIONALLY LEFT BLANK

LIST OF ACRONYMS AND ABBREVIATIONS

E	East
ECMWF	European Center for Medium Range Forecasts
ERA-Interim	ECMWF Re-Analysis Interim
EPS	Ensemble Prediction System
GPH	Geopotential Height
hPa	hecto-Pascals
JTWC	Joint Typhoon Warning Center
K	Degrees Kelvin
km	kilometers
LTM	Latent Trajectory Model
MCS	Mesoscale Convective System
MDR	Main Development Region
MM5	Mesoscale Model 5th Generation
N	North
NWP	Numerical Weather Prediction
OLR	Outgoing Longwave Radiation
PV	Potential Vorticity
PVU	Potential Vorticity Unit
RHS	Right-hand Side
s	seconds
SEC	Strong Extratropical Cyclone
SST	Sea Surface Temperature
TC	Tropical Cyclones
TCS-08	Tropical Cyclone Structure 2008
TIGGE	THORPEX Interactive Grand Global Ensemble
TS	Tropical Storm
THORPEX	The Observing system Research and Predictability Experiment
TT	Tropical Transition
TUTT	Tropical Upper-Tropospheric Troughs
UKMO	United Kingdom Meteorological Office

UTC	Universal Time Coordinates
WEC	Weak Extratropical Cyclone
WISHE	Wind Induced Surface Heat Exchange
WNP	Western North Pacific
WWRP	World Weather Research Program

ACKNOWLEDGMENTS

There are numerous people I am indebted to and would like to thank for help in completion of this thesis. First, I would like to thank Professor Moore for being my thesis advisor; providing guidance and much needed feedback throughout the entire process. Also thanks to Professor Harr for being the second reader for this thesis.

A special thanks to Professor Michael Montgomery for providing the Advanced Tropical Meteorology class. I learned a lot from both Tropical and Advanced Tropical.

I'd like to thank the entire NPS Meteorology department faculty for their excellent teaching and time devoted to each and every student. I think our whole class benefited from it.

Also, to my family for giving me support and to my wife, Susannah, for sharing my frustrations and enduring my long hours. Without you, none of this would be possible.

THIS PAGE INTENTIONALLY LEFT BLANK

I. INTRODUCTION

A. MOTIVATION

Tropical cyclones (TCs) are the most powerful storms on earth. They produce copious amounts of rainfall, strong-damaging winds and, if they encounter coastal regions, a significant storm surge capable of causing severe flooding. While TCs have been a central research focus for well over 50 years, tropical cyclogenesis remains a challenging forecast problem (Montgomery and Farrell 1993; Emanuel 2005). Accurately forecasting when and where a tropical cyclone will form is of great interest to both civilian and military personnel. In addition to the inherent danger to property and life posed to all humans, tropical cyclones can greatly impact military operations as well as necessitate costly relocations of militarily-important equipment to avoid TC-related damage.

While conventional wisdom suggests tropical cyclogenesis is purely a tropical process, a growing body of work has indicated a significant fraction of TCs form as a direct result of an extratropical precursor. Perhaps the first examples of tropical cyclogenesis influenced by the extratropics were presented by Sadler (1976, 1978), wherein it was shown that tropical upper-tropospheric troughs (TUTTs) can play an integral role in the tropical cyclogenesis process in the western North Pacific (WNP). More recently, the focus shifted to the Atlantic basin: it has been shown that nearly half of Atlantic basin TCs form in conjunction with an extratropical precursor (McTaggart-Cowan et al. 2008). The dynamical process via which this occurs was termed tropical transition (TT) by Davis and Bosart (2004).

The overarching goal of this work is to re-examine TT research in the WNP. This will be accomplished via the synthesis of climatological and case-study approaches. The former encompasses a subjective examination of all TC events that occurred in the WNP during the years 2002–2008. Based on the investigation of relevant dynamical fields, storms are classified as TT or non-TT events. The latter approach involves a detailed case

study analysis of a particularly intriguing TT event that occurred during the Tropical Cyclone Structure (TCS-08) field program (Elsberry and Harr 2008) in September 2008. Specifically, we hope to gain insight into the dynamical evolution of the storm in question through the examination of ensemble prediction data.

B. RELEVANT TROPICAL TRANSITION RESEARCH

1. TC Genesis

A tropical cyclone is defined as a non-frontal synoptic-scale low-pressure system originating over tropical or subtropical waters with organized convection and a cyclonic surface wind circulation (Emanuel 2005). As an incipient tropical disturbance becomes organized and intensifies, a naming system invoking maximum sustained near-surface winds is employed: tropical depression [up to 17 m s^{-1} (33 knots)], tropical storms [between 18 to 32 m s^{-1} (34–63 knots)], and tropical cyclones [greater or equal to 33 m s^{-1} (64 knots)]. Terminology for a tropical cyclone varies depending on geographic location. For example, TCs are referred to as hurricanes in the Atlantic Basin and typhoons in the WNP. We will use the terminology "tropical cyclone" herein.

The following ingredients have been deemed required for TC formation (Gray 1968; DeMaria et al. 2001; Emanuel 2003):

1. Sea surface temperatures (SST) greater or equal to 26.5^{o}C
2. Potentially unstable atmosphere
3. Moist mid troposphere
4. Sufficient amount of the Coriolis parameter (i.e., latitudes poleward of 5^{o})
5. Low vertical wind shear of the horizontal winds
6. Pre-existing low-level disturbance providing sufficient low-level cyclonic vorticity

It is important to note that, while these are necessary ingredients for tropical cyclogenesis, their mere presence does not guarantee a TC will form. In fact, the precise dynamical processes that lead to TC formation remain an active area of research.

2. Tropical Transition

a. Western North Pacific

There has been a growing appreciation in the scientific community that tropical cyclogenesis need not be a purely tropical process in that an incipient disturbance (criteria number six in the previous subsection) can be of non-tropical origin. Sadler (1976, 1978) illustrated that anomalies along the dynamic tropopause that emanate from the extratropics [Sadler used the term tropical upper-tropospheric troughs (TUTTs)] can provide a forcing mechanism for TC development in the WNP. In his 1976 paper, Sadler presents three generalized synoptic patterns over the WNP and discusses the interactions of tropical systems with each pattern. The first involves a scenario in which the tropical system is located under tropospheric easterlies with a subtropical ridge (STR) to the north (Figure 1). In this case the outflow circulation from the tropical system encounters resistance and, thus, this pattern is not favorable for TC development.

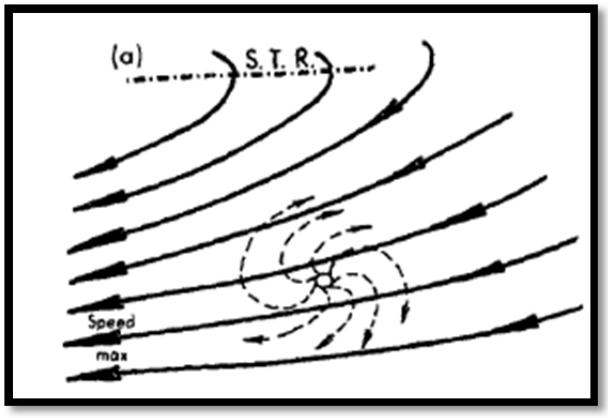

Figure 1. Tropospheric-level interaction of a TC outflow (dashed lines) with tropospheric easterlies (thick black lines) [Figure 1(a) from Sadler 1976].

The second scenario represents a trough in the westerlies penetrating into the tropics (Figure 2). This provides a "channel for facilitated outflow" (Sadler, 1976). Sadler points out that this case is mostly found in late season (October and November) when deep troughs in the westerlies penetrate onto the WNP basin. One can think of these 'deep troughs' as the equivalent of the potential vorticity (PV) streamers that will be discussed in detail in this work.

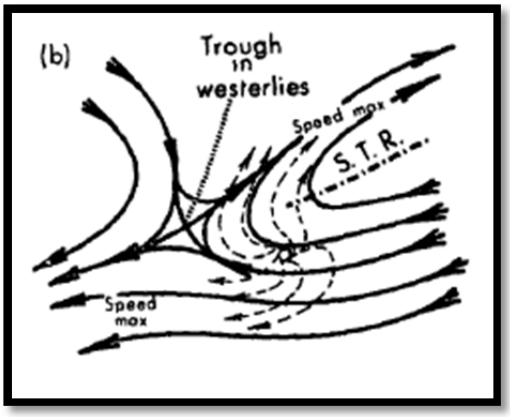

Figure 2. Tropospheric-level winds (solid black lines) with a trough in westerlies providing a channel for facilitated outflow (dashed black lines) for a tropical system in low-levels [Figure 1(b) from Sadler 1976].

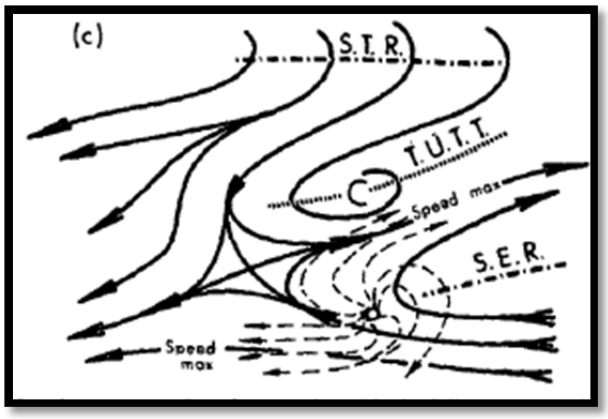

Figure 3. Tropospheric-level winds (solid black lines) with tropical system outflow (dash lines) [Figure 1(c) from Sadler 1976].

Sadler (1976) goes on to say, "during summer, troughs in the mid-latitude westerlies seldom extend in the tropical WNP; therefore, we must look to some other circulation feature for an outflow channel to westerlies." This leads to Sadler's third scenario: a TUTT cell between the STR to the north and the subequatorial ridge (SER) to the southeast (Figure 3). In this synoptic pattern, the TUTT cell also provides the needed "channel for facilitated outflow." This scenario is more consistent with observed flow patterns that are present during the early to mid-season when the "deep troughs in westerlies" case is seldom present. Sadler (1976) goes on to describe how the TUTT played a critical role in the development of three typhoons (which is "almost twice the normal for the WNP" as noted by Sadler for the month of June) in the WNP (Freda, Gilda and Harriet in June of 1971).

In 1978, Sadler attempted to apply his TUTT model to four simultaneous typhoons in July 1972 (Rita, Phyllis, Tess and Susan). He found that the genesis pathways of Typhoons Rita, Phyllis, and Tess were consistent with scenario 3 (Figure 3). In contrast, Susan encountered a synoptic pattern more equivalent to scenario 1 (Figure 1) with tropospheric easterlies aloft. In the latter case of Susan, the disturbance only achieved minimal typhoon status as reported by the Joint Typhoon Warning Center (JTWC).

b. North Atlantic

More recently, the focus has shifted to the Atlantic basin. After noting that "nearly half of the Atlantic tropical cyclones from 2000 to 2003 depended on an extratropical precursor (26 out of 57)," Davis and Bosart (2004) coined the term tropical transition (TT) to describe the avenue to tropical cyclogenesis that involves an extratropical precursor. A clear motivation of their work was the forecast challenge TT presented forecaster along the east coast of the United States and in throughout the Caribbean. They noted that "while TT storms typically do not exceed Category 2 intensity, their tendency to form close to North America can create significant forecast and evacuation problems."

Davis and Bosart (2004) classified TT cases as strong extratropical cyclone (SEC) or weak extratropical (WEC) events. The SEC cases "involve extratropical precursors of sufficient strength to trigger wind-induced surface heat exchange (WISHE)" whereas "in WEC cases, the baroclinic zone is an organizing agent for convection." Davis and Bosart (2004) discuss the synoptic and mesoscale features of SEC cases in the Atlantic with a composite synoptic analysis for four SEC cases (Florence 2000; Michael 2000; Karen 2001; Gustav 2002). Davis and Bosart make the following observations of the composite analysis: i) "The composite structure shows a pronounced, localized anomalous trough in the upper troposphere to the west of the surface low just prior to TT" (Figure 4) and ii) "The lower-troposphere temperature pattern exhibits warm and cold anomalies consistent with horizontal transport due to the precursor cyclone and anomalous warmth across the northeastern United States and eastern Canada" (Figure 4).

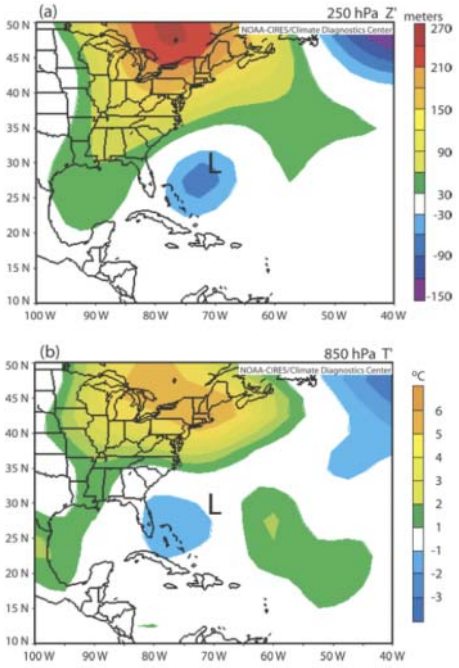

Figure 4. Top image shows the 250 hPa geopotential height anomaly and bottom image show the 850 hPa temperature anomaly for the four SEC cases [Flourence (2000), Michael (2000), Karen (2001) and Gustav (2002)]. The "L" indicated the position of the composite surface low center (Figure 1 from Davis and Bosart 2004).

In addition to SEC cases, Davis and Bosart (2004) revisited previous studies of non-developing cases. They conclude that the tropical cyclogenesis failed to occur due to the fact "the occluding cyclone is embedded within a mean current that translates it over cool water before TT can occur" or the "primary cyclone is prevented from occluding" (i.e., an upper-level disturbance moves in providing increased vertical wind shear).

For WEC cases, while the baroclinic zone is too weak to allow for cyclogenesis, persistent convection leads to midtropospheric vorticies that subsequently initiate tropical cyclogenesis. Davis and Bosart (2004) comment that "considerable research remains to understand how convection organizes in systems with weak precursors" thus, "it is difficult to derive a set of forecast rules." However, they point out that "PV debris" were a common occurrence at upper levels over the tropical Atlantic in September 2001 and it was theorized that these PV anomalies had to persist for 1–2 days over a weak baroclinic zone to provide mesoscale ascent. They conclude, "favorable conditions for WEC cases of TT involve mid-upper-tropospheric cyclonic PV anomalies encountering lower-tropospheric baroclinicity (and, hence, vertical shear)."

The TT process has been documented via a number of case studies in the Atlantic basin spell out ampersands (Bosart and Bartlo 1991; Davis and Bosart 2003; Hulme and Martin 2009a; Hulme and Martin 2009b). The initial development of TS Diana (September 1984) was studied by Bosart and Bartlo (1991). The development was presented as a three-stage process: i) a positive PV anomaly cut-off from the main upper-level flow over a stalled frontal zone located near the central Florida coast resulted in cyclogenesis in the southwestern flank of the PV anomaly; ii) following cyclogenesis was a period of intensification via deep tropospheric ascent associated with sloping isentropes from the PV anomaly aloft; finally, iii) the system took on more tropical characteristics with the destruction of the PV anomaly aloft.

Davis and Bosart (2003) looked at ten tropical cyclones from the 2000 and 2001 Atlantic hurricane season that started in highly sheared environments (greater than

12 to 15 m s^{-1} as defined by Gray (1968) and DeMaria et. al. (2001) and went through a process which resulted in reduced vertical wind shear. Hurricane Michael (2000) was an intriguing case they chose to simulate using the fifth-generation Pennsylvania State University-National Center for Atmospheric Research Mesoscale Model (MM5). Initial vertical wind shear over Michael was calculated to be in the 30 m s^{-1} range clearly placing it into a "high-shear" environment. Within 24 hours, the vertical wind shear was reduced by 20 m s^{-1} leading to a more conducive environment for tropical cyclogenesis. The authors concluded that diabatic effects acted to reduce and redistribute the PV anomaly thus reducing the vertical wind shear. Non transitioning cases (that did not undergo tropical cyclogenesis) were also examined. It was determined that the upper-level PV anomaly was either sustained by various shortwave troughs (hence sustained high vertical wind shear) or the storm moved over cooler waters (SST < 26^{o}C) before transition could occur.

Hulme and Martin (2009a) looked at six TT cases in the Atlantic basin (Michael 2000; Karen 2001; Noel 2001; Olga 2001; Delta 2005; Epsilon 2005) with strong extratropical precursors [classified as SEC by Davis and Bosart (2004)]. They note that "several similarities in the six cases appear to be the result of convection and its organization by, and interaction with, synoptic-scale features. They also suggest that the "extratropical occlusion accelerated by diabatic heating" can lead to tropical transition. In a companion paper, Hulme and Martin (2009b) investigated one of the TT events (Hurricane Karen) with numerical simulations using version 2 of the Weather Research and Forecasting (WRF) model. Their results supported the conclusions of Davis and Bosart (2003), being consistent with the three step process outlined above.

McTaggart-Cowen et al. (2008) produced an objective climatology of all tropical cyclogenesis events in the Atlantic basin from 1948 to 2004.Their goal was to "provide an objective method for framing studies and discussions of tropical cyclogenesis in analyses, forecast models, and climate prediction systems." The study addressed the issue of TC spinup by developing a dynamically-based classification scheme. After investigating the possible influence of a large number of dynamical fields, the authors

settled on two primary metrics to identify possible external forcing in the local environment and, thusly, classify all events. One metric was indicative of quasigeostrophic forcing for ascent, while the other assessed lower-level baroclinicity.

The "latent trajectory model" (LTM) is schematically illustrated in Figure 5 in terms of a phase space that is comprised by the magnitude of the two metrics (Thickness Asymmetry on the y-axis and Q-vector Convergence on the x-axis). For each storm (496 total in their dataset), the two metrics were calculated using the National Center for Environmental Prediction reanalysis data for the near-vortex environment over a 36-hour period leading up to the initial storm report per National Hurricane Center best track data. Mean Q-vector convergence for 400–200 hPa within a 6^{o} radius of the storm center was used to represent the upper-level forcing. The maximum difference in 1000–700 hPa thickness values within 10^{o} of the storm center was used to represent the low-level baroclinicity.

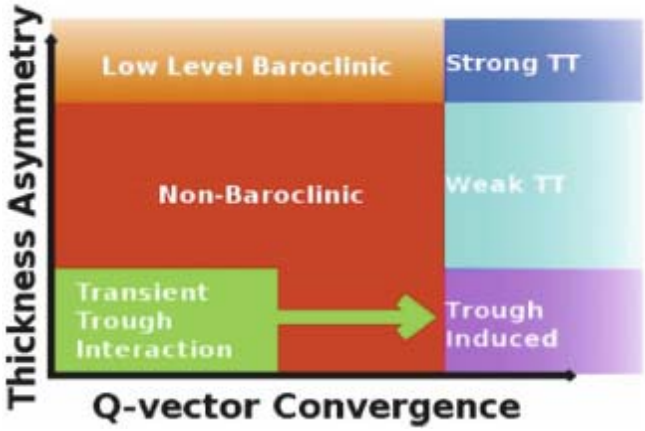

Figure 5. Simplified description of the Latent Trajectory Model devised by McTaggart-Cowen et al. (2008) as a means for objectively classifying TC genesis. Q-vector convergence represents the quasigeostrophic forcing for ascent while thickness asymmetry represents low-level baroclinicity (Figure 9 from McTaggart-Cowen et. al. 2008).

The seven groups along with the corresponding percentage of storms belonging to that group and a brief description of that group's classification are present in Figure 6. Also depicted are the three Th groups with corresponding percentage of storms

belonging to that group. Using just the Q and Th metrics alone yields 21 different categories, thus the LTM was devised and each pair (Q,Th) were placed into the category of nonbaroclinic, low-level baroclinic, transient-trough interaction, trough induced, weak TT or strong TT (as show schematically) in Figure 5 and in tabular form in Figure 7.

Metric	Group identifier	Membership percentage (π_x)	Summary description
Q	1	13.8	Constant low
	2	28.9	Constant low
	3	14.8	Medium, increasing toward T_o
	4	19.4	Constant medium
	5	10.9	Medium, decreasing toward T_o
	6	9.4	Constant high
	7	2.8	High, increasing toward T_o
Th	1	25.3	Constant low
	2	44.3	Constant medium
	3	30.4	Constant high

Figure 6. Table showing the 7 Q categories and 3 Th categories with percentage of storm falling into that category alongside a brief description of the category (Table 2 from McTaggart-Cowen et. al. 2008).

Category	Membership percentage	Q group	Th group
Nonbaroclinic	40	1	1
		2	1
		5	1
		1	2
		2	2
		5	2
Low-level baroclinic	13	1	3
		2	3
		5	3
Transient–trough interaction	16	3	1
		3	2
		3	3
Trough induced	3	4	1
		6	1
		7	1
Weak TT	13	4	2
		6	2
		7	2
Strong TT	15	4	3
		6	3
		7	3

Figure 7. Table showing the 6 Tropical cyclogenesis categories (column 1) with percentage of storms belonging to that category (column 2) and respective Q-group (column 3) and TH-group (column 4) numbers. These 6 categories are based on the 21 possible Q/Th combinations and is graphically depicted in Figure 5 (Table 3 from McTaggart-Cowen et. al. 2008).

The largest fraction of tropical cyclogenesis events fall into the nonbaroclinic category (40%). They represent what one thinks of as a "typical pathway" to TC formation with weak upper-level forcing (Q-vector convergence) and small values of low-level baroclinicity (thickness asymmetry). Geographically, these systems develop over the warm SSTs of the tropical Atlantic (Figure 8). McTaggart-Cowen et. al. (2008) note that this region represents the central and western sections of the [Main Development Region] MDR, an area characterized by warm SSTs at the west end of the subtropical high." Low-level baroclinic systems have weak upper-level forcing (Q-vector convergence) but strong low-level baroclinicity (thickness asymmetry). Figure 8 shows that most of these occurrences are in the Cape Verde and western Caribbean regions where low-level baroclinicity can be found late in the hurricane season.

Transient trough interaction events represent systems that initially developed in a region of weak upper-level forcing (Q-vector convergence) but, nearer to the initial storm report (within six hours), the storm encounters strong upper-level forcing. The upper-level feature in question subsequently translates away from the developing system, thusly reducing the vertical wind shear. Geographically these systems tend to occur in the Gulf of Mexico where a TC, in early stages of development, encounters a trough moving south from the North American continent.

Trough-induced cases are the smallest category out of the six comprising only three-percent of the systems evaluated in their dataset. These cases occur with strong upper-level forcing (Q-vector convergence) over a region of low baroclinicity (thickness asymmetry). These cases are confined mostly to the Gulf of Mexico where SSTs are near their peak for the season (Figure 8). McTaggart et. al. (2008) highlight that "warm SSTs modify the overlying lower atmosphere to eliminate baroclinicity, and strong trough penetrations from the North American continent are common late in the hurricane season." This lack of low level baroclinicity and trough penetrations from a continental landmass is comparable to the WNP region of interest in this study.

Weak and strong TT cases comprise 13 and 15%, respectively, and are characterized by relatively high upper-level forcing (Q-vector convergence) as in the trough-induced cases but have stronger low-level baroclinicity (thickness asymmetry) with the magnitude of the baroclinicity delineating the two categories. Figure 8 shows that these cases occur closer to land where low-level baroclinic zones are more prevalent and also in the vicinity of the Gulf Stream (a natural persistent baroclinic zone).

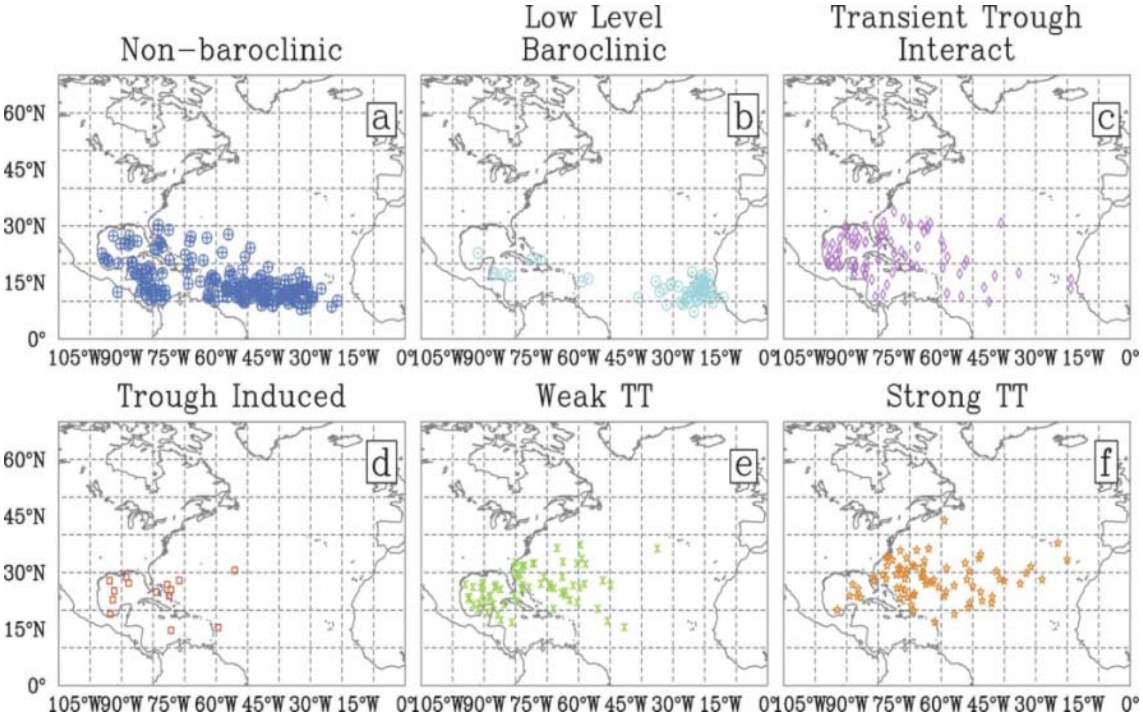

Figure 8. Spatial Distribution of tropical cyclogenesis events for each of the 6 categories (a) Nonbaroclinic (b) Low Level Baroclinic (c) Transient Trough Interaction (d) Trough Induced (e) Weak TT (f) Strong TT (Figure 10 from McTaggart-Cowen et. al. 2008).

Category	April	May	June	July	August	September	October	November	December
Nonbaroclinic	0	2	8	20	52	86	26	5	1
Low-level baroclinic*	0	0	0	3	26	26	6	1	0
Transient–trough interaction	0	2	7	12	21	20	15	2	0
Trough induced	0	0	1	1	7	3	1	1	0
Weak TT	0	0	11	7	15	22	9	2	0
Strong TT**	2	3	2	3	11	20	22	8	2
Total	2	7	29	46	132	177	79	19	3

Figure 9. Intraannual distribution of tropical cyclogenesis events for the 6 categories (Table 5 from McTaggart-Cowen et. al. 2008).

3. PV Concepts

a. General Concepts

Potential vorticity (PV) provides a useful tool for analyzing the atmospheric dynamics. Ertel's PV is defined as follows (Ertel 1942; Holton 2004):

$$PV = (\zeta_\theta + f)(-g\frac{d\theta}{dp}) \tag{1.1}$$

$\zeta_\theta$is the relative vorticity on an isentropic surface and f is the Coriolis parameter, thus the first term in the parenthesis on the right-hand-side (RHS) of Equation 1.1 represents absolute vorticity. The second term is a measure of static stability, which can be visually interpreted as the distance or separation of potential temperature lines on a vertical cross section. The lager (smaller) the spacing between isentropes the less (more) stable the atmosphere. Potential vorticity is measured in Potential Vorticity Units or PVUs with 1 PVU equivalent to 10^6 K kg^{-1} m^2 s^{-1}.

One of PV's most useful aspects is illustrated by the so-called invertibility principle. Simply stated, if one knows the distribution of PV in the atmosphere, given an appropriate reference state and boundary conditions, then one can calculate the absolute vorticity and static stability individually. This allows one to quantify the balanced state associated with the PV field, in terms of variables such as geopotential height and potential temperature. Positive PV anomalies are synonymous with higher vertical wind shear because PV and geopotential height are related based on Equation 1.2.

$$q = \frac{1}{f_0}\nabla^2\varphi + \frac{f_0}{\sigma}\frac{\partial^2\varphi}{\partial p^2} + f = \Lambda(\varphi) + f \tag{1.2}$$

Where q is the quasigeostrophic PV, φ is the geopotential height and f is the Coriolis parameter. While it is agreed that vertical wind shear is "inimical to genesis," (Emanuel 2005) no consensus on a threshold value for vertical wind shear has been reached.

b. PV Anomaly Forcing of Convection

Recent studies in the tropical regions have suggested a connection between intrusions of high PV air into the tropics and the occurrence of deep convection (Kiladis and Weickman 1992; Montgomery and Farrell 1993; Funatsu and Waugh 2008). Further examining the climatology of intrusions into the tropical upper troposphere prepared by Waugh and Polvani (2000), Funatsu and Waugh (2008) noted that deep convection nearly always occurred on the downstream side of a PV streamer and that the PV streamer *preceded* the deep convection. They hypothesized that the deep convection was a result of reduced static stability and enhanced vertical motions associated with the PV streamer.

Hoskins et al. (1985) showed that a positive PV anomaly aloft will cause a decrease in static stability below the anomaly resulting in a sloping isentropic surface (Figure 11). The decrease in static stability in conjunction with the motion of the PV anomaly can result in non-zero vertical velocities associated with air parcel flow along vertically-sloping isentropes (see Figure 12, Funatsu and Waugh 2008).

In addition to their climatological analysis, Funatsu and Waugh (2008) examined a PV intrusion that occurred 13–17 January 1987. They conducted numerical simulations of the event using MM5 in order to test their hypothesis that convection occurring downstream [marked by low outgoing longwave radiation (OLR) in their study] was directly tied to the presence of the PV intrusion. Using simulations that remove latent heat release and / or the PV anomaly the authors were able to illustrate the direct link between the PV intrusion and the deep convection. These results are summarized in Figure 10, where there is a noticeable absence of deep convection upon the removal of the PV intrusion.

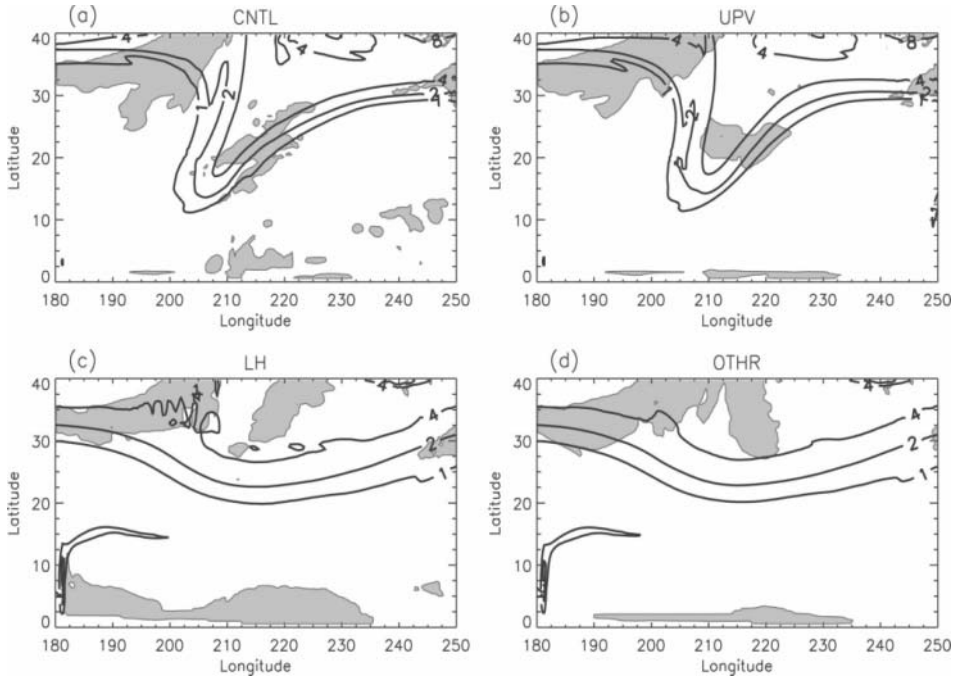

Figure 10. Potential vorticity (contours of 1, 2, 3 and 8 PVU) on the 200 hPa level and OLR less than 210 W m^{-2} shaded at 1200 UTC 15 January, 1987 for (a) MM5 control simulation (CNTL), (b) MM5 simulation with latent heat release removed (UPV), (c) MM5 simulation with PV anomaly removed and (d) MM5 simulation with both latent heat release and the PV anomaly removed (OTHR)(Figure 7 from Funatsu and Waugh 2008).

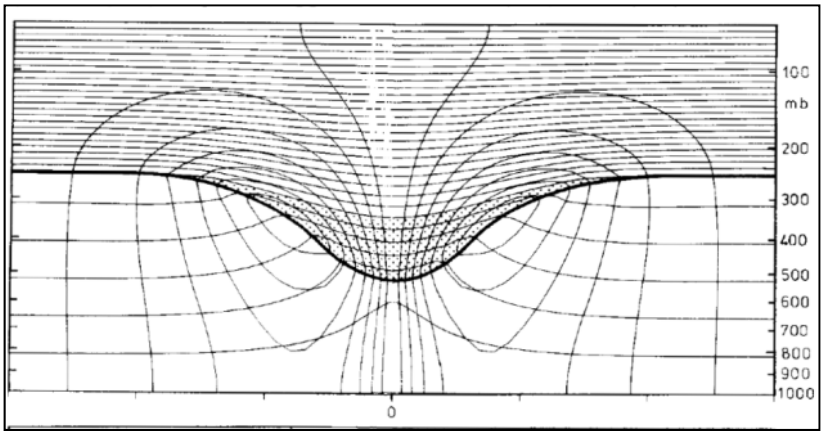

Figure 11. Structure of a positive PV anomaly aloft. The thick line represents the dynamic tropopause. The two sets of thin black line represent isentropes every 5 K and transverse velocity every 3 m s^{-1} [Figure 15(a) from Hoskins et. al. 1985].

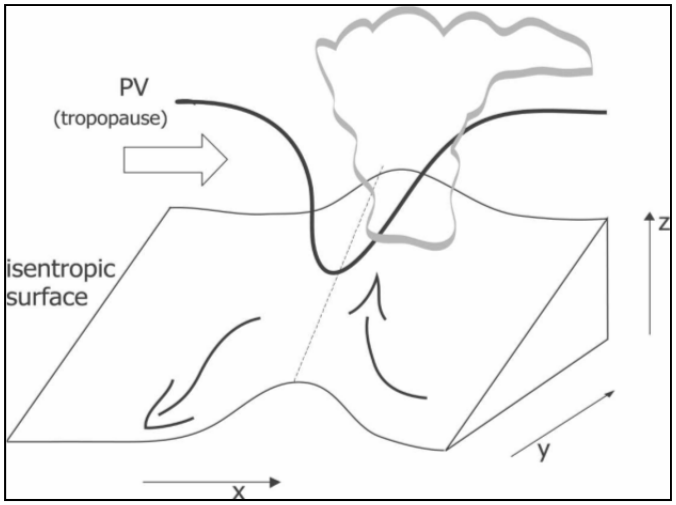

Figure 12. Schematic representation of the proposed mechanism for the occurrence of convection. Based on Dixon et al. (2003). The presence of an upper-level PV trough causes a parcel of air on an isentropic surface to move northwestward and upward on its downstream side, providing conditions favorable to trigger convection (Figure 1 from Funatsu and Waugh 2008).

The study of Funatsu and Waugh only examined the dynamics associated with PV intrusions in the eastern Pacific. However, given that wave breaking events are prevalent during the summer and fall seasons in the central North Pacific and, to a lesser extent, the WNP (Figure 13), it is not unreasonable to hypothesize the same dynamical processes involving linking upper-level PV anomalies and deep convection are at work. Furthermore, given the relatively high SSTs in the WNP, the local conditions are likely more favorable for the deep convection to ultimately result in tropical cyclogenesis.

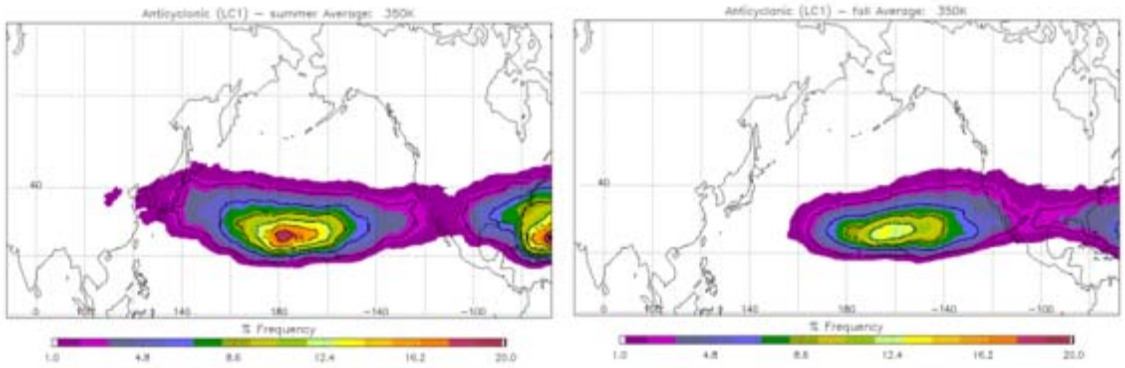

Figure 13. Left Image: Frequency (%) of the occurrence of anticyclonic breaking waves for the Pacific Basin for summer months (June, July and August). Right Image:Frequency (%) of the occurrence of anticyclonic breaking waves at the tropopause for the WNP basin for fall months (September, October and November).

c. Repercussion of Diabatic Processes on PV Structure

PV is conserved in the absence of friction and diabatic processes. When these processes are present, PV can be generated and/or destroyed.

For the present study, we are primarily focused on the impact of diabatic processes on the three-dimensional PV structure. The previous studies of TT and PV intrusions into the tropics outlined above have illustrated how an upper-level PV anomaly can induce deep convection. The repercussion of deep convection in a vertical column is to re-distribute PV. In the presence of diabatic heating, PV is generated below and depleted above the level of maximum heating. An equation representing the change in PV can be written as in Equation 1.3 (Martin 2.6).

$$\frac{d}{dt}(PV) = -g(\zeta_\theta + f)\left(\frac{d\theta}{dp}\right) \qquad (1.3)$$

Consistent with this notion, Wernli and Davies (1997) showed through an air parcel trajectory analysis that an air parcel gains PV below the level of maximum diabatic heating and then loses PV above that level. Figure 14 shows the PV tendency for air parcels from a Lagrangian perspective with the bold lines representing the trajectory

and the shaded region representing the region of diabatic heating and the hatched region indicating the positive PV anomaly.

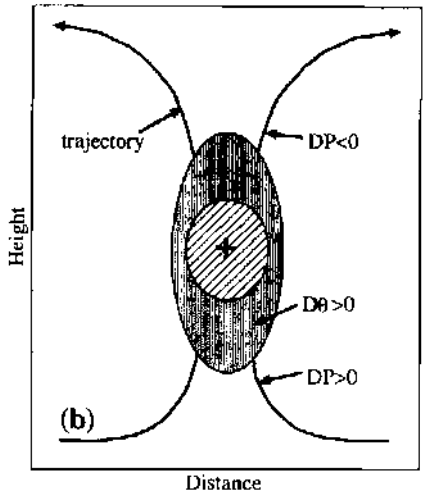

Figure 14. Diabatic heating effects on PV. The bold lines represent Lagrangian air parcel trajectories with PV production (DP >0) below the region of max heating (+) and PV depletion above (DP<0) [Figure 4(b) from Wernli and Davies 1997].

4. Tropical Storm 16W

Schönenberger (2010) conducted a detailed case study on Tropical Circulation System 037 (TCS-037) which occurred in September 2008, during the TCS-08 field program of 2008 (Elsberry and Harr 2008). TCS-08 "provided a unique opportunity to study a developing system with an extratropical precursor (TCS-037) developing into Tropical Storm 16W (TS 16W)" (Schönenberger 2010). This subsection summarizes the results and conclusions of this study, thereby serving as a foundation for the analysis of ensemble prediction data for this case (Chapter IV).

A broad region of convection developed in the WNP (Figure 15) at approximately 168^{o}E and 17^{o}N on 3 September 2008 and was designated as TCS invest 37. From Figure 18, one can see that the convection is associated with a PV anomaly aloft. Figure 17 shows the SSTs in this region were approximately 28^{o}C, satisfying necessary condition number one discussed previously.

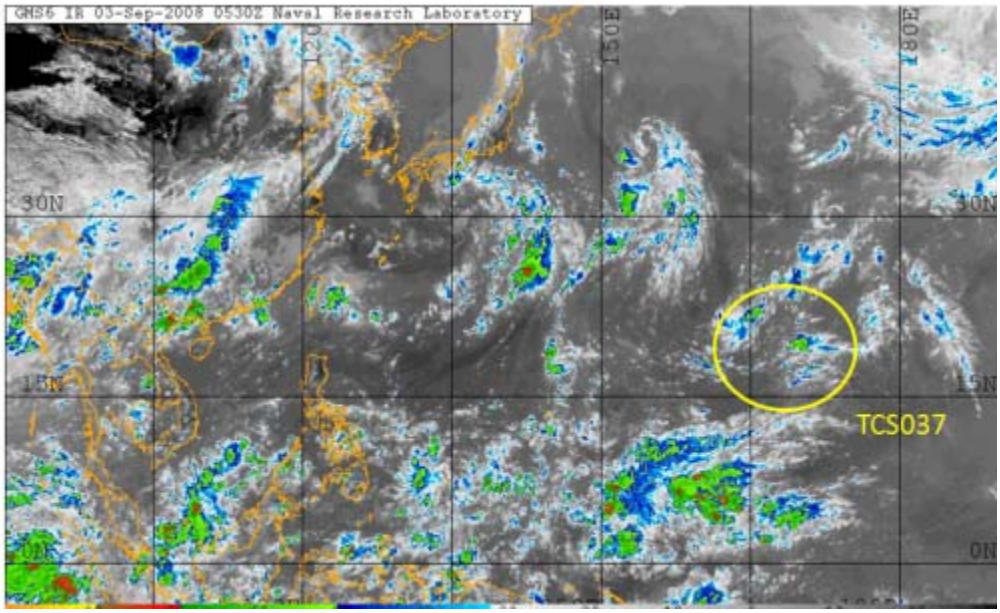

Figure 15. METSAT IR imagery valid 0530 UTC 3 September 2008. The area of convection designated TCS-037 is circled in yellow. The upper-level trough can be seen to the northeast of TCS-037.

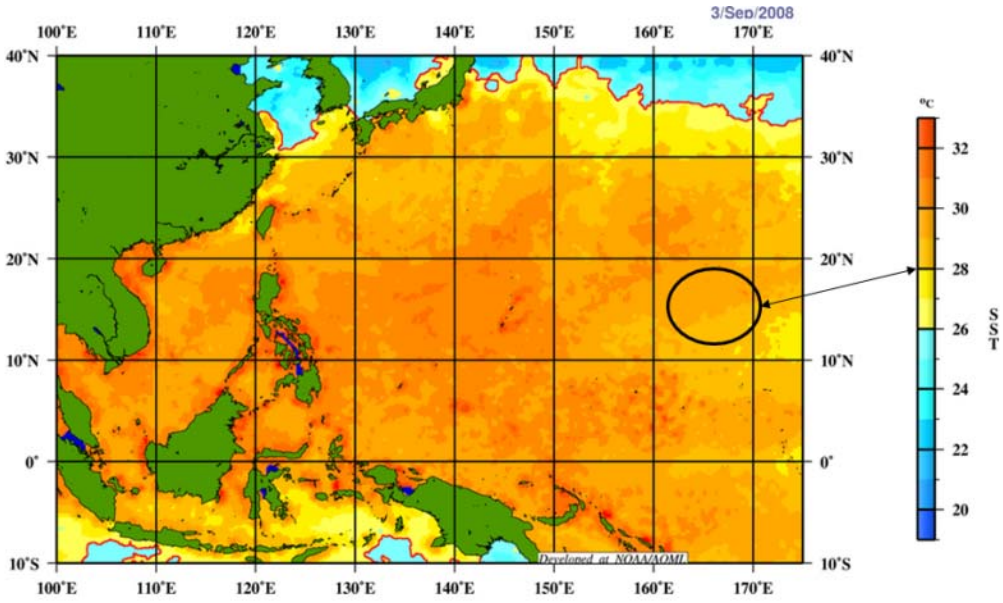

Figure 16. Sea Surface Temperatures (^{o}C) over the western Pacific valid 0000 UTC 3 September 2008. The general location of TCS037 circled in black. SSTs in this area are roughly 28^{o}C (necessary condition #1). Image retrieved from TCS08/TPARC website: http://catalog.eol.ucar.edu/tparc_2008/index.html

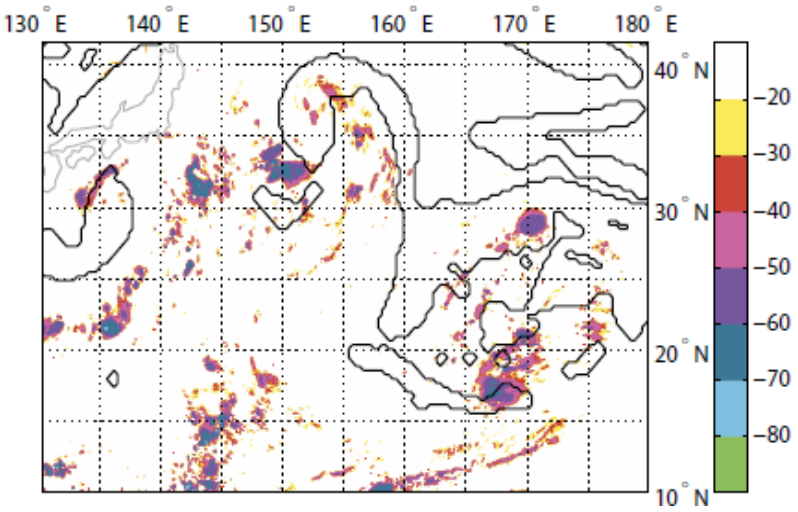

Figure 17. METSAT IR cloud top temperatures (°C).Black line indicates 1 PVU on the 345 K. Valid 1800 UTC 3 September 2008 (Figure 4.3 from Schönenberger 2010).

Moderate to strong vertical wind shear existed in the region with the PV anomaly overhead (Figure 18). Convection persisted to the southeast of the upper-level PV anomaly through 4 September until convection decreased from 0000 UTC to 1200 UTC 5 September. Two MCS started forming at 1500 UTC 5 September with the upper-level divergence growing in response to the convection.

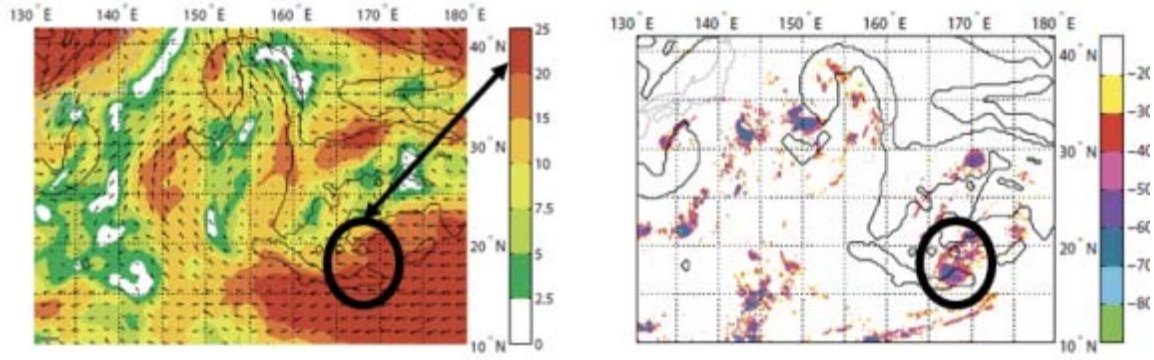

Figure 18. Left image – Deep Vertical Wind Shear (850 – 200 hPa) with flow field for 900 hPa (15 m s^{-1} reference). Right Image – METSAT IR cloud top temperatures (°C). Both images valid 1800 UTC 3 September 2008 and the black line is 1 PVU on the 345 K surface. Thick black circle indicates relative position of TCS-037 at the given time (Figure 4.4 and 4.5 from Schönenberger 2010).

Figure 19 shows two Mesoscale Convective Systems (MCS) (approximately 17.5°N/162°E and 25°N/161°E) were generated (in response to the upper-level forcing associated with the PV streamer) and decayed with no distinct low level circulation forming during this time.

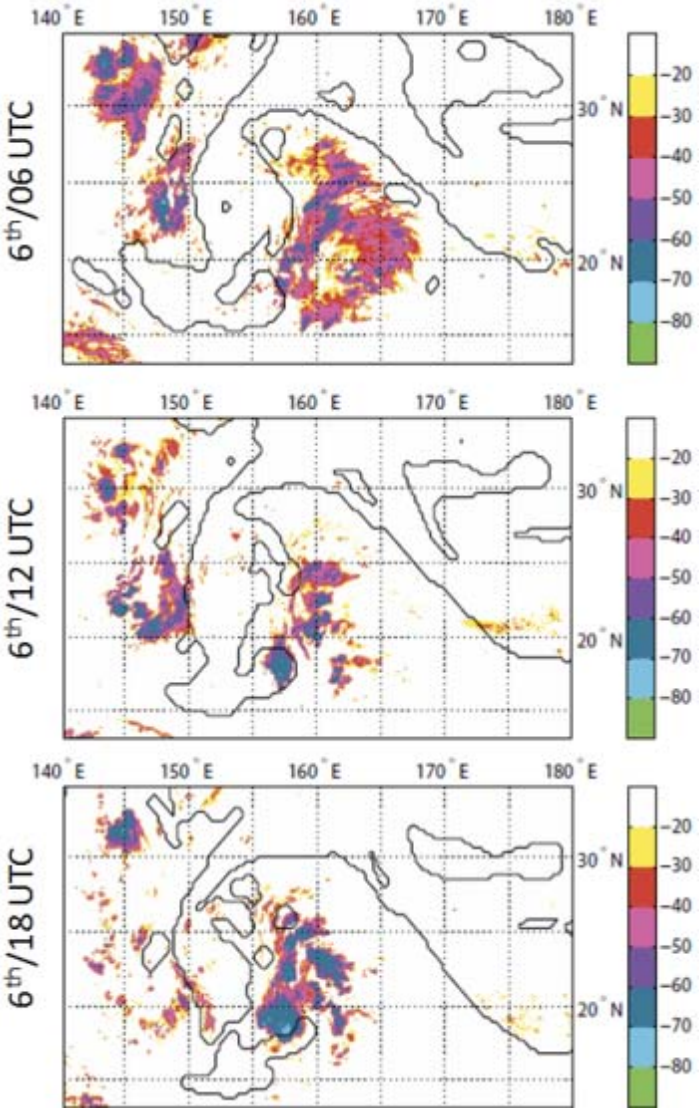

Figure 19. METSAT IR cloud top temperatures 0000 through 1800 UTC 6 September 2008 with black line showing 1 PVU on 345 K surface (Figure 4.10, 4.11 and 4.12 from Schönenberger 2010).

With convection becoming more organized on 7 September, Schönenberger showed that the PV anomaly enhanced convection along its southwest flank shown in the vertical cross section in Figure 20. In this figure, it is important to note the upward bowing of the isentropes (solid gray lines) directly beneath the PV anomaly to about 700 hPa. Schönenberger elaborates by stating, "as we would expect from theory, a particle will be lifted as the tilted isentropes below the streamer approach it and convection can be triggered, as is the case at this point in time" consistent with stage one of our hypothesis described in subsection 7.

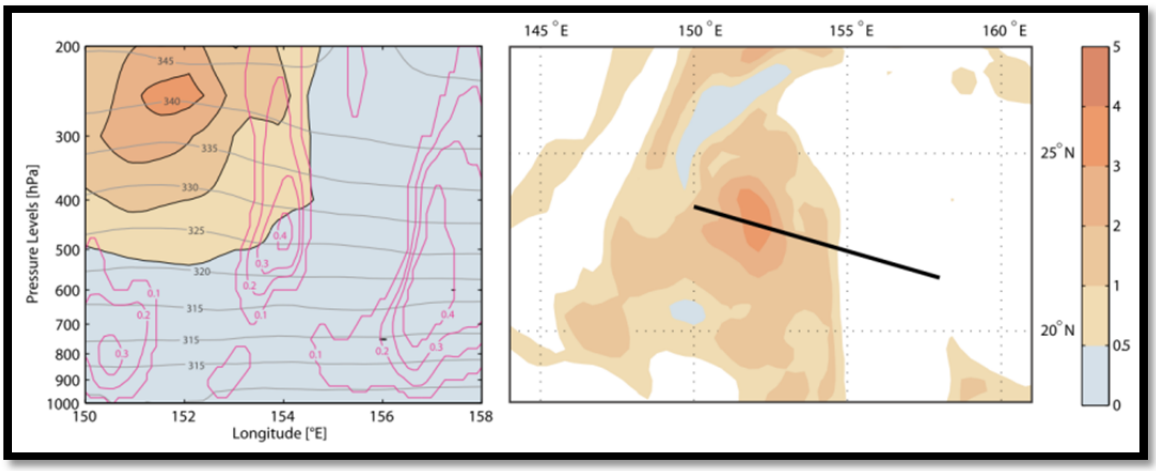

Figure 20. Vertical cross-section through PV streamer shown on the right at 0000 UTC 7 September 2008. The black line shows the location of the cross-section. The image on left shows potential temperature in thin gray solid lines, PVU in shaded colors and vertical velocities in magenta lines. Upward vertical motion is shown on the southwest flank where the convection was located (Figure 5.9 from Schönenberger 2010).

In situ measurements from C-130 flight dropsondes as well as ECMWF analysis show a weak surface circulation at 0000 UTC 7 September centered roughly 19°N/155°E with a minimum central pressure of 1006 hPa. Also the PV structure begins to cut off on 7 September with respect to the 1 PVU surface on the 345 K potential temperature surface (Figure 21).

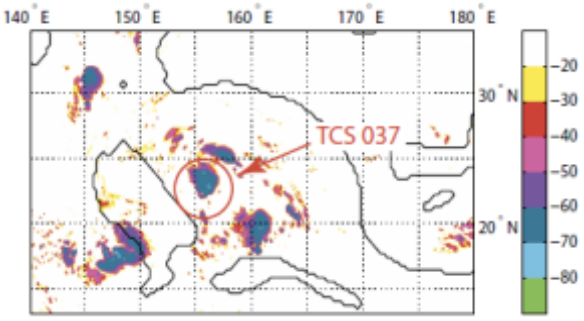

Figure 21. METSAT IR cloud top temperatures 1600 UTC September 7 2008 with the black line showing 1 PVU on 345 K surface (Figure 4.16 from Schönenberger 2010).

ECMWF analysis data and observations showed that on 8 September the circulation was better defined at 850 and 700 hPa and that it appeared vertically stacked. The PV anomaly completely cuts off from the stratospheric reservoir of high PV between 0000 and 1800 UTC (see Figure 22) resulting in a "channel" of relatively low PV air. This channel is associated with substantially lower values of vertical wind shear (on the order of 5–10 m s^{-1}) (Figure 23) and it represents the region where a coherent low-level vorticity feature forms and subsequently intensified as it traveled to the northwest.

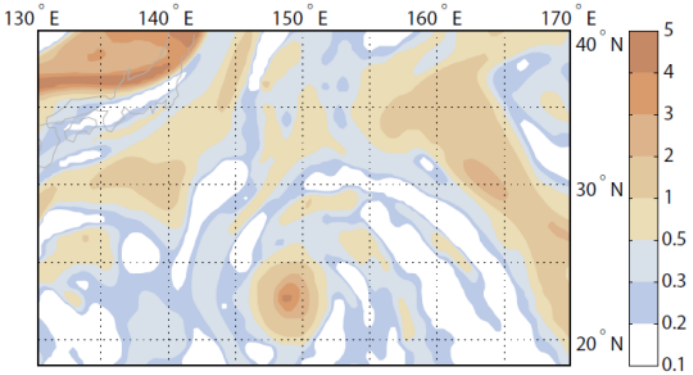

Figure 22. PV (PVU shaded colorbar to the right) on the 345 K potential temperature surface. PV streamer (~23°N/149°W) is shown here cutoff from the larger PV structure to the northeast leaving a noticeable "channel" of relatively lower PV air oriented from the southeast to northwest (Figure 4.21 from Schönenberger 2010).

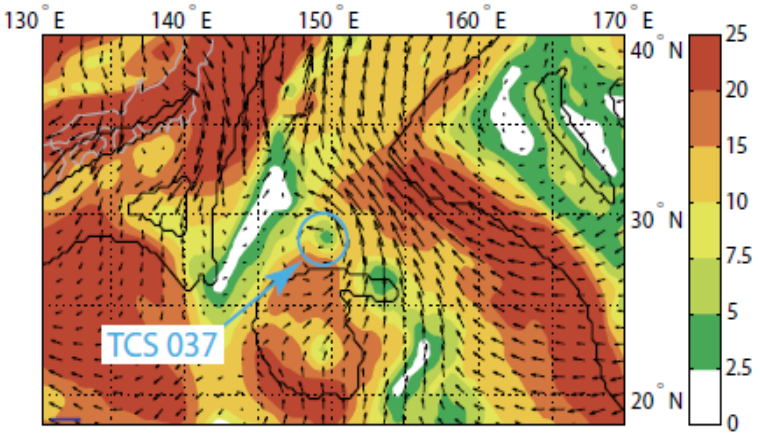

Figure 23. Deep Vertical Wind Shear (850 – 200 hPa) in m s^{-1} for 1800 UTC 8 September 2008 with flow field on 900 hPa (15 m s^{-1} reference). Black contour is 1 PVU on 345 K potential temperature surface. Shows corresponding "channel" of reduced vertical wind shear (Figure 4.23 from Schönenberger 2010).

In an effort to quantify the impact of diabatic processes on the PV-cutoff process and concomitant reduction in vertical wind shear, Schönenberger (2010) conducted backward trajectory analyses from the region of the upper-level PV channel (i.e., reduced upper-level PV). The study identified all air parcels that underwent a 40 Kelvin (K) warming during a 96-hour period ending at the predefined endtimes of 1200 and 1800 UTC 7 September and 0000 and 0600 UTC 8 September with the goal of capturing diabatic processes associated with air parcels ascending via convection. Figure 24 shows the trajectory analysis for the time periods described above. Nearly all of these air parcels originated in the atmospheric boundary layer (below approximately 900 hPa).

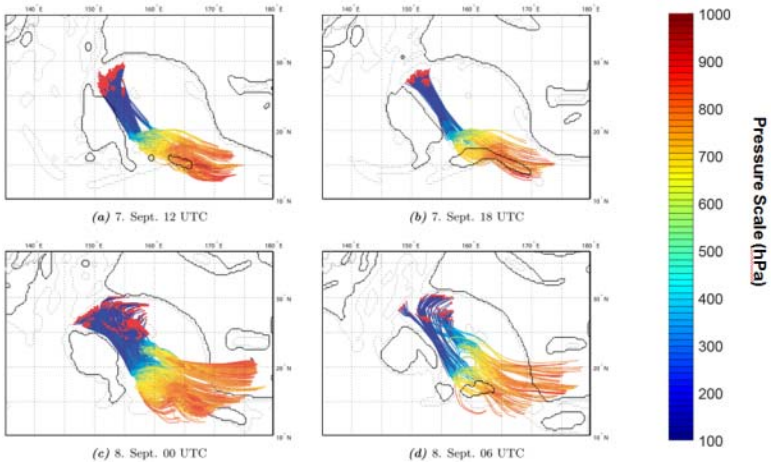

Figure 24. Trajectory analyses for air parcel undergoing 40K of warming during the previous 96hrs ending at: (a) 1200 UTC 7 Sept 2008, (b) 1800 UTC 7 Sept 2008, (c) 0000 UTC 8 Sept 2008, and (d) 0600 UTC 8 Sept 2008. Pressure levels indicated by a color scheme shown on the right [Figure 5.10(a)-(d) from Schönenberger 2010].

Further analysis of the air parcel trajectories by Schönenberger revealed that above the maximum heating rate, PV was decreasing showing that diabatic processes were responsible for the dramatic alteration of the dynamic tropopause (stage two of our hypothesis described in subsection 7) above the convective region.

Figure 25 shows the statistical evaluation of the trajectory analysis for each day. Schönenberger (2010) used the minimum potential temperature (K) as the reference state to calculate the change and assuming a subjective heating threshold of 15 K to differentiate between air parcels that are warmed due to simple advection (i.e., $<$ 15K warming) and those that are diabatically enhanced (i.e., $>$ 15 K warming). One notices a sharp increase in the percentage of diabatically heated air parcels from 0000 UTC to 1800 UTC 7 September. Schönenberger (2010) notes that this was the time period when the PV anomaly becomes cutoff showing the diabatic effects depleting the PV aloft. Figure 26 shows the heating rate (left panel) alongside the PVU (right panel) for all parcels undergoing 40 K of warming. There are two peaks in diabatic heating rate (-48h and -36h) and the PVU shows increasing values up to that second peak in diabatic heating (at -

36hr) and then begins to decrease highlighting the PV depletion due to diabatic effects consistent with stage two described in Subsection 7.

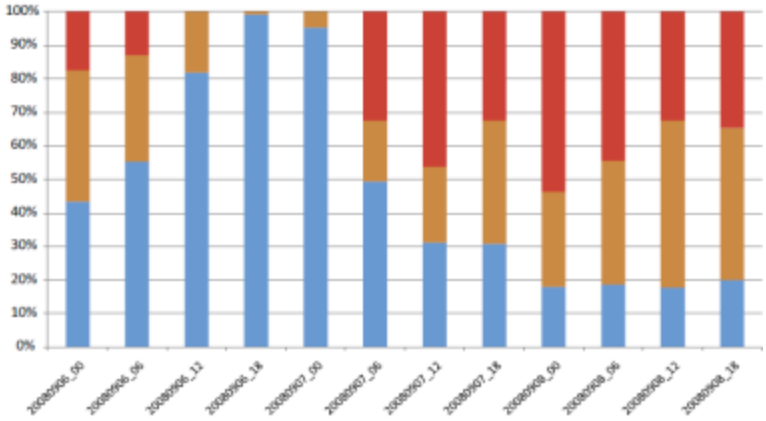

Figure 25. Statistical representation of the percentage of advected trajectories with heating values lower than 15 K (blue) and diabatically enhanced trajectories with heating values above 15 K (15–35 K = orange, 35–50 K = red). All trajectories were started on a equidistant 20km grid on the 345 K isentropic surface (Figure 5.11 from Schönenberger 2010).

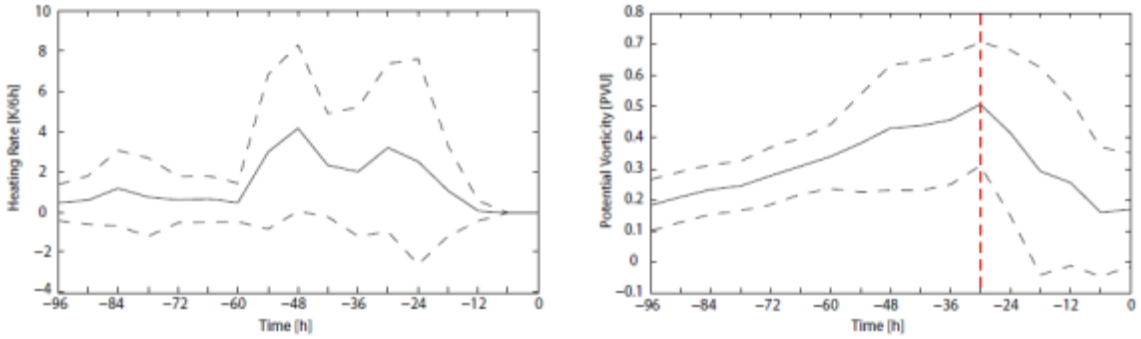

Figure 26. Lagrangian history of all backward trajectories, heated more than 40 K, concerning instantaneous diabatic heating (left panel) and PV (right panel). Solid lines represent mean values, dashed lines show the standard deviation [Figure 5.13(a)–(b) from Schönenberger 2010].

5. Probabilistic Weather Prediction

In the past few decades, the focus of Numerical Weather Prediction (NWP) has shifted from deterministic to probabilistic prediction. Lorenz's classic 1963 paper, Deterministic Nonperiodic Flow, brought forth the idea that non-periodic systems are unstable and, therefore, that bounded systems have a finite limit of predictability (Lorenz 1963). Lorenz (1965) estimated the limit of predictability of the atmosphere to be less than a month but more than a week. The limit of predictability exists as a result of errors that arise from a variety of sources, including imperfect observations, imperfect models, and/or imperfect analysis (Hacker 2011).

This phenomenon is presented in schematic form in Figure 27. The red-outlined circles represent the forecast in phase-space, while the circled T's represent the true state of the atmosphere. The initial state is the left-most T-circle and the gray cloud shows the uncertainty in phase space of the actual true state of the atmosphere. Essentially a deterministic forecast takes an initial condition from this "cloud" and forecasts the future state. The distance between the truth circles and the red forecast circles shows the forecast error within this phase space. The error is expected to grow with time. In summary, the figure illustrates the relatively simple fact that one can never know the exact state of the atmosphere at any one time and the error from this uncertainty coupled with "model deficiencies" causes the NWP forecasts to deviate from the true state of the atmosphere (Hacker 2011).

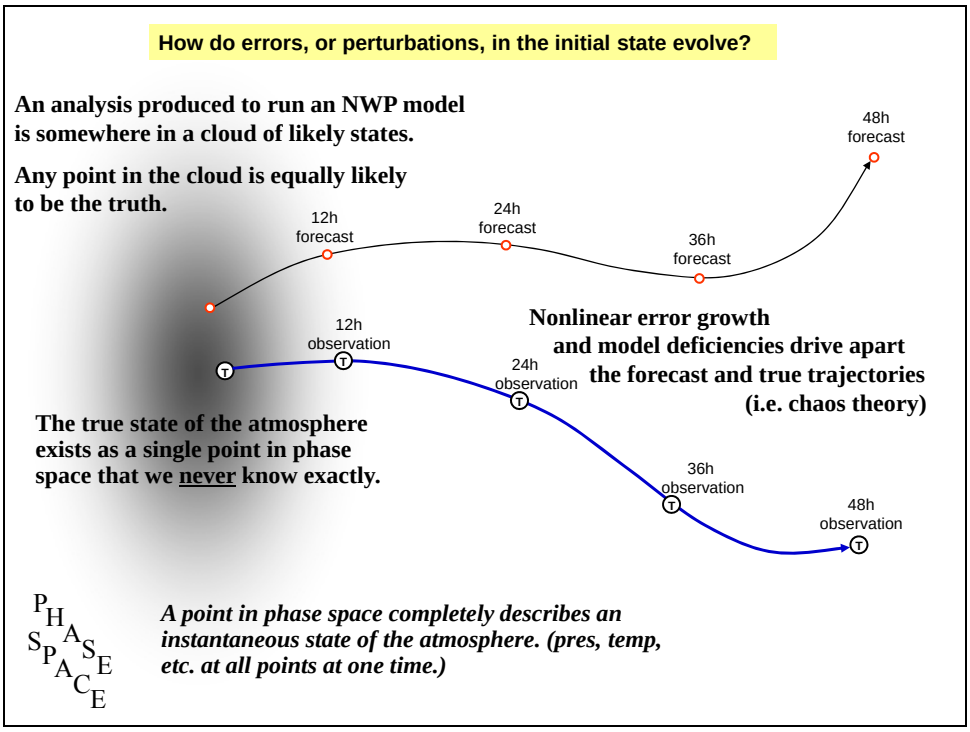

Figure 27. Schematic representation of the initial state uncertainty and error growth producing forecast deviations from the truth.

To attempt to account for the chaotic nature of the atmospheric system, Epstein (1969) introduced the notion of stochastic dynamic forecasting. The idea is to treat the atmosphere as a system that deterministically obeys a certain set of fundamental laws but, at the same time, to recognize that the state of the atmosphere can only be known in probabilistic form. An ensemble prediction system (EPS) attempts to account for the uncertainty in model construction to determine the range of possible forecast outcomes, to estimate the probability of any individual forecast outcome, and hopefully determine the most likely forecast outcome. An EPS can attempt to account for a number of uncertainties, including those related to the initial condition, model configuration, physical parameterizations and even the numerical model employed (i.e., create a multi-model ensemble).

The most common approach used today is related to initial condition uncertainty. Data assimilation techniques are used to calculate the best guess of the initial condition

and to estimate the amount of initial condition uncertainty. This information can then be used to construct an EPS with the goal to not only estimate the most likely forecast outcome (the ensemble mean), but also the forecast uncertainty (via EPS spread). This is accomplished by creating initial condition perturbations that attempt to account for the initial condition uncertainty. An EPS system compromises the ensemble control (ensemble member initialized with the best guess of the initial condition) and a number of ensemble perturbations (members run from the analyses that are changed to reflect the initial condition uncertainty). Different methods have been employed to generate appropriate initial conditions perturbations, including but not limited to the Breeder Method, Singular Vectors, and Ensemble Transform Kalman Filter (Stone 2011).

As intimated above, the use of probabilistic forecasting is well suited for scenarios wherein there exists significant initial condition uncertainty. Furthermore, a measure of forecast uncertainty that can be provided by an EPS is extremely useful for dynamical situations that exhibit significant sensitivity to initial condition error. It is these features that make the use of probabilistic forecasting appropriate for the study of TT in the WNP. This is a region almost entirely devoid of in-situ measurements (implying significant initial condition uncertainty). As hypothesized in Subsection 7, the dynamical evolution of the TT process involves a wide variety of temporal and spatial scales (ranging from synoptic to mesoscale). Diabatic processes are also known to be critical to the observed evolution of TT systems. All of these facts indicate that a probabilistic methodology should be utilized.

6. Probabilistic Forecast of Typhoon Dolphin

Typhoon Dolphin was a tropical cyclone that underwent tropical transition in December 2005 in the WNP basin (the best track data for JTWC is presented in Figure 28). Stehrenberger (2009) studied the evolution of Dolphin within the context of ensemble prediction data by comparing the ensemble forecasts of two ensemble prediction systems with the observed evolution. Using ECMWF and United Kingdom Meteorological Office (UKMO) ensemble data, Stehrenberger (2009) computed the

maximum 850 hPa vorticity, sea-level pressure minimum and mean vertical wind shear for each six-hour time step utilizing a tracking routine of her design to compare these data with the ERA-interim representation. Next, she categorized each ensemble member (Figure 29) based on the storm tracks as compared with the actual track.

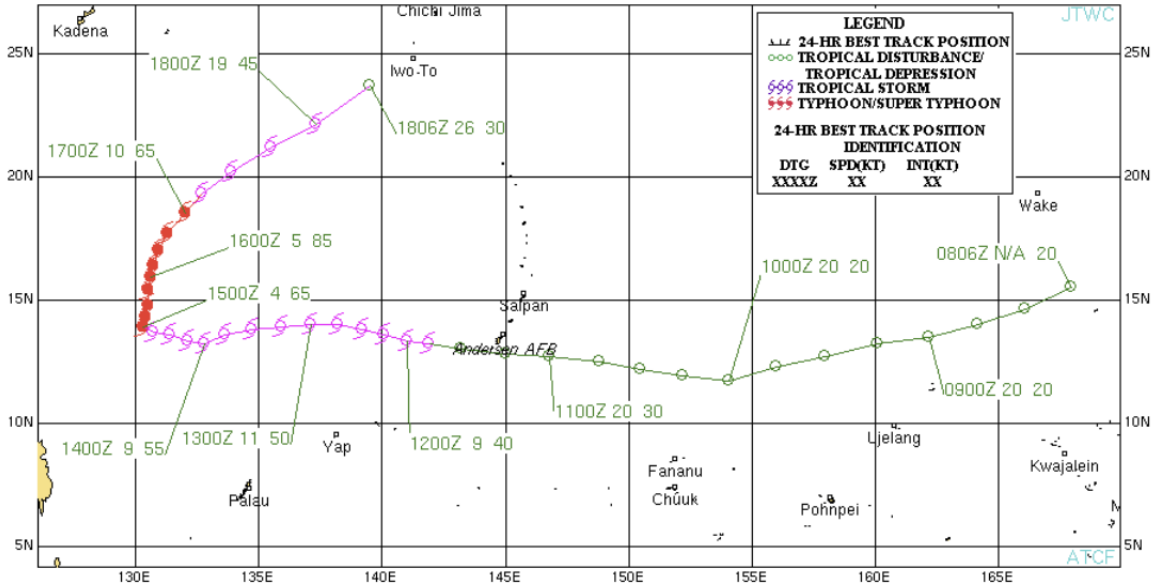

Figure 28. JTWC best track for Typhoon Dolphin from the 2008 Annual Tropical Cyclone Report. Storm's position is shown as green circles (tropical disturbance), pink tropical storm symbols (tropical storm) and red typhoon symbols (typhoon).

ECMWF Ensemble Members (Start on 4 Dec)	Characteristics
1, 2, 6, 8, 12, 15, 17, 19, 23, 27, 32, 35, 38, 43, 46, 47, 49	Track similar to real one, slightly west/north of the real track, vortex moves rather fast tracked minimum SLP eventually turns south.
3, 9, 11, 13, 16, 21, 22, 25, 26, 29, 30, 33, 34, 39, 40, 41, 48	Track similar to real one, slightly east/south of it
4, 5, 7,10, 14, 18, 20, 28, 36, 42, 44	Vortex moves eastwards into the extratropics
24, 37, 45, 50	Heading south-east, later southwards
31	Vortex stays around 25°N

Figure 29. Categorizations on the 50 ECMWF ensemble members based on predicted tracks of the maximum 850 hPa relative vorticity and minimum sea-level pressure.

The evolution of each ensemble member was subjectively classified according to its track characteristics. Looking closer at ECMWF ensemble member 34, which she indentifies as a "relatively good forecast" (group tracks colored red in Figure 30) and ECMWF ensemble member 44 classified as a "bad forecast" (group tracks colored blue in Figure 30). Further examination of the dynamical evolution of the bad forecast illustrated that the resulting track error was due to the positional error in the location of the upper-level trough: it remained too far to the north, thereby serving to recurve the incipient disturbance into the extratropics (compare Figures 31 and 32).

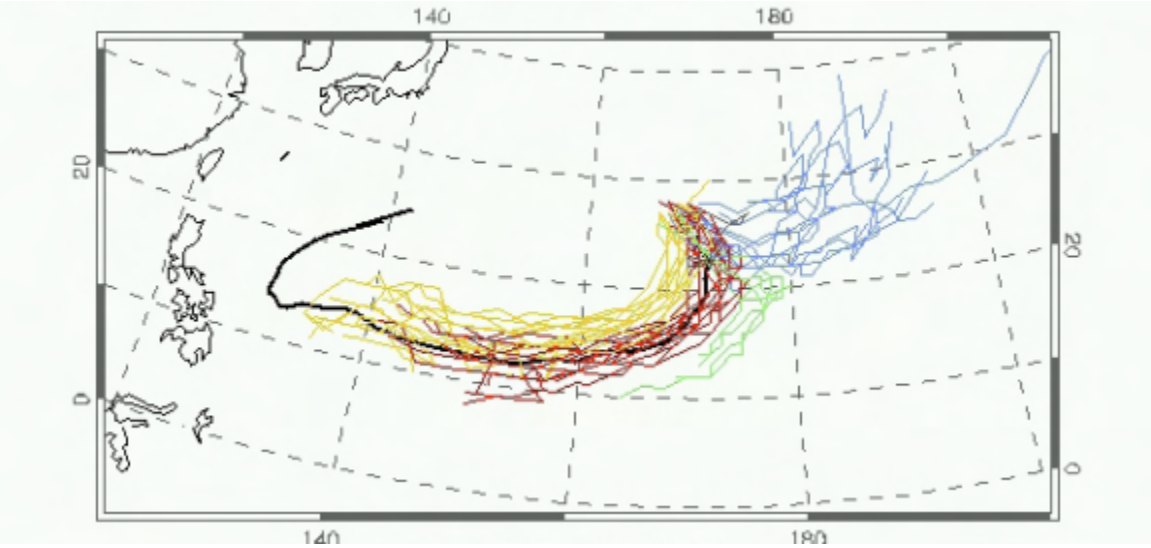

Figure 30. ECMWF ensemble member track color-coded [track similar to the real one only slightly west/north) (yellow), track similar to the real one only slightly east/south (red), vortex moves east into extratropics (blue), heads southeast and later south (green), and vortex remains stationary around 25°N] based on groupings in Figure 29 (Figure 12 from Stehrenberger 2009).

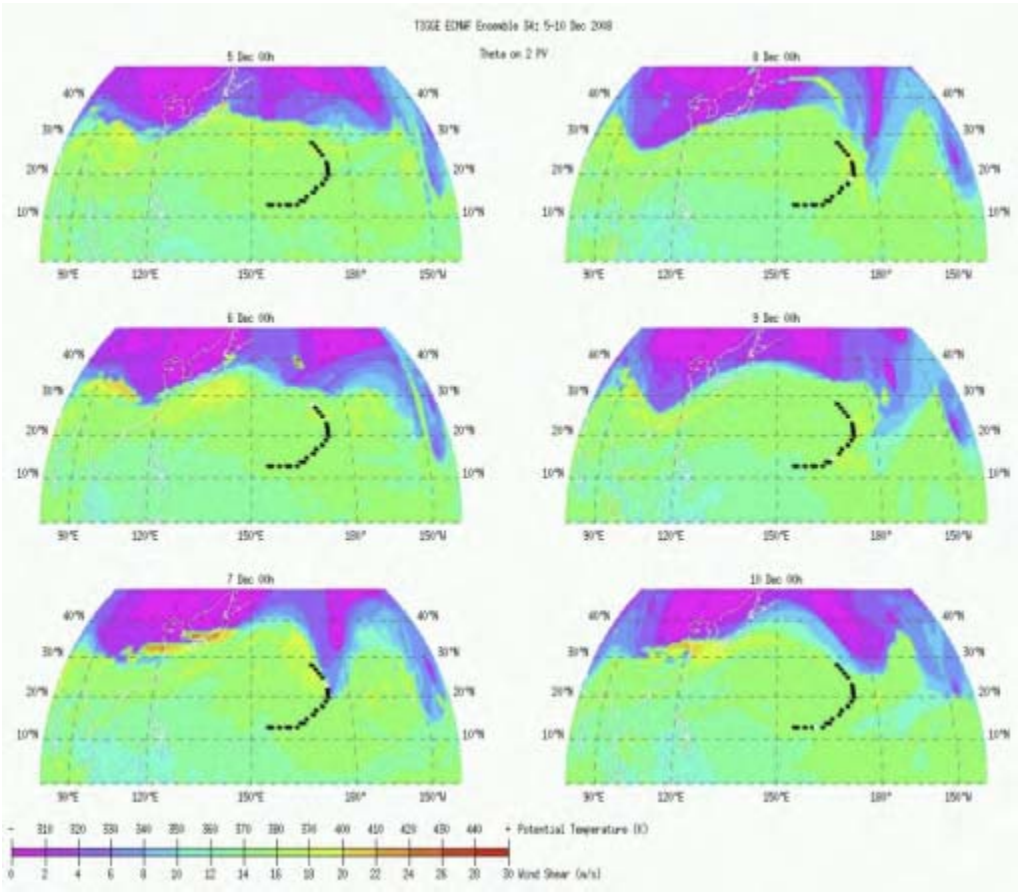

Figure 31. Ensemble member 34 (good forecast) showing the potential temperature (shaded) on the 2 PVU surface starting 0000 UTC5 December showing every 24 hours top to bottom then left to right ending 0000 UTC 10 December. Black dots show the forecast track of the Dolphin precursor. Upper-level trough is clearly to the east of the storm and continues east after the low-level vortex (white dot) develops and moves on (Figure 14 from Stehrenberger 2009).

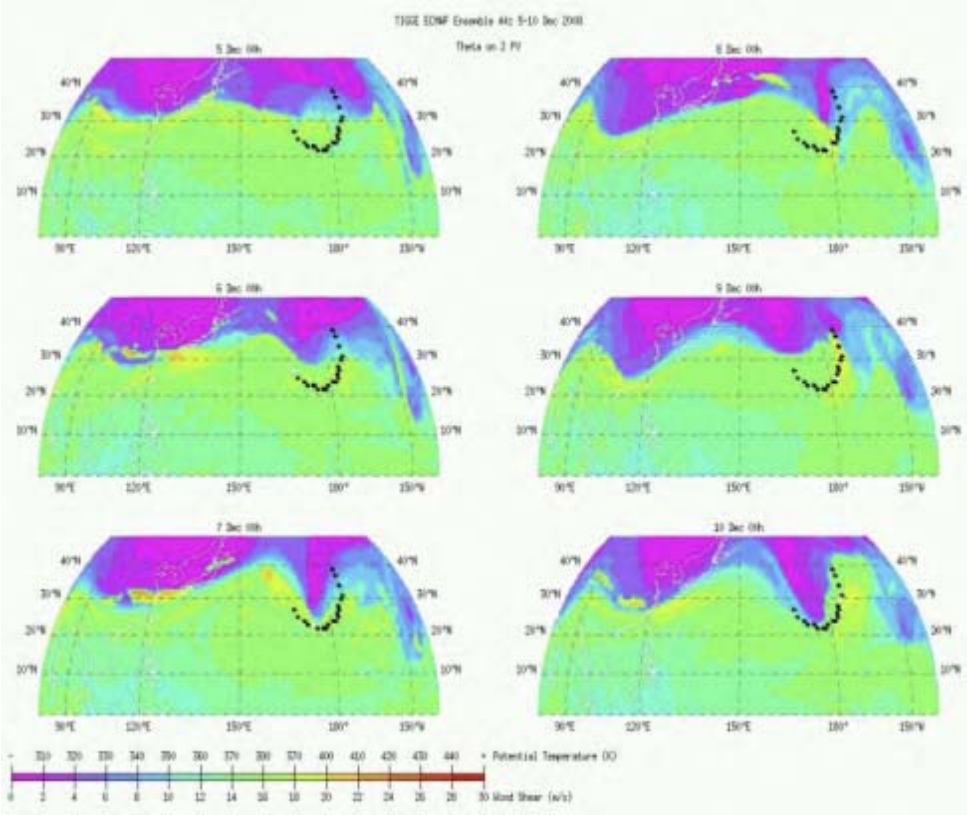

Figure 32. Ensemble member 44 (bad forecast) showing the potential temperature (shaded) on the 2 PVU surface starting 0000 UTC5 December showing every 24 hours top to bottom then left to right ending 0000 UTC 10 December. Black dots show the forecast track of the Dolphin precursor. Upper-level trough stalls to the north and west of the low-level vortex (white dot) and the resulting steering flow recurves the precursor (Figure 17 from Stehrenberger 2009)..

Stehrenberger (2009) concludes that "for two completely different evolutions, the upper-level structure and vertical wind shear investigated can make a large difference."

7. Study Hypothesis and Thesis Outline

The breaking of synoptic scale Rossby waves is a common occurrence along the extratropical waveguide (as seen in Figure 13). During such events, stratospheric intrusions into the troposphere of PV air retain only a thin connection to or completely cutoff from the stratospheric body of air. In some cases, these so-called PV streamers can

extend a significant distance equatorward, concomitantly serving as an atmospheric destabilization mechanism. It has been shown that these so-called PV streamers / cutoffs can serve as a forcing mechanism for deep convection and, in some case, as a precursor to tropical cyclogenesis (i.e., TT).

In the WNP, the most common avenue for TT appears to be of either trough-induced or weak TT categories (using the nomenclature of McTaggart-Cowen et al. 2008).In this context, it is hypothesized that TT is a two-stage process:

Stage One: The first stage involves the near-continuous forcing of deep convection by a tropopause-level PV anomaly (i.e., the PV streamer). Deep convection is a necessary ingredient for tropical cyclogenesis. It can both moisten the mid-troposphere (necessary condition 3) and generate a low-level vorticity anomaly that can serve as an incipient disturbance (necessary condition 6). However, a large-magnitude upper-level PV anomaly is associated with strong upper-level horizontal winds. Therefore, the presence of a significant PV anomaly is likely associated with significant vertical wind shear.

Stage Two: Given that large vertical wind shear is deleterious for formation of a tropical cyclone (necessary condition 4), the second stage must involve the reduction of vertical wind shear. The hypothesis is that diabatic processes associated with latent heat release in regions of deep convection serve to erode or rearrange the upper-level PV structure in such a way as to reduce the vertical wind shear and allow tropical cyclogenesis to occur.

The overarching goal of this thesis is to re-examine the relevance of the TT process in the western Pacific basin in the context of the proposed dynamical evolution. Specifically, we will test the above hypothesis in a number of frameworks.

The first involves a climatological analysis designed to ascertain the relevance of TT concepts via a subjective examination of all TC events during a seven-year time period (2002–2008). This analysis will help to elucidate the frequency in time and space

of TT events. Subsequent to a presentation of the data and methodology employed in this thesis (Chapter II), the climatological results will be presented in Chapter III.

The dynamical evolution of TCS-037 that is provided by Schönenberger (2010) and summarized in Subsection 5 provides a foundation for the subsequent examination of ensemble prediction system the data for this case (Chapter IV). It is hypothesized that the ensemble data will provided significant insight into the dynamical evolution of TCS-037 / TS16W as well as the predictability of this event. Finally, study conclusions and a discussion are presented in Chapter V.

THIS PAGE INTENTIONALLY LEFT BLANK

II. DATA AND METHODOLOGY

A. CLIMATOLOGICAL ANALYSIS

In order to subjectively investigate tropical cyclone (TC) genesis over an extended period of time in the WNP, ECMWF-Interim (ERA-Interim) data are incorporated for the 2002–2008 TC seasons. The data are reduced form their native resolution to comprise one degree resolution in both latitude and longitude and 60 vertical model levels. The data are available every six hours.

In addition to the typical meteorological fields provided by ECMWF, a number of additional, dynamically-relevant parameters are calculated. These include, but are not limited to, vorticity, potential vorticity (PV), potential temperature, relative humidity, diabatic heating, and PV generation rate. In addition two representations of the dynamic tropopause are created: i) potential temperature on the 2.0 PVU isosurface, and ii) PV on a number of potential temperature surfaces (335, 340, 345, 350 K).

For the subjective climatological analysis, the dynamical evolution that lead to TC genesis was viewed as a series of multi-panel plots for each relevant six-hour time period. An example is provided in Figure 33 for the case of Tropical Storm Vongfong at 1800 UTC 11 August 2008. The left panels represent PV on respective potential temperature surfaces (350 to 335K from top to bottom). The right panels represent deep-layer (850 to 200 hPa) vertical wind shear, 200 hPa vorticity, 850 hPa vorticity and sea level pressure. For all right panels, the 2.0 PVU PV contour on 350 to 335K are shown in black.

The general methodology that was used focuses on the formation of a coherent 850 hPa vorticity center that can be directly tied to the TC genesis. The identification of this feature is straightforward: one simply tracks the TC 850 hPa vorticity anomaly backwards in time to the point in time and space it forms (i.e., the first step when a coherent anomaly can be identified). If, at this time and place, the vorticity feature is associated with an extratropical feature (apparent in the dynamic tropopause maps), the TC genesis event is termed a tropical transition (TT) case. If no such extratropical feature

is present, the storm in question is deemed a non-TT case. In this way, we can identify cases that are associated with extratropical precursors.

Using this methodology, TS Vongfong was catalogued as a TT storm. To illustrate this point, we refer to Figure 33. The incipient 850 hPa vortex formed at approximately 22^{o}N/137^{o}W (location shown inside the black circle in Figure 33). The extratropical precursor (it terms of a breaking wave along the dynamic tropopause and its attendant PV streamer) is indicated by the black arrow (identifying the 2 PVU contour on potential temperature surfaces). The features are within approximately 200 km of each other. This number is comparable to the proximity of the PV streamer and vertical velocities (deemed to be collocated with maximum low-level vorticity) identified in a vertical cross section for the convective outbreak associated with a PV streamer examined by Funatsu and Waugh (2008) and discussed in the previous section (see Figure 34), on an outbreak of convection initiated by a PV streamer and discussed in the previous section.

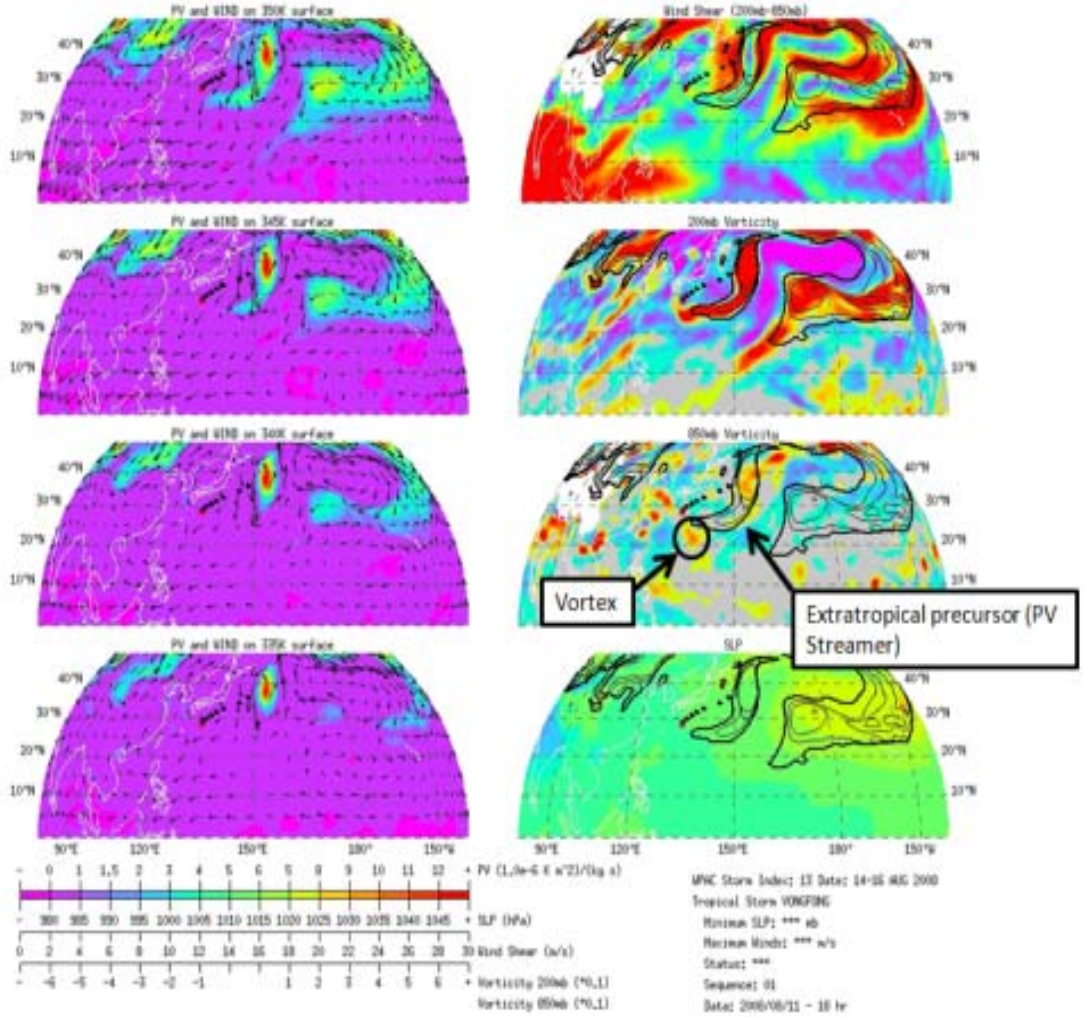

Figure 33. ERA-Interim data for the case of TS Vongfong at 1800 UTC 11 August 2008. PV (shaded, PVU) on the 350, 345, 340, 335 K potential temperature surfaces are shown in the left panels (top to bottom). Right panels presents deep vertical wind shear (200–850 hPa), 200 hPa vorticity, 850 hPa vorticity and sea level pressure (top to bottom). The 2.0 PVU PV contour on 350, 345, 340, and 335 K potential temperature surfaces are shown on right panel plots.

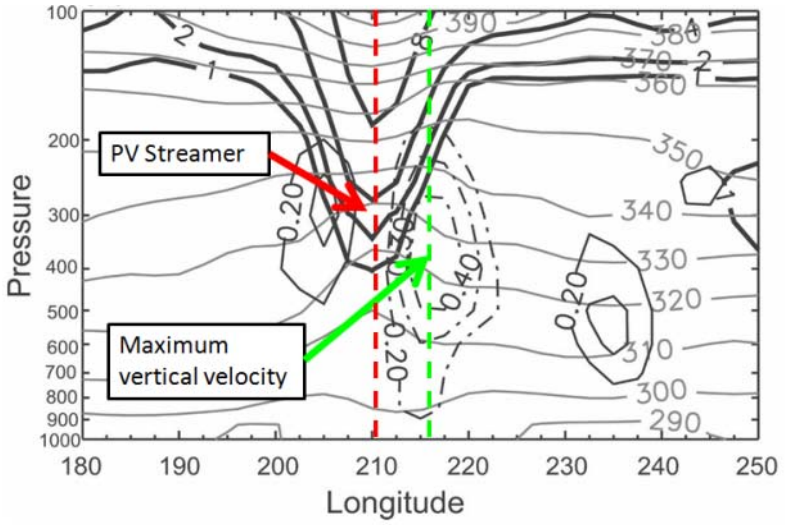

Figure 34. Vertical cross-section at 25°N through PV streamer on 15 January 1987. Thick black lines show PV (1, 2, 4 and 8 PVU) on the 200 hPa pressure surface. Thin dashed and solid line represent rising motion and sinking motion (ω in Pa s^{-1}). Gray lines show the isentropic surfaces (θ values in K) (Figure 3 from Funatsu and Waugh 2008).

In cases where the influence of the PV streamer was not clear, an examination of additional meteorological fields from ERA-interim dataset (i.e., 3D structure of the vertical velocity and potential temperature on the 2 PVU surface) was undertaken to more accurately identify the nature of the event.

B. DYNAMICAL EVOLUTION OF TS16W

The European Center for Medium-Range Weather Forecasts (ECMWF) analysis data are used to describe and investigate the dynamical evolution of Tropical Cyclone Structure Invest 37 (TCS-37). The disturbance subsequently was identified by the Joint Typhoon Warning Center (JTWC) as Tropical Storm 16W (TS 16W) at 0000 UTC September 10 2008. The spatial resolution of the data is TL799L91 equating to a total wave number of 799 (~25 km grid length) with triangular truncation providing 91 vertical levels. The temporal resolution is every six hours (0000, 0600, 1200, and 1800 UTC). Similar to the methodology for the ERA-Interim data, additional meteorological parameters are generated and dynamic tropopause maps are created.

Given the general lack of in-situ observation in the region of interest, the ECMWF analysis data is used as a 'best guess' of both the environmental conditions and the evolution of the storm system in question.

C. ENSEMBLE DATA

To examine the predictability and provide dynamical insight in to the evolution of one particular TT event (TS 16W), ensemble data are obtained from THe Observing System Research and Predictability Experiment (THORPEX) Interactive Grand Global Ensemble (TIGGE). TIGGE is a part of the World Weather Research Program (WWRP) hosting a comprehensive data base of ensemble data from a number of operational centers.

For this work, we incorporate ensemble data from ECMWF. The ensemble prediction system is comprised of one control member and 50 perturbed members. The resolution of the ECMWF ensemble system (used generating the control member analysis) is TL799L91 (a spectral model with a total wave number of 799) equating roughly to a 25 km grid at the equator with 91 vertical levels (TIGGE 2012).

ECMWF TIGGE data are available in four separate files: pressure level data (1000, 925, 850, 700, 500, 350, 250, 200, and 50 hPa), potential vorticity on the 320 K potential temperature surface, potential temperature on the 2.0 PVU PV surface, and single level data. For this study, we focused on the evolution of the 925 hPa vorticity, potential temperature on the 2.0 PVU PV surface and six-hourly accumulated precipitation to represent the TC vortex, structure of the dynamic tropopause, and diabatic processes, respectively. Deep layer vertical wind shear (200 to 850 hPa) data were also generated and examined.

The data are obtained for a number of initialization times: 0000 UTC 4 through 8 September 2008. All ensemble data were examined at six-hour intervals for the initialization time to 0000 UTC 11 September 2008 (the time JTWC downgraded TS 16W to a tropical disturbance.

In order to examine the evolution of environmental parameters relevant to the TT genesis process for the large number of ensemble forecasts, it is necessary to devise an objective method to track the path of the TCS-037 / TS 16W storm system. Schöenenberger (2010) constructed a subjective best track of the storm system by examining the 850 hPa flow field and identifying the center of cyclonic circulation at each six-hour time step. Such an approach is impractical here due to the investigation of four initialization times and the large number of ensemble members (51). This would require 204 subjective best tracks.

An objective "best track" methodology was therefore devised, focusing on the low-level (925 hPa) relative vorticity field in the ECMWF analysis data. The first step was to ascertain the time and location of the emergence of the low-level vortex that subsequently became TS 16W. The exact location was deemed to coincide with the 925 hPa vorticity maximum at 1200 UTC 8 September. It was located approximately 27^{o}N and 152^{o}E (Figure 35). The next step was to determine the track going forward at each six-hour time step. This was accomplished by establishing the 925 hPa vorticity maximum at the subsequent time step (six hours later), by searching within a circle of 150 km radius centered on the previous position. A schematic representation for generating the ensemble member tracks is presented in Figure 35. This procedure is used not only to identify the "best track" in the ECMWF analysis data, but also for each ensemble member. In this way, we establish the track of a coherent low-level vortex (if one exists) for all ensemble forecasts.

In addition to tracking the low-level coherent vortex at 925 hPa, the deep-layer vertical wind shear was also catalogued. Once the center was established at the 925 hPa level for a particular time step, the average deep-layer (200 to 850 hPa) vertical wind shear within the circle of 150 km radius is calculated.

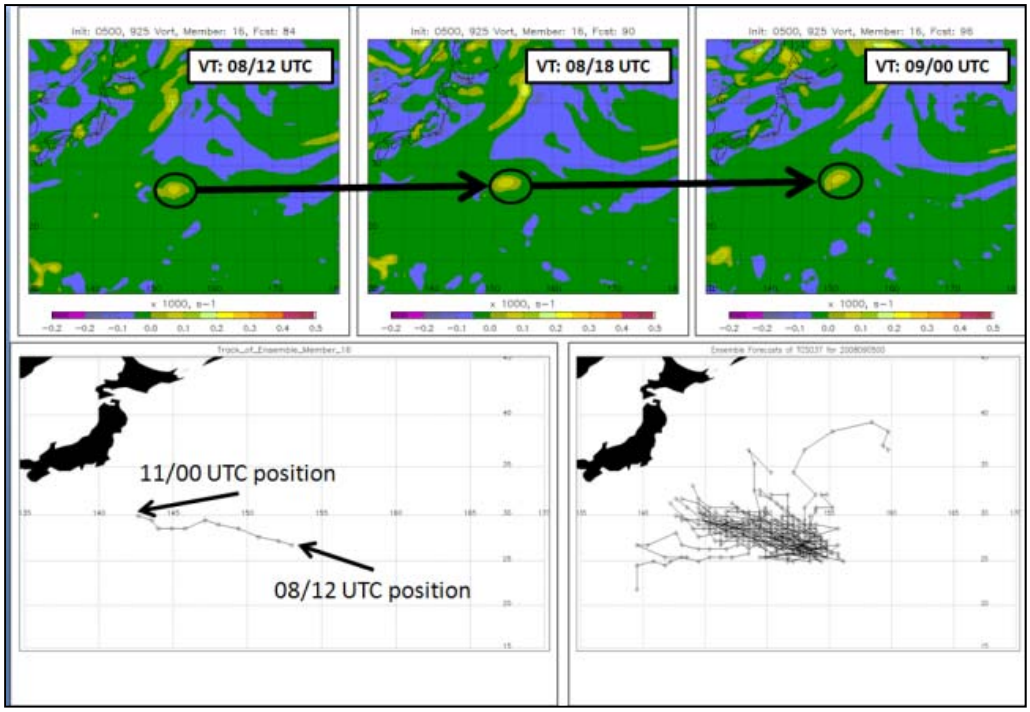

Figure 35. Schematic representation of tracking code used to generate plots of the 51 ensemble member storm tracks. Upper three images are 925 hPa relatively vorticity fields from the ECMWF ensemble member 16 for 1200 UTC 8 September (upper left), 1800 UTC 8 September (upper middle) and 0000 UTC 9 September (upper right). Bottom left shows the plotted locations for the vorticity maxima for ensemble member 16 beginning 1200 UTC 8 September and terminating at 0000 UTC 11 September. Bottom right shows tracks for all 51 ensemble members.

THIS PAGE INTENTIONALLY LEFT BLANK

III. CLIMATOLOGY

This section presents the results of a subjective classification of all tropical cyclogenesis events that occurred in the WNP during the years 2002–2008. Via the methodology outlined in Chapter II and briefly discussed below, each storm is classified as either a TT or non-TT case. For the former, an upper-level PV anomaly of extratropical origin is deemed to play an important role in the dynamical evolution leading to tropical cyclogenesis. In contrast, non-TT storms exhibit no extratropical forcing. Such an approach allows one to catalog the frequency and location of TT events during this seven-year time period. In this way, we can both investigate the relevance of the TT paradigm in the WNP (in terms of how often and where these events occur) and, furthermore, glean important dynamical insight into TT dynamics.

As described in Chapter II, the time of primary interest for the subjective classification of TC events is centered on the formation of a coherent 850 hPa vorticity feature. The time and location of the formation of this feature is determined by tracking the well-defined 850 hPa vorticity center associated with the TC backward in time to the point when it is no longer evident. During this formation time period, a number of relevant model fields are examined to subjectively determine if the formation of the 850 hPa vorticity feature is associated with an extratropical precursor. Model fields examined in addition to the 850 hPa vorticity include PV on potential temperature surfaces from 335–350 K, deep layer (850–200 hPa) vertical wind shear, 200 hPa vorticity and sea-level pressure. If it is determined that the generation of the 850 hPa vorticity is associated with a feature of extratropical origin, the event is deemed to be a TT. Conversely, the lack of a precursor of extratropical origin indicates a non-TT case.

In terms of defining the presence of lack of an extratropical precursor, the primary field used is PV on potential temperature surfaces. In a dynamical sense, what is being identified is the presence or lack of a tropopause-level PV anomaly. It has been shown that a tropopause-level PV anomaly can induce tropical deep convection. The co-location

of a PV anomaly and an emerging 850 hPa vorticity center is therefore taken as a direct indication that convective processes associated with the PV anomaly are responsible for the low-level generation of vorticity.

To put this approach in the context of the objective analysis of Atlantic storms conducted by McTaggart-Cowen et. al. (2008), we are essentially equating TT storms as those that have significant Q-vector convergence (Figure 5). In their classification system, these would be so-called "trough induced," "strong TT" or "weak TT" cases, depending on the amplitude of the thickness asymmetry metric. In contrast, non-TT cases would be of the "non-baroclinic" or "low-level baroclinic" variety (given the relative lack of upper-level forcing). In general, low-level baroclinicity is quite weak in the region of interest (in contrast to the western North Atlantic). Therefore, in practical terms, we are most likely describing either trough-induced or weak TT cases for our "TT storms." Using similar logic, the vast majority of our "non-TT storms" are likely of the non-baroclinic variety.

A. EXAMPLE CASES

To more specifically illustrate the methodology, two cases are presented in detail below. The first represents a case that was identified as a TT event, while the latter was deemed a non-TT case. Results of the subjective climatology are shown in Appendix A.

1. TT Case

Typhoon Shanshan formed in the western North Pacific in mid-September of 2006 shown in Figure 36. Shanshan reached a maximum wind speed of 120 kts with gusts to 145 kts (category 4 on Saffir-Simpson scale) and a minimum central pressure of 919 hPa sustaining typhoon status for eight days. Shanshan's main forecast challenge appeared to be the track (best track presented in Figure 37) as it neared populated areas like Taiwan, Japan and South Korea. Shanshan eventually passed over southwestern Japan as a weaker typhoon (category 1) but still resulted in 200 injuries and 11 deaths. A

tornado was even reported to have occurred in Nobeoka, Miyazaki, Japan as a result of land falling Shanshan (Wikipedia, The Free Encyclopedia 2012).

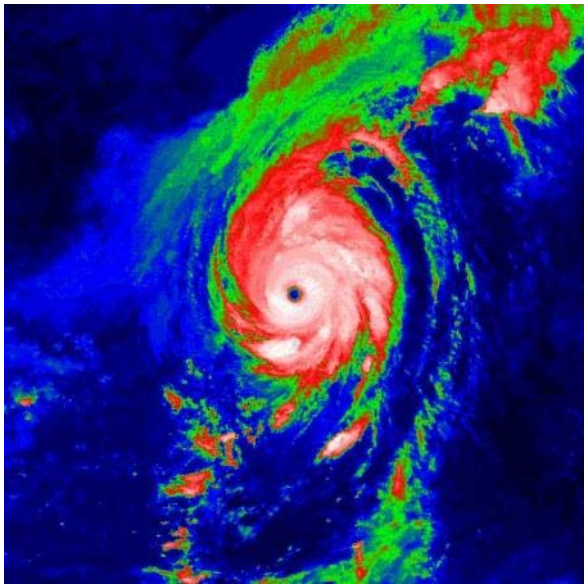

Figure 36. METSAT infrared imagery of Typhoon Shanshan at 0300 UTC 16 September 2008 (image retrieved from Digital Typhoon 2012).

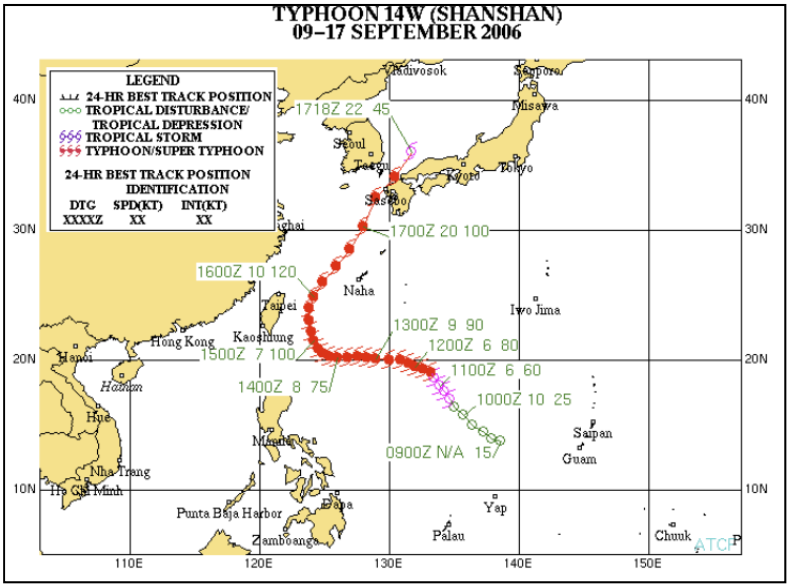

Figure 37. JTWC best track for Typhoon Shanshan from the 2006 Annual Tropical Cyclone Report. Storm's position is shown as green circles (tropical disturbance), pink tropical storm symbols (tropical storm) and red typhoon symbols (typhoon).

Figure 38 shows when Shanshan is easily identifiable via the 850 hPa vorticity as a coherent vortex centered approximately 17.5°N, 134.5°E at 1800 UTC 10 September 2008. Shanshan was classified a TS prior to this time with 40 kt winds and a central pressure of 994 hPa according to JTWC best track data. Tracing this vorticity center backwards in time to the point at which it first emerges (at approximately 18 UTC September), allows us to examine the formation mechanism of this feature. At this crucial evolutionary juncture, a distinct PV streamer (as evidenced by the 2 PVU PV contour on the 335–50 K potential temperature surfaces in Figure39) is observed at approximately 20°N, 148°E to the north and east of the broad region of vorticity that would subsequently become Typhoon Shanshan.

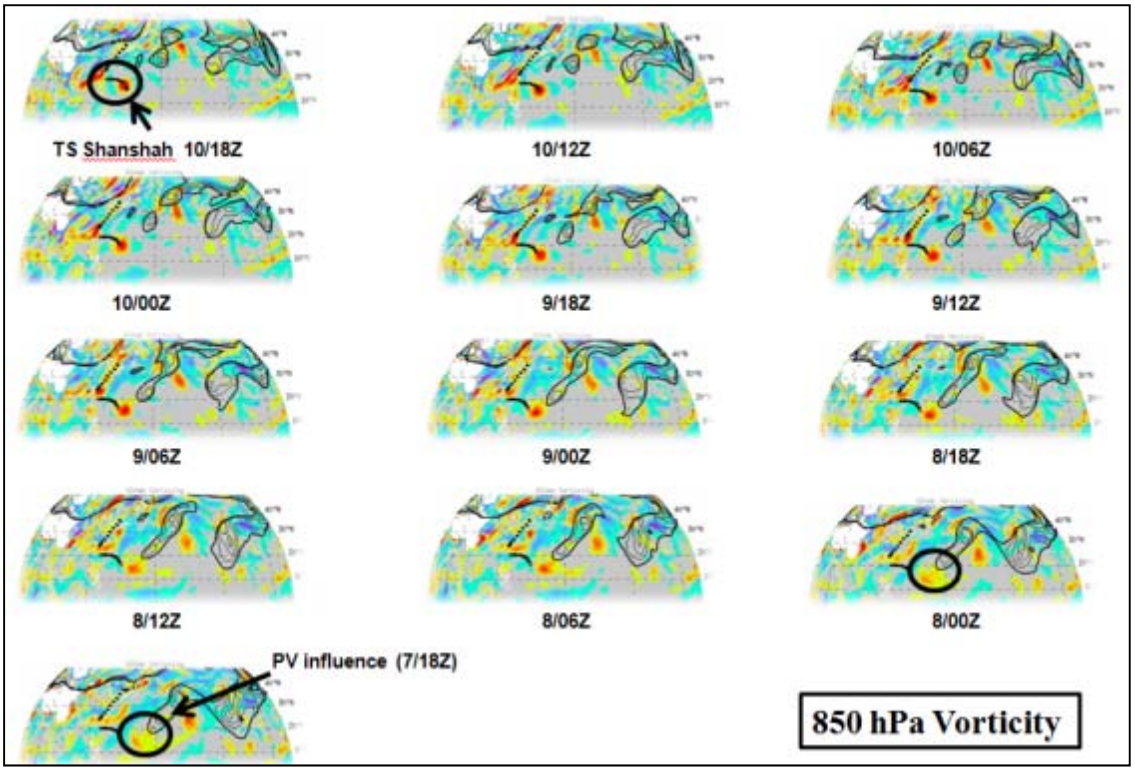

Figure 38. 850 hPa relative vorticity tracing then TS Shanshan backwards in time (from left to right and top to bottom) from 1800 UTC 10 September to 1800 UTC 7 September 2008 where there is clearly some influence from a PV streamer (thin black lines).

To examine the formation of the PV streamer in question and properly identify it as a feature of extratropical origin, PV and wind vector data on the 345 K potential temperature surface are presented in Figure 39. High values of PV, representing stratospheric air, are observed extend as far south as 15°N in the vicinity of the dateline in early September with a persistent upper-level ridge centered on 150°E. The ridge takes on a more positive tilt as Typhoon Ioke passes to the south and west of the ridge. The upper-level trough becomes positively tilted as a shortwave trough moves over the ridge. The broad region of PV eventually becomes elongated and cutoffs from a broad PV trough that continues moving east past the dateline. This PV streamer is shown clearly in Figure 39 at 1800 UTC 7 September and it is this feature that initiates the deep convection responsible for the formation of low-level vorticity.

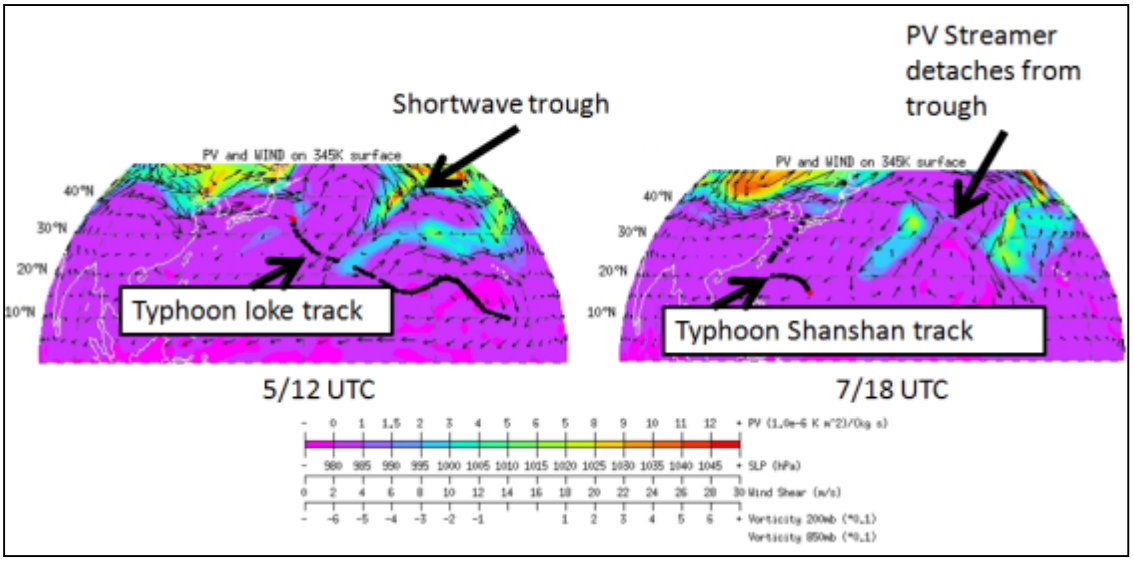

Figure 39. PV (PVU) and wind vectors on the 345 K potential temperature surface for 1200 UTC 5 September and 1800 UTC 7 September illustrating the evolution of the PV streamer as a shortwave trough moves into the base of the stationary trough and eventually the PV streamer detaches from the main PV anomaly.

2. Non-TT Case

Tropical Storm Noul was a purely tropical TC genesis event (nonbaroclinic according to the terminology of McTaggart-Cowen et. al. 2008) with minimal upper-level forcing and minimal low-level baroclinicity. The best track data from JTWC is presented in Figure 40. Noul was first classified by JTWC as a *Poor* area 0600 UTC 13 November 2008, then *Fair* at 1400 UTC on the same day. JTWC issued its first Tropical Cyclone Formation Alert (TCFA) at 2030 UTC on 15 November before issuing the first warning (classifying it as a tropical disturbance) at 0000 UTC 17 November. TS Noul made landfall near Nha Trang, Vietnam approximately 0600 UTC 17 November 2008. The storm quickly lost strength as it encountered high terrain on its trip inland. Copious amounts of precipitation associated with the land-falling tropical storm caused landslides and widespread flooding resulting in 21 deaths (Wikipedia, The Free Encyclopedia 2012).

The 850 hPa vorticity and 2 PVU PV evolution are shown in Figure 41. It is quite clear that there is no interaction between an extratropical feature (a PV streamer) in this case.

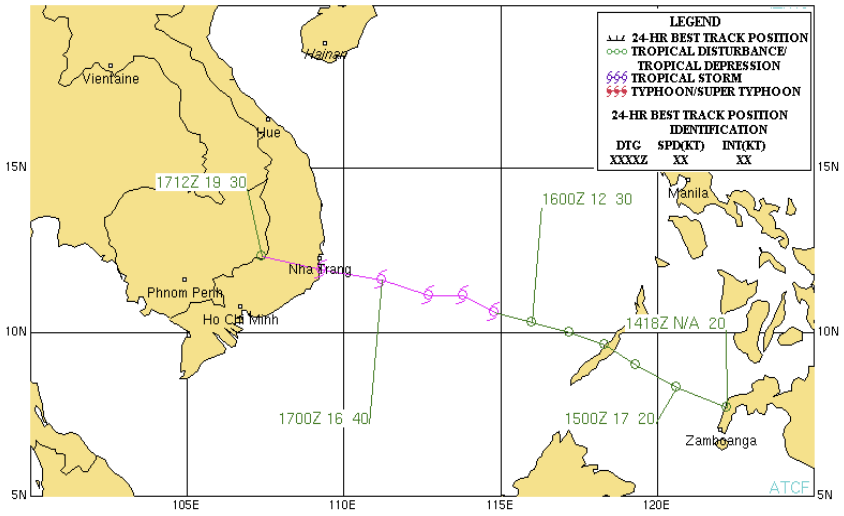

Figure 40. JTWC best track for TS Noul from the 2008 Annual Tropical Cyclone Report. Storm's position is shown as green circles (tropical disturbance), pink tropical storm symbols (tropical storm) and red typhoon symbols (typhoon).

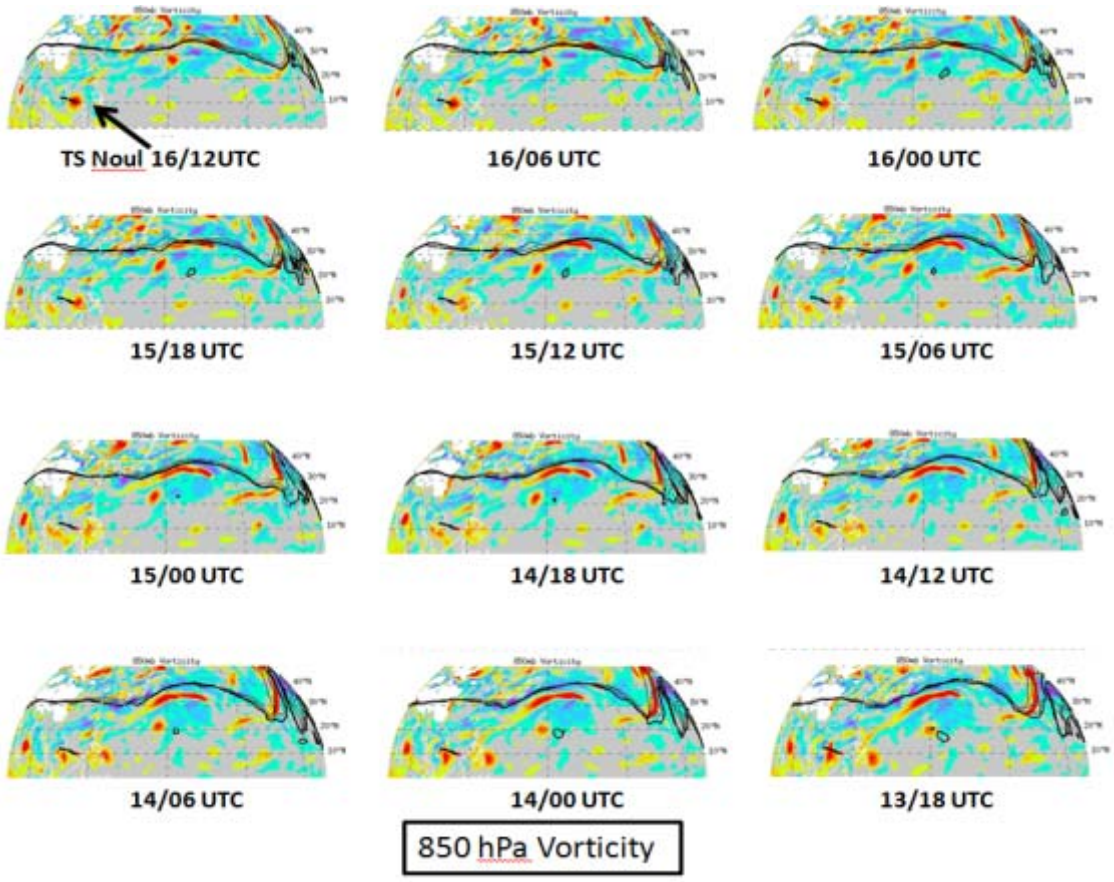

Figure 41. Similar to Figure 39 showing the relative vorticity tracing the vorticity maximum deemed the position of TS Noul at 1200 UTC 12 September 2008 backwards in time (left to right then top to bottom). Note the low level vortex is never in the vicinity of the dynamic tropopause (thin black line showing 1 PVU on 345 K potential temperature surface).

B. CLIMATOLOGY RESULTS

Figure 42 shows the total number of TT cases for each year (blue) in addition to the total number of tropical cyclones for the year in question (red) to illustrate the relative frequency of TT events. The relative frequency of TT events in presented in Table 1. The total number of TT cases from 2002–2008 was 27 out of 195 storms (13.8%) This indicates that TT events are relatively rare, but are also non-negligible in terms of tropical cyclogenesis in the WNP. Figure 42 also illustrates there can be a large interannual variability. This is most apparent when looking at the 2008 TC season in comparison to

the rest of the study time period. In 2008, TT cases represent 33% of all events. This is contrast to the relatively consistent average of approximately 11% from 2002–2007. In addition, while not shown herein, it has been suggested that the 2009 season also exhibited a relatively high frequency of TT events (personal communication, P. Harr).

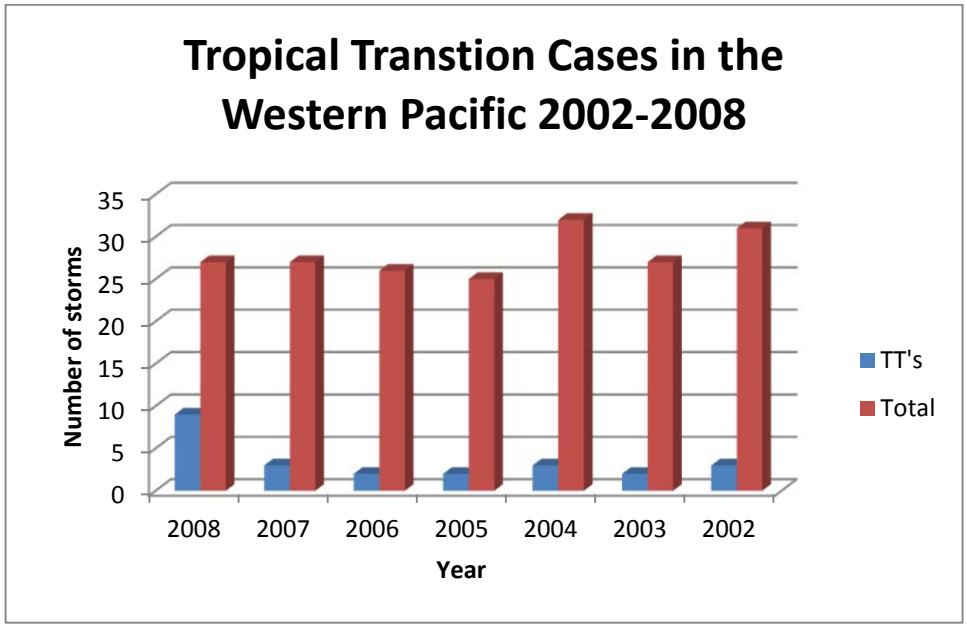

Figure 42. Subjective climatology of TT case in the western North Pacific from 2002–2008. Blue bar indicates the number of TT cases for the respective year and the red bar indicates the total number of TCs for the respective year.

Year	**Percentage of all TC's classified as TT**
2008	33
2007	11
2006	8
2005	12
2004	9
2003	15
2002	10

Table 1. Frequency of TT events as a percentage of total TC events for the western North Pacific 2002–2008.

The data was further broken down by month to ascertain the seasonal frequency of TT cases (Figure 43). There is a noticeable lack of TT cases in the early half of the year most likely due to the lack of large scale environmental factors necessary for TC genesis (high SSTs). There is a peak in the late summer and early fall months (July through September) which seems to make sense with warm SSTs persisting along with the presence of breaking waves along the extratropical waveguide, suggesting that there may a "sweet-spot" for the occurrence of TT events. The monthly climatology still shows a relatively small number of TT events persisting until the end of the year (October through December).

For comparison, the monthly data for non-TT events are presented in Figure 44. Non-TT events also exhibit a frequency maximum in the late summer / early fall. This peak coincides with the time period when local conditions are climatologically most conducive for tropical cyclogenesis. In contrast to the absence of TT cases in the first half of the year (January through June), non-TT events are present throughout this time period (with a significant amount in the months of May and June). This distinct difference is almost assuredly the result of TT cases requiring both a conducive local environment, *and* the presence of a breaking wave. During this time of year, there is a relative lack of breaking waves in this region. Hence, while the overall synoptic environment might be conducive to non-baroclinic development, it is not well suited to the process of TT.

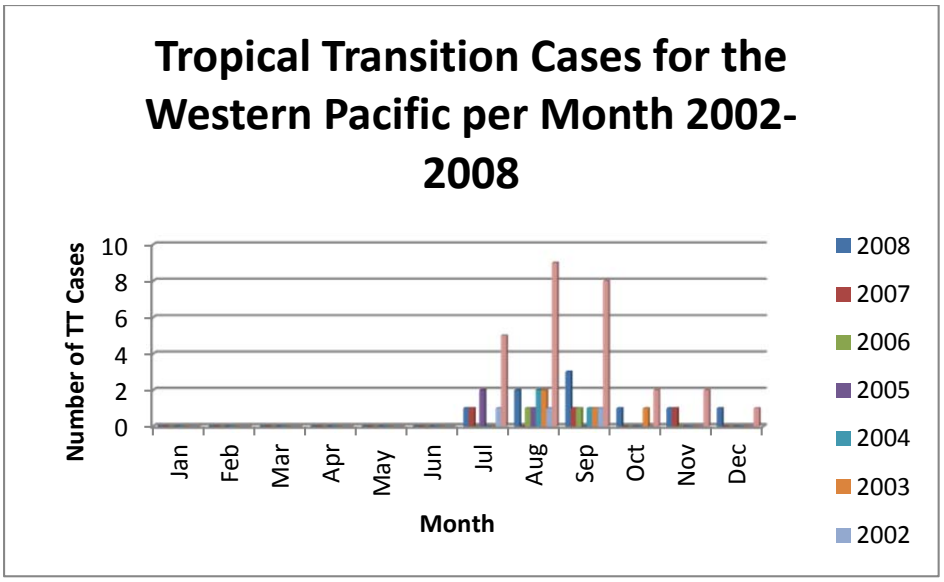

Figure 43. Subjective climatology of TT case in the western North Pacific broken down into months. Number of TT cases per month plotted for the years 2002–2008.Total is the total number of storms for the respective month for the 2002–2008 period.

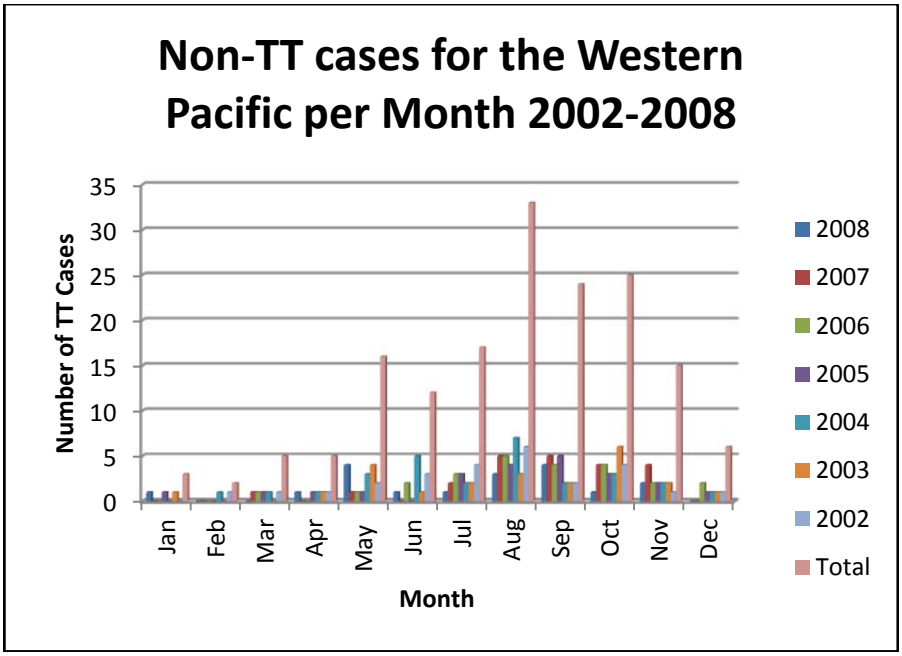

Figure 44. Subjective climatology of non-TT case in the western North Pacific broken down into months plotted for the years 2002–2008. Total is the total number of storms for the respective month for the 2002–2008 period.

Figure 45 shows the position of the subjectively classified TT cases in the WNP in relation to all TC events (right panel) and the seasonal distribution of TT events (left panel). Although no distinct seasonal distribution is readily apparent a few conclusions can be drawn about the general location of TT events as compared to all TC events. They tend to occur farther north between roughly 15^{o}N and 35^{o}N. Given the limited climatology for the WNP presented here, it is difficult to conclude that TT event tend to form closer to land masses as Davis and Bosart (2004) mentioned with a large number of TT events occurring in the middle of the WNP basin. The frequency of extratropical wave breaking events coupled with warm SSTs appear to be the driving factors in where TT events occur.

It is found, however, somewhat consistent with the result of Davis and Bosart (2004), it appears that TT storms are both relatively weak (rarely exceed Category 2 strength) and short-lived. One of the outliers in Figure 46, was Typhoon Dolphin (summarized in Chapter I). The incipient low-level vorticity feature that becomes Dolphin was associated with an occluded extratropical cyclone (a strong TT case in the terminology of McTaggart-Cowen et. al. 2008). It becomes a major typhoon.

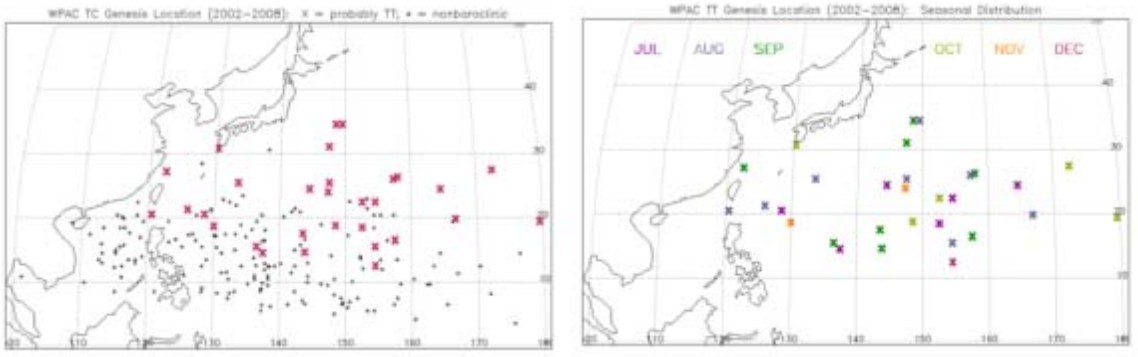

Figure 45. Left image shows the locations of all subjectively classified TT events (red X) and non-TT event (black asterisk) for the WNP from 2002–2008. Right image shows a color-coded seasonal distribution of the subjectively classified TT events.

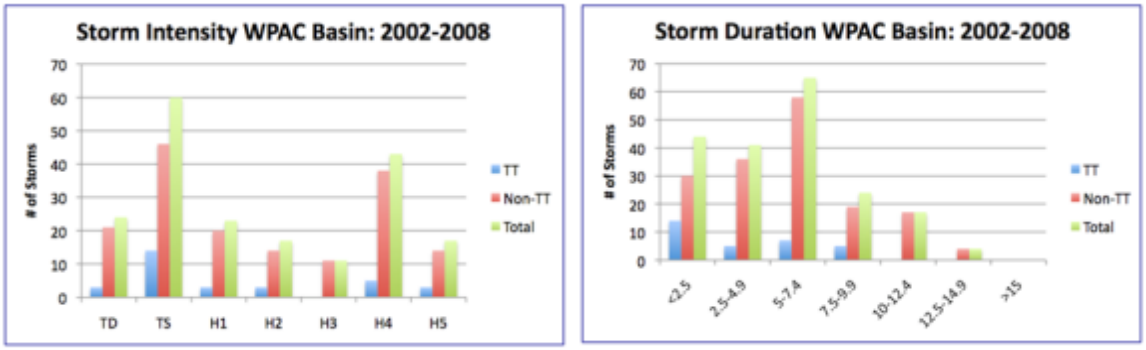

Figure 46. Right image shows a bar graph showing the number of storms on the x-axis storm intensity on the y-axis (Saffir-Simpson scale) for TT events (blue), Non-TT events (red) and both TT and non-TT events (green). Using the same color scheme as the right image, the left image depicts a bar graph of the number of storms on the x-axis and storm duration in days on the y-axis.

IV. PROBABILISTIC FORECASTS

The goals of this section are to evaluate the predictability of TCS-037 and to investigate the two-stage hypothesis via an examination of ensemble prediction data. As stated in Chapter I, given the general lack of in-situ measurements in the WNP (likely resulting in significant initial condition uncertainty) and the primacy of diabatic processes inherent in the hypothesized two-stage evolution of TT events, the use of probabilistic forecasting techniques is advisable (as opposed to relying on a single deterministic forecast that provides no measure of forecast uncertainty).

The goal of an ensemble prediction is not only to provide a best guess of the possible outcome, but also to provide a measure of uncertainty as to the best guess. As such, the utilization of ensemble prediction data can serve a number of purposes when examining a particular TT event. The first of which is to provide an estimation of the predictability of the event. If a suite of ensemble members predominately capture the dynamical evolution of the storm in question with little spread, the event is likely quite predictable. In contrast, if a number of different evolutionary pathways are identified, this implies significant forecast uncertainty.

Given the latter situation, a second purpose that can be served is insight into the dynamical processes that are at work. By examining in detail evolutionary pathways that are different than observed, one can attempt to identify the environmental inconsistencies responsible. In this way, it is possible to glean information regarding the important dynamical processes at work.

For the case of TCS-037 / TS 16W, we hereby examine ensemble prediction data from the ECMWF to investigate these issues. Data are acquired for a number of initializations times (to ascertain the importance of forecast lead time) for the 4 through 7 September 2008. All initialization times are for 0000 UTC.

A. PREDICTIBILITY

1. Ensemble Forecast (0000 UTC 7 September 2008)

The ensemble members initialized 0000 UTC 7 September all appeared to produce a coherent vortex at low-levels with the only noticeable issue being differing tracks. Figure 47 shows the tracks of the 51 ensemble members (left panel) compared to the automated best track (described in detail in Section II) from the ECMWF analysis (right panel). All members indentify a coherent vortex that, once formed, moved to the west-northwest towards Japan. With the exception of one member, none recurve during this time period. This is the case with the automated best track (right panel of Figure 47).

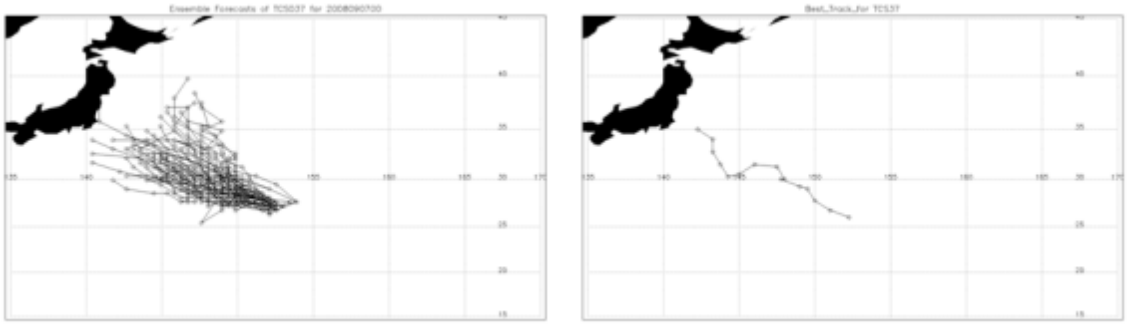

Figure 47. Storm tracks for each of the 51 ensemble members initialized on 0000 UTC on 7 September 2008 (left panel) starting on 1200 UTC 8 September 2008 marking the storm position every six hours (black circle) until 0000 UTC 11 September. Best track based on the ECMWF analysis data (right panel) withstorm position (black circle) every six hours from 0600 UTC 8 September until 0000 UTC 11 September.

2. Ensemble Forecast (0000 UTC 6 September 2008)

Ensemble forecasts initialized 0000 UTC 6 September also produced coherent vortices at 925 hPa. Figure 48 compares the ensemble members forecast track (left panel) compared to the automated best track (right panel) similar to Figure 48. The forecast tracks appear to lag the actual path outlined by the automated best track, and therefore, remain farther offshore than the automated best track (right panel). There are also a

higher fraction of ensemble members that recurve (approximately four members) within this time period, in comparison to the 0000 UTC 7 September initialization time.

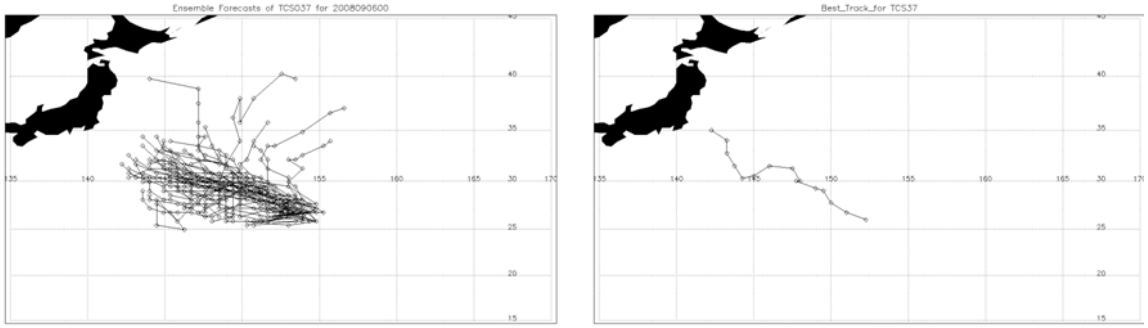

Figure 48. Storm tracks for each of the 51 ensemble members initialized on 0000 UTC 6 September 2008 (left panel) starting on 1200 UTC 8 September 2008 marking the storm position every six hours (black circle) until 0000 UTC 11 September. Best track based on the ECMWF analysis data (right panel) withstorm position (black circle) every six hours from 0600 UTC 8 September until 0000 UTC 11 September.

Figures 49 and 50 show the maximum 925 hPa vorticity and deep vertical wind shear (200–850 hPa), respectively, for the ensemble members with the black line indicating the ensemble mean and the thick green line representing the calculated maximum vorticity based on the automated tracking data for the ECMWF analysis data. The maximum 925 hPa vorticity ensemble mean shows a steady increase, while the ECMWF analysis indicates some fluctuation from 90 hours to 114 hours. Deep vertical wind shear is greater in the ensemble mean than the ECMWF analysis data, especially in the latter half of the forecast, with differences as great as 6 m s^{-1}. Although it might appear trivial, the ensemble mean value near 13 m s^{-1} put the forecast close to an unfavorable environment for tropical cyclogenesis whereas the ECMWF value of 7 m s^{-1} is more conducive for tropical cyclogenesis. Members with higher vertical wind shear typically exhibited lower vorticity values as illustrated with ensemble member 4 (Figure 51).

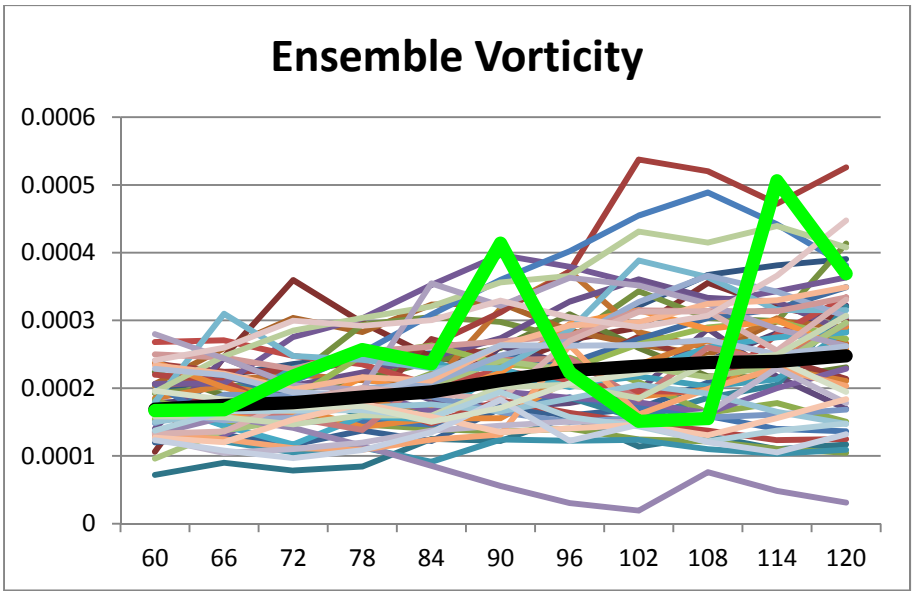

Figure 49. 925 hPa maximum vorticity (s^{-1}) for TCS037 from 1200 UTC 8 September to 0000 UTC 11 September for 51 ensemble members. Thick black line shows the ensemble mean and the thick green line shows the calculated maximum vorticity based on the automated tracking from the ECMWF analysis data.

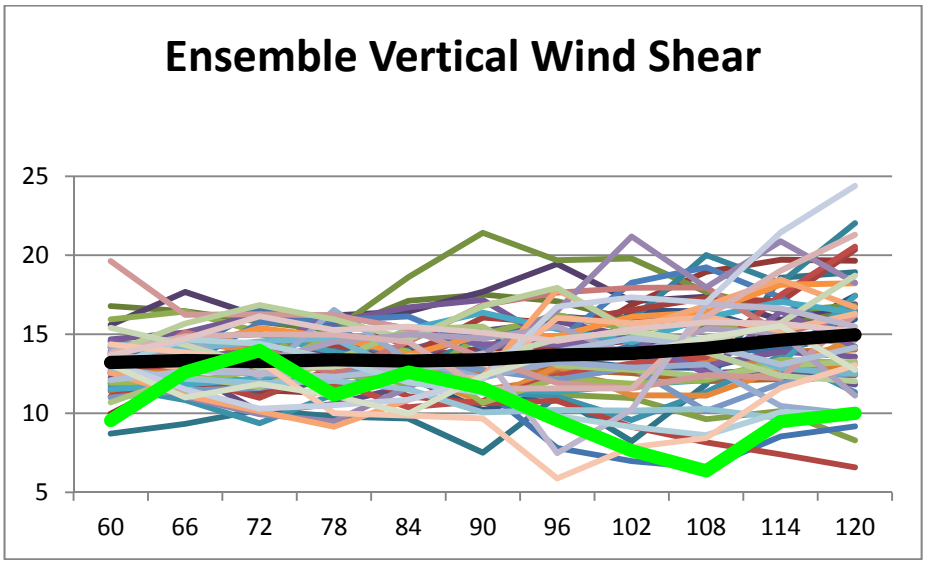

Figure 50. Averagedeep vertical wind shear (200 hPa – 850 hPa) for 150 km radius circle around TCS-037 storm center (deemed collocated with maximum vorticity location). Thick black line shows the ensemble mean and the thick green line shows the calculated deep vertical wind shear based on the automated tracking from the ECMWF analysis data.

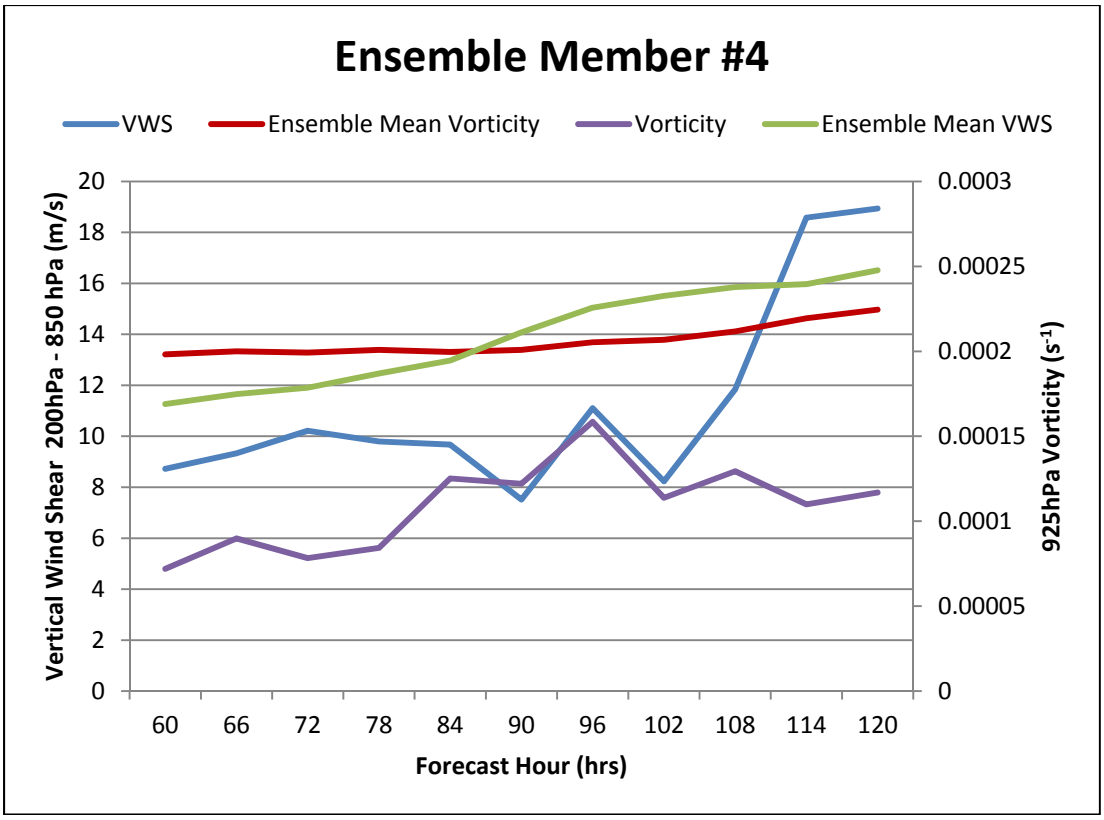

Figure 51. Ensemble Member 4 (initialized 0000 UTC 6 September 2008) maximum vorticity (purple) and ensemble mean vorticity (red) compared to vertical wind shear (blue) and ensemble vertical wind shear (green). 925 hPa vorticity values on the right y-axis and deep vertical wind shear values (200–850 hPa) values on the left y-axis. Forecast time is on the x-axis.

3. Ensemble Forecast (0000 UTC 5 September 2008)

Ensemble forecast initialized on 0000 UTC 5 September showed more variability with respect to storms track and vortex strength at the 925 hPa level. All ensemble members still produced a coherent low-level vortex. A few members started showing a propensity for early recurvature.

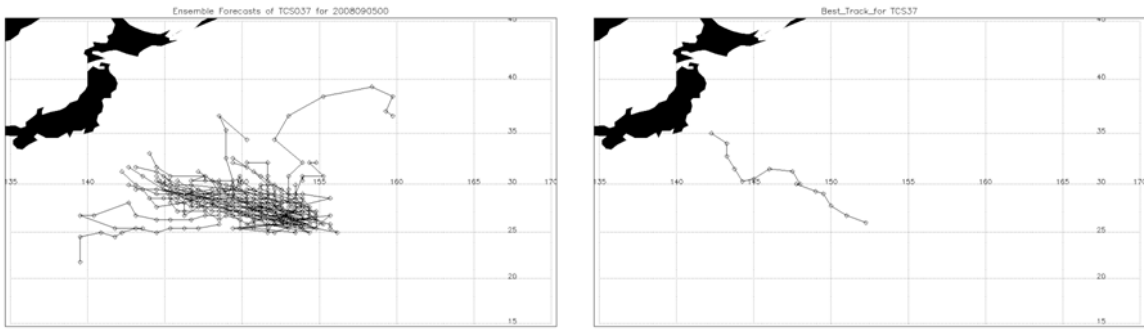

Figure 52. Storm tracks for each of the 51 ensemble members initialized 0000 UTC 5 September 2008 (left panel) starting 1200 UTC 8 September 2008 marking the storm position every six hours (black circle) until 0000 UTC 11 September. Best track based on the ECMWF analysis data (right panel) with storm position (black circle) every six hours from 0600UTC on 8 September until 0000 UTC 11 September.

Figures 53 and 54 show maximum 925 hPa vorticity and deep vertical wind shear (200 – 850 hPa), respectively, for the ensemble members with the black line indicating the ensemble mean and the green line showing the observed vorticity and wind shear calculated from the automated best track method from the ECMWF analysis data. Similar to the 6 September maximum vorticity, 5 September shows a gradual increase missing the observed fluctuation. However, the deep vertical wind shear is slightly different with the ensemble mean being lower than the ECMWF analysis by 2 to 3 m s^{-1} for the first half of the forecast before returning to being greater than the ECMWF analysis values. Both 925 hPa maximum vorticity and deep vertical wind shear show greater variability earlier in the forecast period than the ensemble member that initialized on 6 September. Several members exhibit weak vorticity values, but still show a coherent vortex on the 925 hPa level. The only exception is the case of ensemble member 1, which did not produce a coherent vortex [likely due to moderate values of vertical wind shear above the system (approximately 10–12 m s^{-1})].

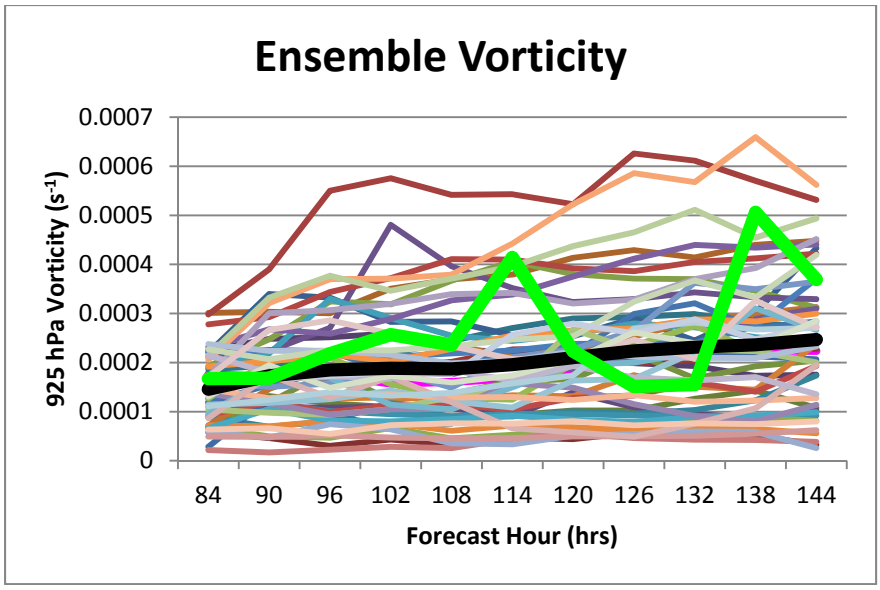

Figure 53. 925 hPa maximum vorticity (s^{-1}) for TCS-037 from 1200 UTC 8 September to 0000 UTC 11 September for 51 ensemble members initialized at 0000 UTC 5 September 2008. Thick black line shows the ensemble mean and the thick green line shows the calculated maximum vorticity based on the automated tracking from the ECMWF analysis data.

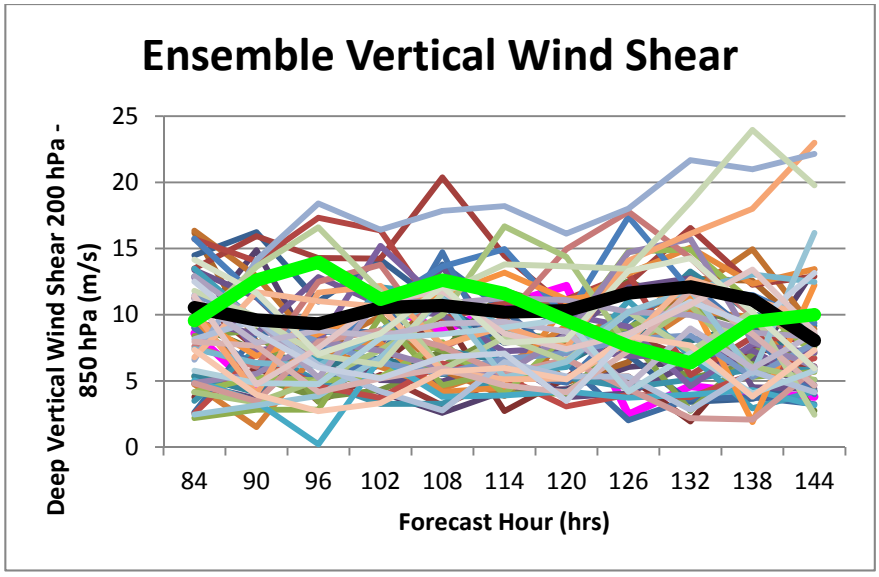

Figure 54. Averagedeep vertical wind shear (200 hPa – 850 hPa) for 150 km radius circle around TCS-037 storm center (deemed collocated with maximum vorticity location). Thick black line shows the ensemble mean and the thick green line shows the calculated deep vertical wind shear based on the automated tracking from the ECMWF analysis data.

4. Ensemble Forecast (0000 UTC 4 September)

The ensemble forecast initialized 0000 UTC 4 September showed the greatest variability as one would expect. The ensemble system at this time predicts significantly large track variability (in terms of storms that recurved and storms that did not recurve when compared to the previous three ensemble initializations). In addition, the ensemble system includes members that fail to generate a coherent low-level vortex, as well as vorticity centers that tracks due west with very little northward progression (in contrast to the observed). This variation suggests the ensemble system at this time may be identifying distinctly different dynamical evolutions that, we can hypothesize, are a result of synoptic scale environmental anomalies from the observations. Figure 55 shows the tracks of the 51 members.

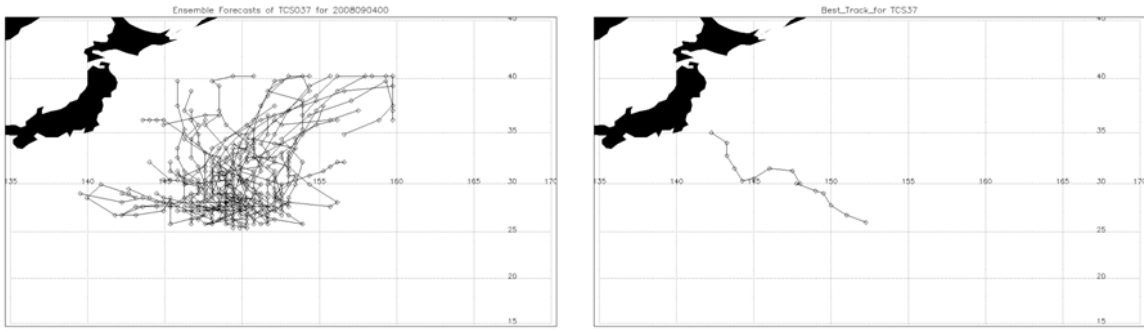

Figure 55. Storm tracks for each of the 51 ensemble members initialized 0000 UTC 4 September 2008 (left panel) starting on 1200 UTC 8 September 2008 marking the storm position every six hours (black circle) until 0000 UTC 11 September. Best track based on the ECMWF analysis data (right panel) with storm position (black circle) every six hours from 0600 UTC on 8 September until 0000 UTC 11 September.

B. DYNAMICAL EVOLUTION OF TS 16W AS VIEWED IN ENSEMBLE DATA

It is evident from an examination of the ensemble forecasts initialized at 0000 UTC 4 September that there are a number of different evolutionary pathways predicted by the forecast system. In this subsection, we hope to take advantage of this fact to

identify the important dynamical processes that lead to the observed evolution of TCS-037 / TS 16W. We will do so in a manner that directly addresses the two-stage evolutionary hypothesis.

To accomplish this analysis, it is first necessary to subjectively identify the different evolutionary pathways represented in the ensemble data. This is done via an examination of 925 hPa vorticity. Five main outcomes are identified:

i. Realistic: The formation of a low-level vortex of similar magnitude and subsequent path as the observed evolution of TCS-37 / TS 16W.

ii. Recurve: the formation of a low-level vortex of similar magnitude to that observed, but undergoing recurvature prior to observed.

iii. Weak Vortex – Realistic: disturbance path similar to observed, but with reduced low-level vorticity.

iv. Weak Vortex – Recurve: similar to category 3, but undergoing recurvature prior to observed.

v. No Vortex: a coherent vortex does not form

The category that each ensemble member falls in is summarized in Table 2.

Category	**Classification**	**Ensemble Members**
1	Formed a coherent low-level vortex that did not recurve	07, 14, 18, 35
2	Formed a coherent low-level vortex that recurved	00, 01, 02, 04, 06, 09, 11, 12, 14, 17, 19, 20, 23, 24, 26, 27, 29, 32, 33, 36, 39, 40, 41, 42, 43, 45, 46, 47, 49, 50
3/4	Form a weak coherent vortex (both recurve and non-recurve cases)	03, 05, 08, 13, 15, 21, 22, 25, 28, 30, 31, 34, 37, 44, 48
5	Failed to form a coherent low-level vortex	10, 16, 3, 8

Table 2. Subjective classification of ensemble members initialized 0000 UTC 4 September.

Having identified five relatively distinct evolutionary pathways in the ensemble data from 0000 UTC 4 September, it is now possible to examine the respective dynamical processes leading to the observed evolution in each category. The goal here is to evaluate the evolution in terms of the hypothesized, two-stage TT evolutionary pathway.

1. Formation of a Low-Level Vortex of Similar Magnitude and Subsequent Path as the Observed Evolution of TCS037 / TS 16W

The ensemble members in this category form a coherent low-level vortex that exhibit a similar evolution in terms of low-level vorticity magnitude and track to that observed. These vortices progress almost due west during the forecast time period. Given this similar evolution to the observed, we hypothesize the two-stage evolution outlined in the case of TCS-037 / TS 16W (Schönenberger 2010, summarized in the Introduction) is also at work. To recount, stage 1 represents the forcing of near-continuous deep convection in response to forcing associated with an extratropical precursor (the PV streamer). During stage 2, diabatic processes help to rearrange upper-level PV in such a way as to reduce deleterious vertical wind shear, thereby allowing for the intensification of the storm system.

To investigate stage 1, we use six-hour precipitation accumulation as a proxy for deep convection. The data for a representative ensemble member (member 18) are presented in Figure 56 for the time-period beginning on 0600 UTC 8 September 2008 at six-hour increments ending at 1200 UTC 9 September 2008. Sustained deep convection (Figure 57) is evident during this crucial juncture of the incipient disturbance's evolution during which time the coherent low-level vortex emerges.

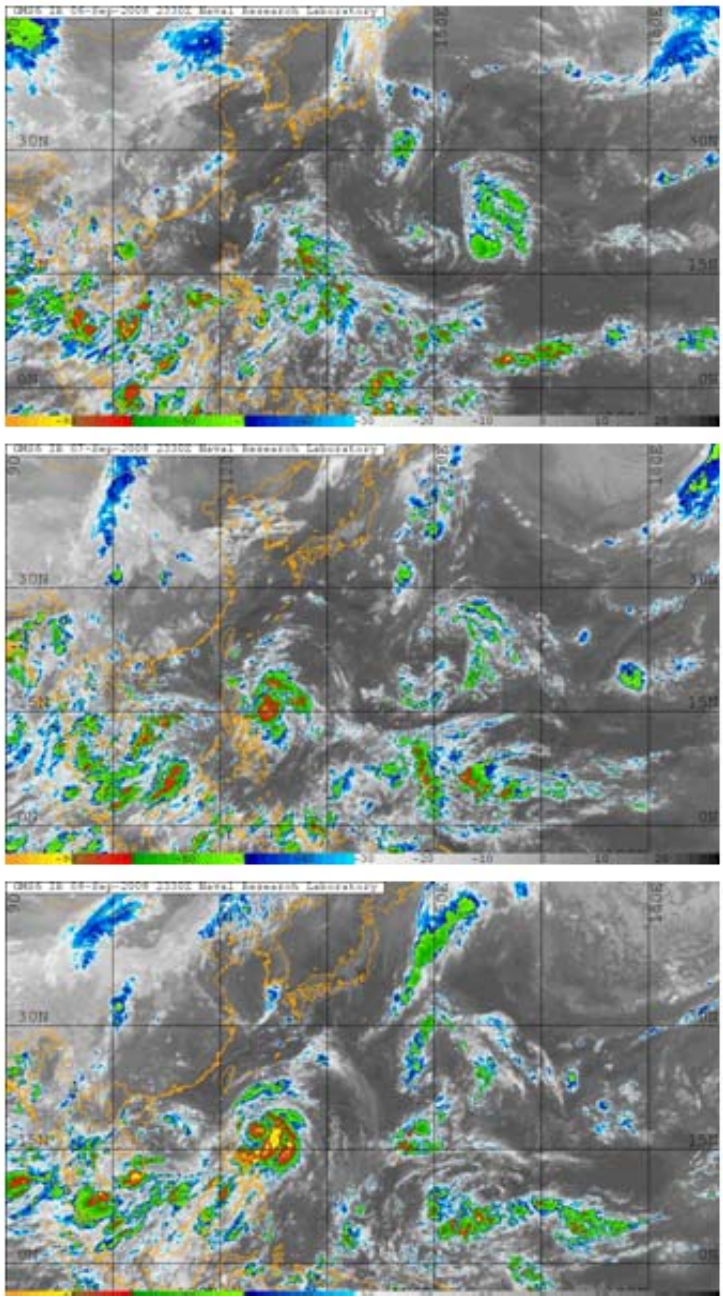

Figure 56. METSAT IR imagery showing cloud top temperatures (color-shaded in ^{o}C) for 0000 UTC 7, 8 and 9 September from top to bottom.

In order to examine stage 2, potential temperature along the dynamic tropopause is presented in Figure 58. In the same region where deep convection is maintained during this time period, there is a clear rearrangement along the dynamic

tropopause: the tail of the PV streamer is observed to cut-off leading to a channel of reduced upper-level PV (as indicated by high values of potential temperature between the stratospheric air to the northwest and the cutoff to the southwest represented by relatively lower values of potential temperature). This evolution is very similar to that observed in Figure 22). As has been diagnosed to TCS-037 / TS 16W, it is the relaxation of the vertical wind shear in association with this rearrangement that allows for the intensification of the storm system.

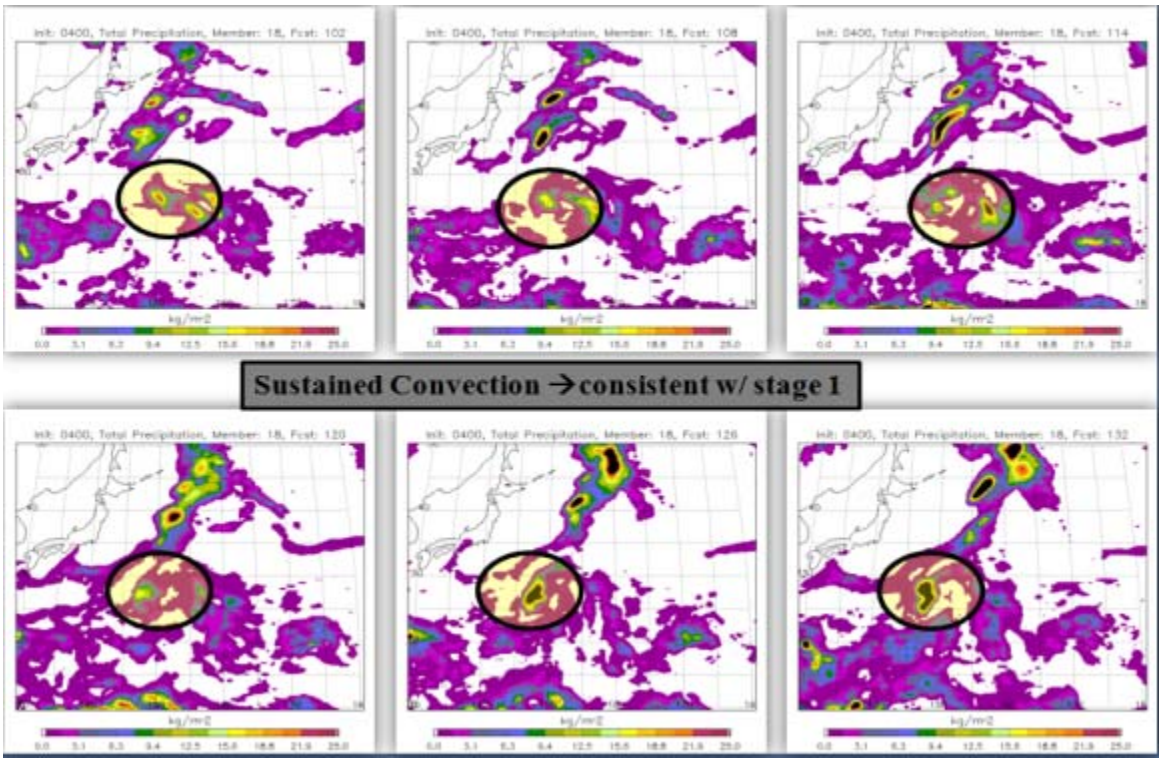

Figure 57. Ensemble member 18 six-hourly total precipitation for 102-hour through 132-hour forecast (0600 UTC 8 September through 1200 UTC 9 September, respectively) in six-hour increments (left to right and top to bottom) for 0000 UTC 4 September initialization time. Amounts of precipitation are in kg m^{-2} roughly equating to the amount in millimeters (mm).

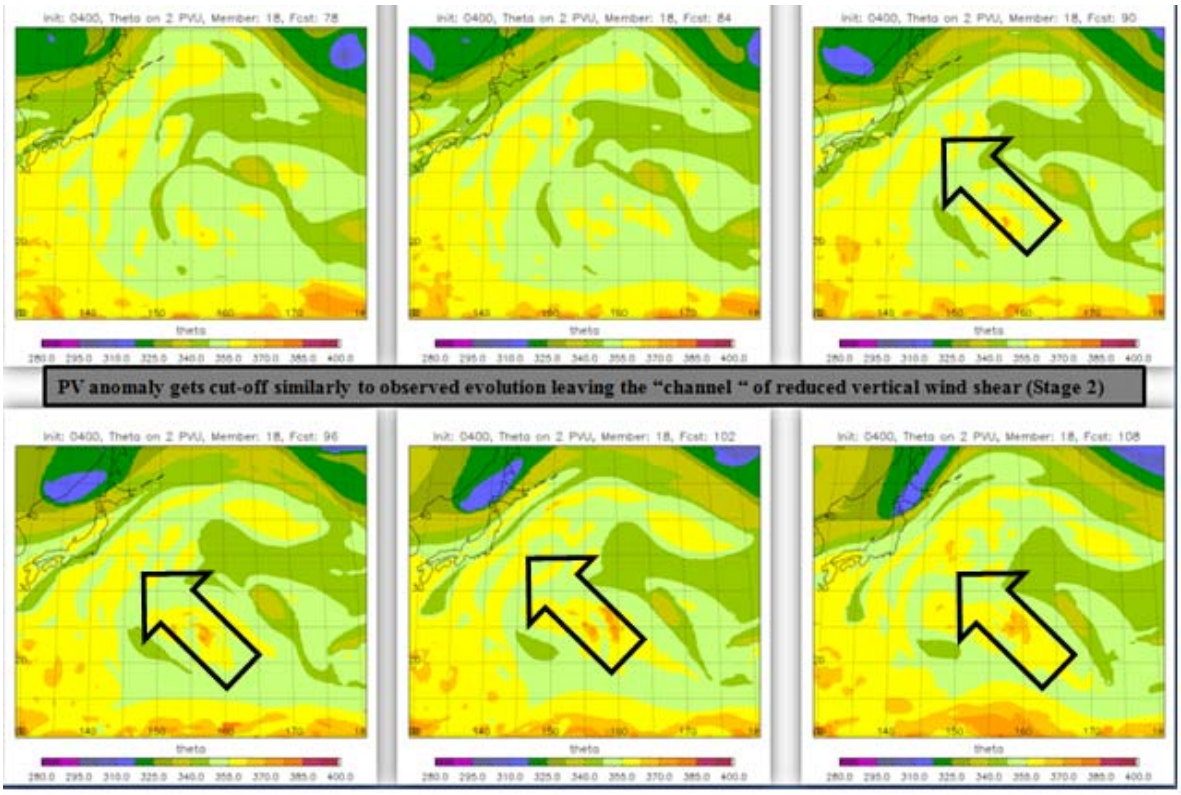

Figure 58. Ensemble member 18 potential temperature (theta) on the 2 PVU surface for 78-hour through the 108-hour forecast (0600 UTC 7 September through 1200 UTC 8 September 2008, respectively) in six-hour increments (left to right and top to bottom) for 0000 UTC 4 September initialization time. Black arrow indicated the *channel* of lower PV air.

2. Formation of a Low-Level Vortex that Recurved

Ensemble members in this category form a coherent vortex at the 925 hPa level, yet the incipient vortex is observed to recurve almost immediately. This forecast track is in stark contrast to that observed. Given that the members in this category are generating a low-level vortex, it is hypothesized that sustained deep convection is represented well by the model leading to the development of a coherent low-level vortex (stage 1). Sustained deep convection then serves to alter the structure of the dynamic tropopause, thus reducing the vertical wind shear (stage 2) as with the previous category. The main difference herein arises from the overall synoptic scale steering-level flow. Further examination revealed that ensemble members within this category predicted a

robust subtropical ridge to the east of the storm and it was this erroneous feature (in comparison to observations) that ultimately led to the premature recurvature.

Figure 60 shows six-hourly accumulated precipitation to represent diabatic processes at 0000 UTC 7 through 9 September. The images illustrate that the convection was sustained throughout this time period. The result is the generation of a low-level vortex (see Figure 59) in response to the near-continuous convection associated with the PV streamer (stage 1), and the rearrangement of the structure along the dynamic tropopause (see Figure 61) resulting in a channel of reduced vertical wind shear (stage 2). With this reduction of vertical wind shear, the environment is conducive for tropical cyclogenesis.

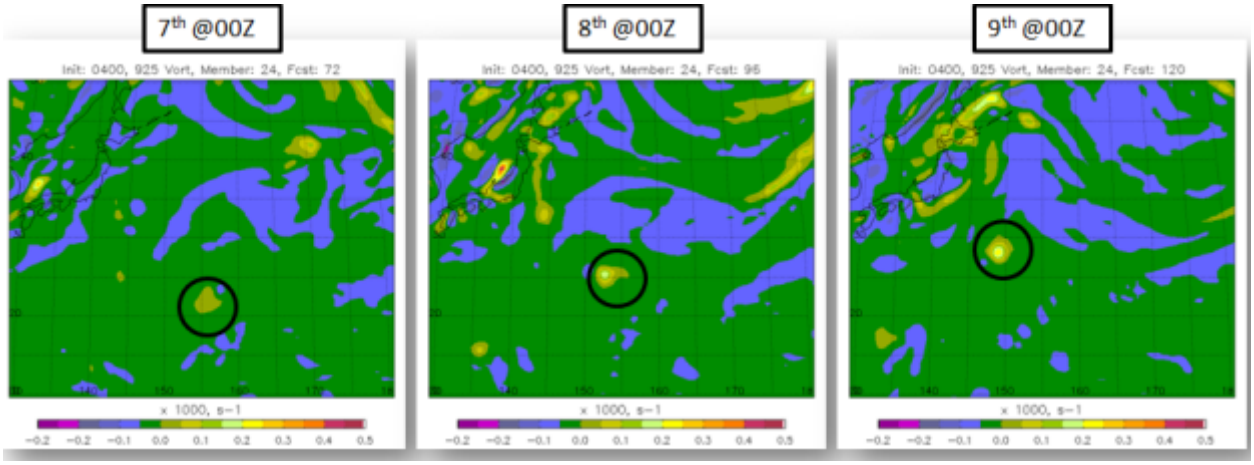

Figure 59. Ensemble member 24 925 hPa vorticity (s^{-1}) initialized 0000 UTC 4 September 2008 valid for 0000 UTC 7, 8 and 9 September. Black circles indicate position of the low-level vortex.

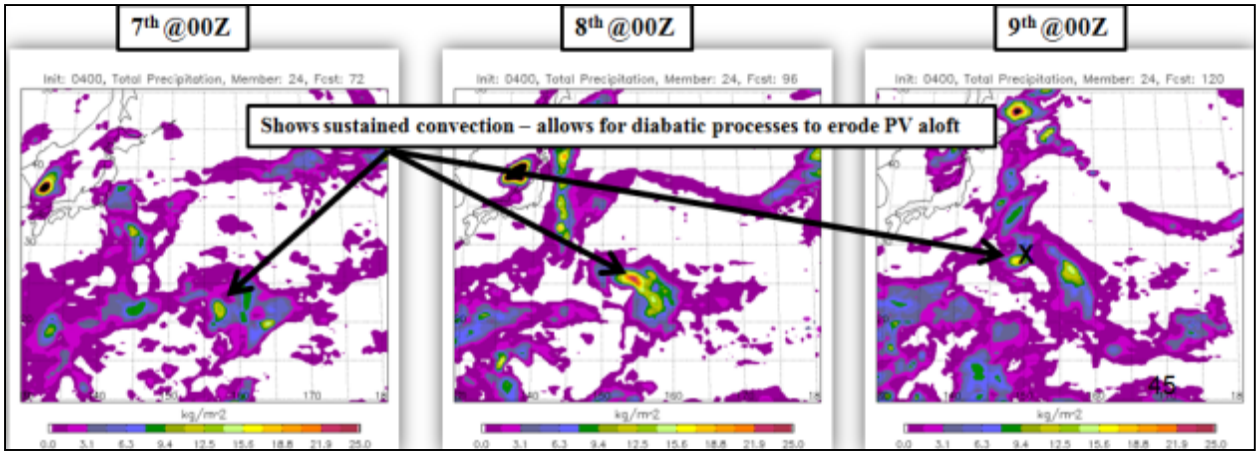

Figure 60. Ensemble member 24 six-hourly total precipitation (mm) initialized 0000 UTC 4 September 2008 valid for 0000 UTC7, 8 and 9 September. X marks the position of the coherent low-level vortex.

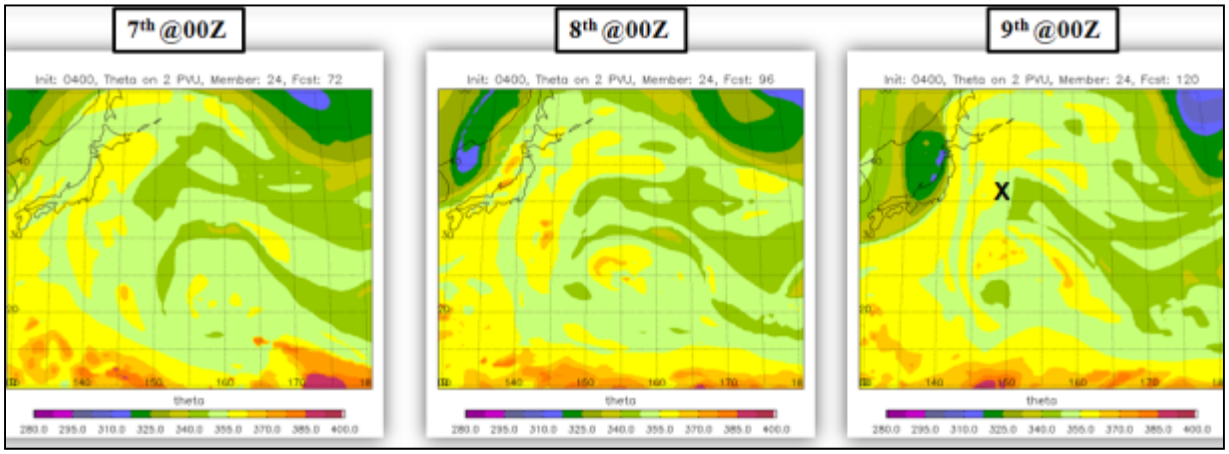

Figure 61. Ensemble member 24 potential temperature (theta) on 2 PVU surface initialized 0000 UTC 4 September 2008 valid for 0000 UTC7, 8 and 9 September. X marks the position of the coherent low-level vortex (TS 16W).

To ascertain the steering flow for TS 16W, 500 hPa geopotential heights are shown in Figure 62. Member 24 (left) shows a fairly sharp ridge along 160°E, thereby explaining the simulated recurvature. In contrast, member 18 (forms a coherent vortex that track similar to that observed) shows a flatter ridge explaining its almost due westerly track.

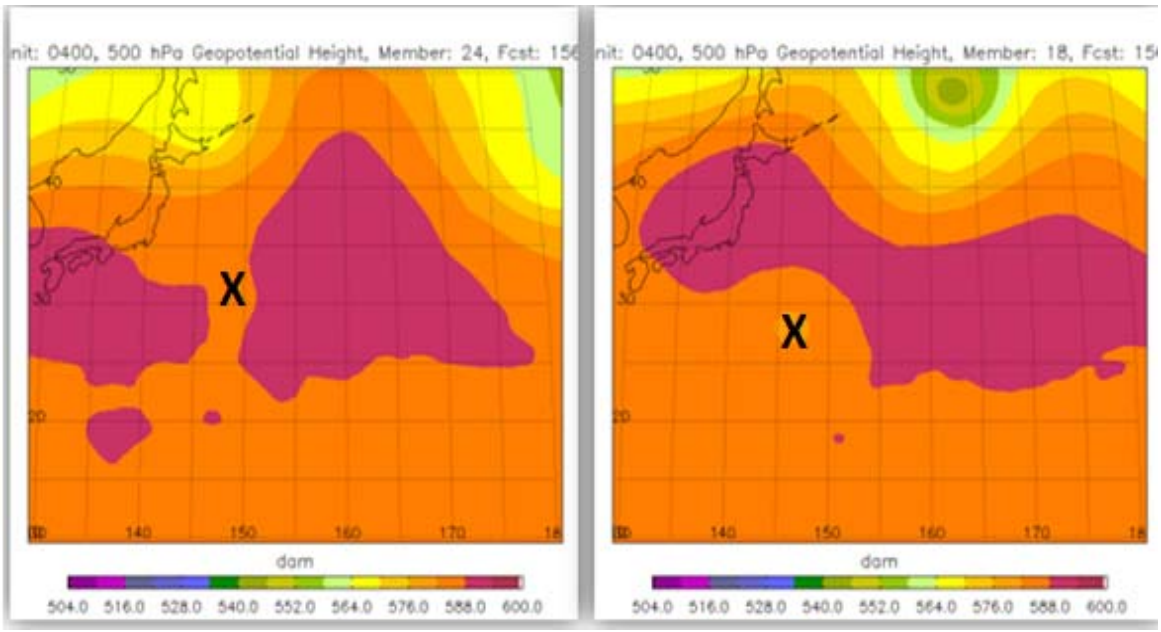

Figure 62. 500 hPa Geopotential Heights (dam) for ensemble members 24 and 18initialized 0000 UTC 4 September 2008 valid for 10 September at 1200 UTC. X marks the position of the low-level vortex.

3. Weak Vortex – Realistic

Within this category, ensemble members did predict the formation of a low-level vortex, however, the vortex was either transitory in nature or weak enough (<0.0002 s^{-1}) that it showed up as a broad region of enhanced vorticity (rather than a coherent vorticity center as in the above two categories). Ensemble member 22 formed a weak vortex with a maximum in 925 hPa vorticity (approximately 0.00014 s^{-1}) at 144 hours (0000 UTC 10 September 2008) but this feature remains weak throughout (Figure 64). Figure 64 shows weaker convection than ensemble member 18 (category 1 see Figure 57). Weaker convection most likely equated to a weaker low-level vorticity generation. The steering flow does not appear to be similar with respect to the subtropical ridge, however, the upper-level trough is further east with a developing ridge over Japan which prevents premature recurvature (Figure 65).

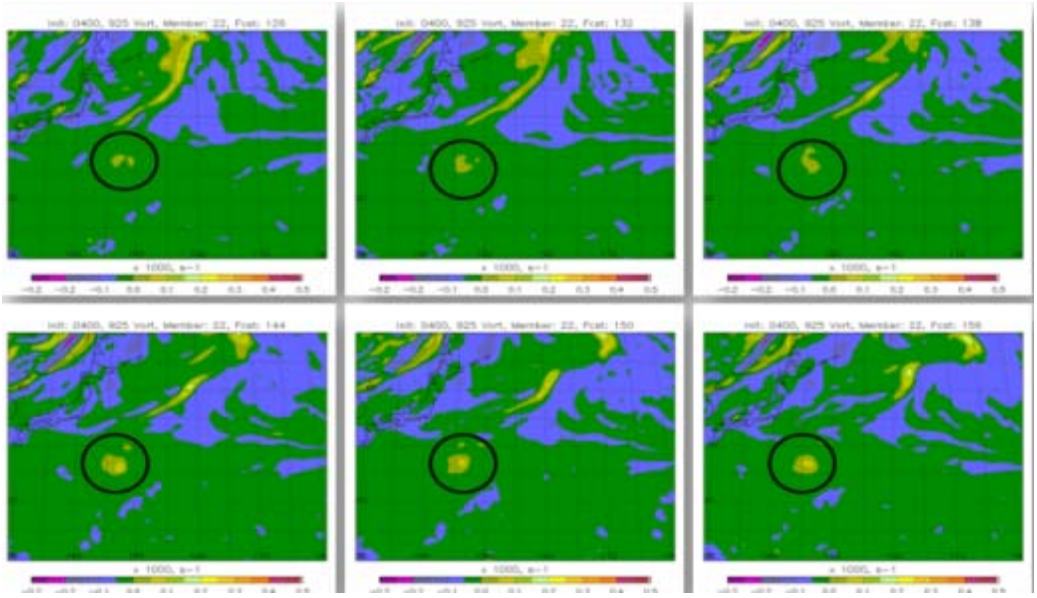

Figure 63. Ensemble member 22 925 hPa vorticity (s^{-1}) 126, 132, 138, 144, 150 and 156-hour (0600 UTC 9 September through 1200 UTC 10 September, respectively) forecasts initialized 0000 UTC 4 September 2008. Black circles indicate position of the low-level vortex.

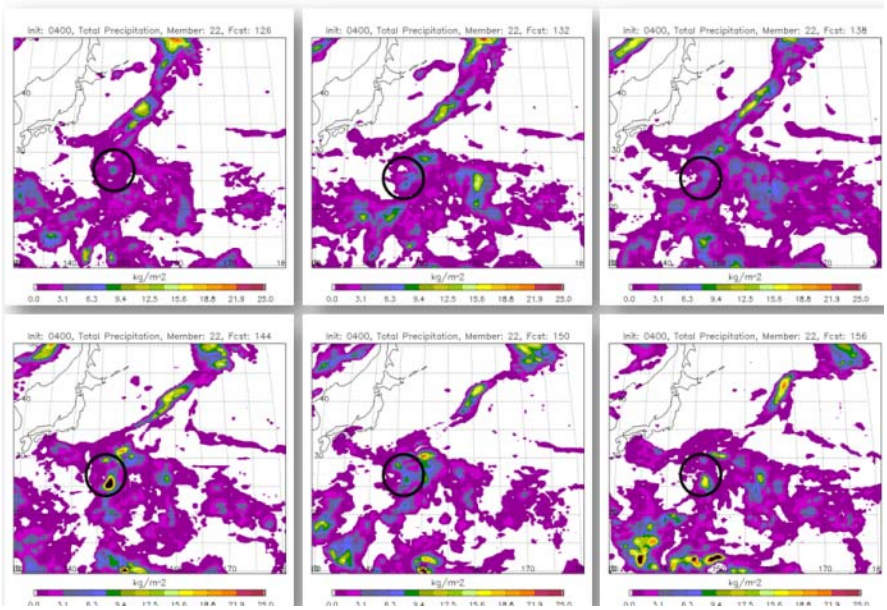

Figure 64. Ensemble member 22 six-hour total accumulated precipitation (mm) 126, 132, 138, 144, 150 and 156-hour (0600 UTC 9 September through 1200 UTC 10 September, respectively) forecasts initialized 0000 UTC 4 September 2008. Black circles indicate position of the low-level vortex.

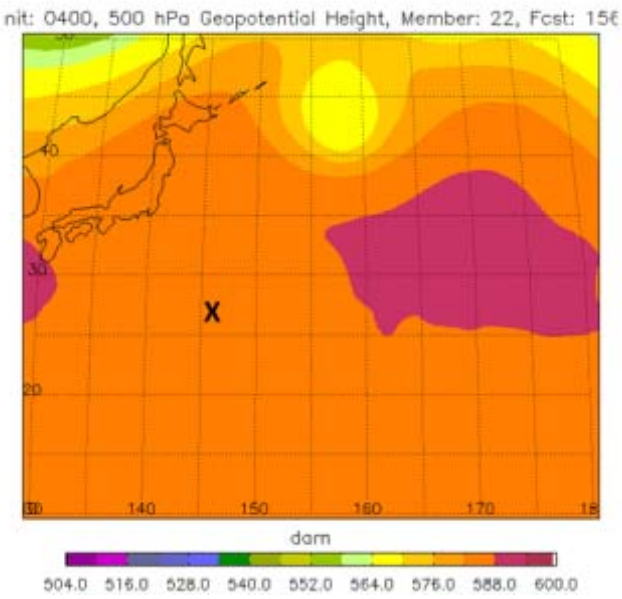

Figure 65. 500 hPa Geopotential Heights (dam) for ensemble member 22 initialized 0000 UTC 4 September 2008 valid on 1200 UTC10 September. X marks the position of the low-level vortex.

4. Weak Vortex – Recurve

Similar to the previous category, ensemble members in this category also form a low-level vortex. Rather than exhibiting a similar track to the observed storm, these weak vorticies are predicted to recurve prematurely (similar to category 2). Figure 66 shows the 925 hPa vorticity for a weak vortex-case (ensemble member 25) that recurved. The convective processes in this case generated a low-level vorticity, however, the upper-level PV anomaly (Figure 68) remained intact (and hence stronger vertical wind shear) thus convection could not be sustained (Figure 67) allowing for the depletion of upper-level PV (stage 2). Figure 69 reveals that the 500 hPa steering flow is similar to that seen in Figure 62 for Category 2.

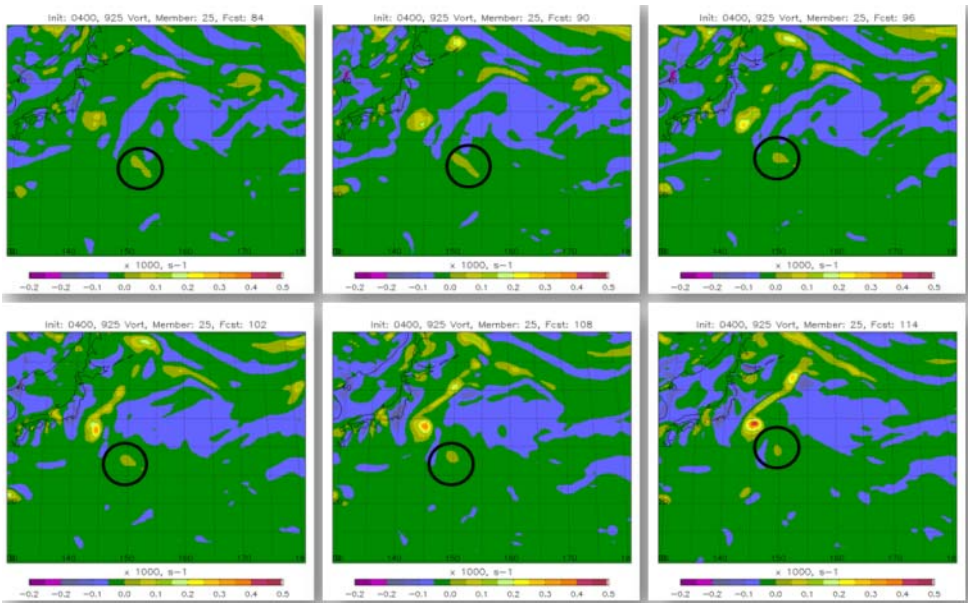

Figure 66. Ensemble member 25 925 hPa vorticity (s^{-1}) 84, 90, 96, 102, 108 and 114-hour (1200 UTC 7 September through 1800 UTC 8 September, respectively) forecasts initialized 0000 UTC 4 September 2008. Black circle show the position of the low-level vortex.

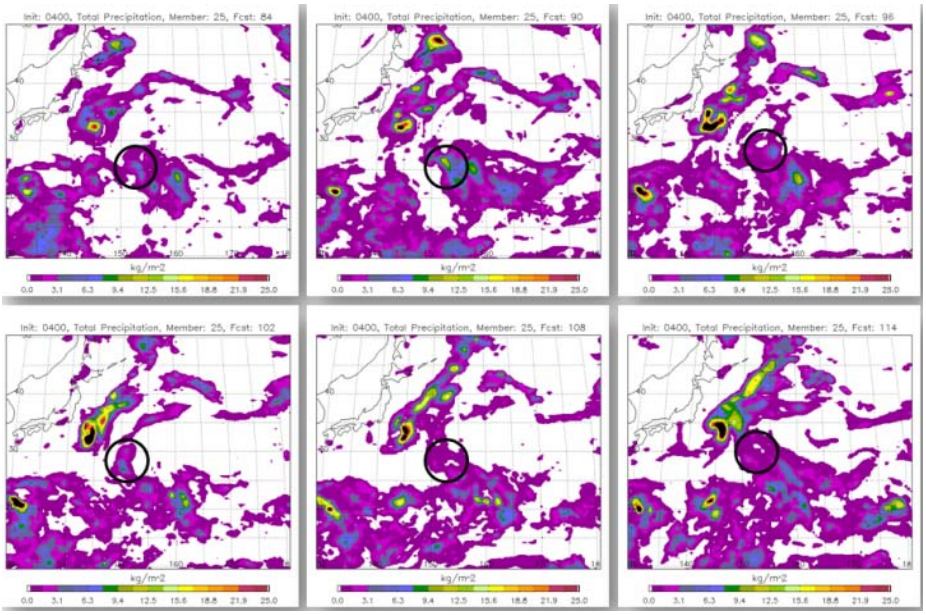

Figure 67. Ensemble member 25 six-hour total accumulated precipitation (mm) 84, 90, 96, 102, 108 and 114-hour (1200 UTC 7 September through 1800 UTC 8 September, respectively) forecasts initialized 0000 UTC on 4 September 2008. Black circles indicate position of the low-level vortex.

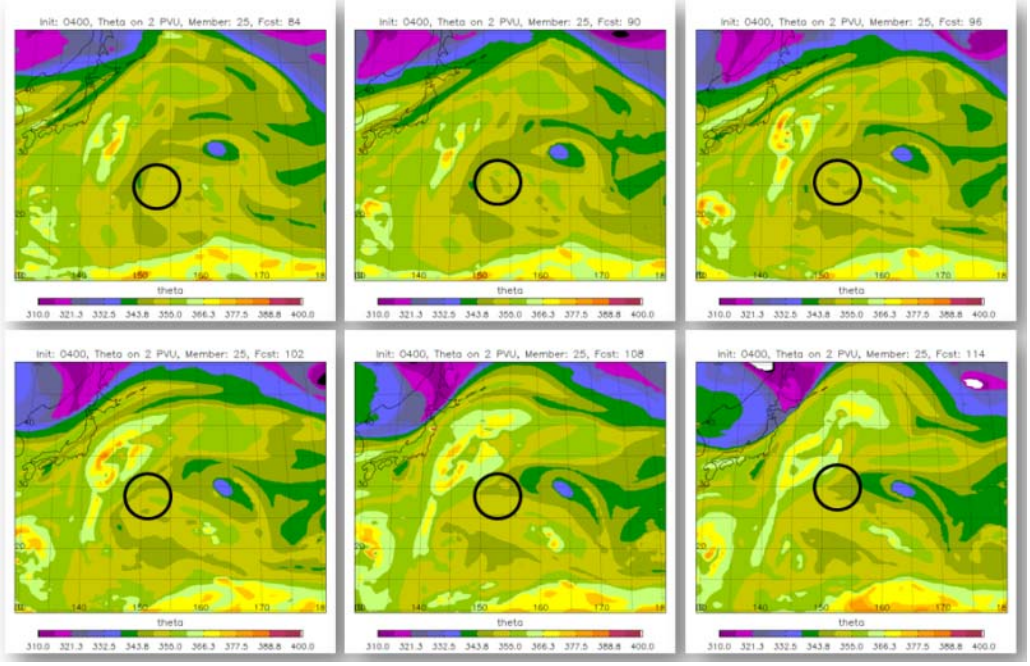

Figure 68. Ensemble member 25 potential temperature (theta) on the 2 PVU surface 84, 90, 96, 102, 108 and 114-hour (1200 UTC 7 September through 1800 UTC 8 September, respectively) forecasts initialized 0000 UTC 4 September. Black circle indicates position of the low-level vortex

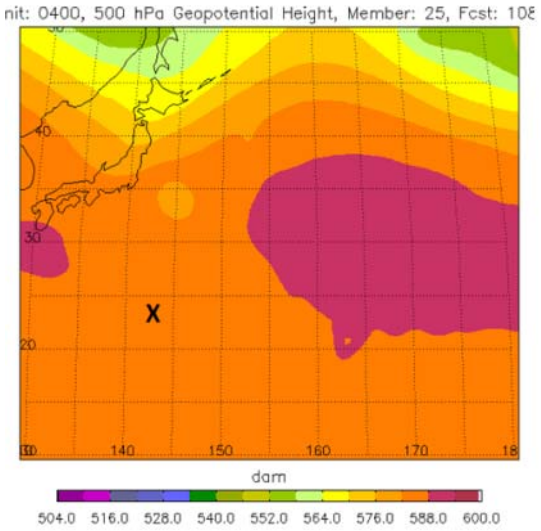

Figure 69. Ensemble member 25 500 hPa GPH (dam) valid 1200 UTC 9 September 2008 (weak vortex – recurve). X marks the position of the low-level vortex.

5. No Vortex

In contrast to ensemble members initialized on 7, 6 and 5 September, the ensemble forecast initialized 0000 UTC 4 September produced members that failed to produce a low-level vortex. It is hypothesized that the model is not representing either of the two stages correctly. Given that the second stage requires the first stage (i.e., sustained deep convection) it is reasonable to say that it must be related to the failure of the model to achieve deep convection or sustain it if it has achieved deep convection.

Figure 70 shows a representative member's (10) total six-hourly accumulated precipitation as a proxy for convection and associated diabatic processes on 0000 UTC 7, 8 and 9 September. Deep convection is evident on 7 September, but dies out and is less evident on 8 and 9 September.

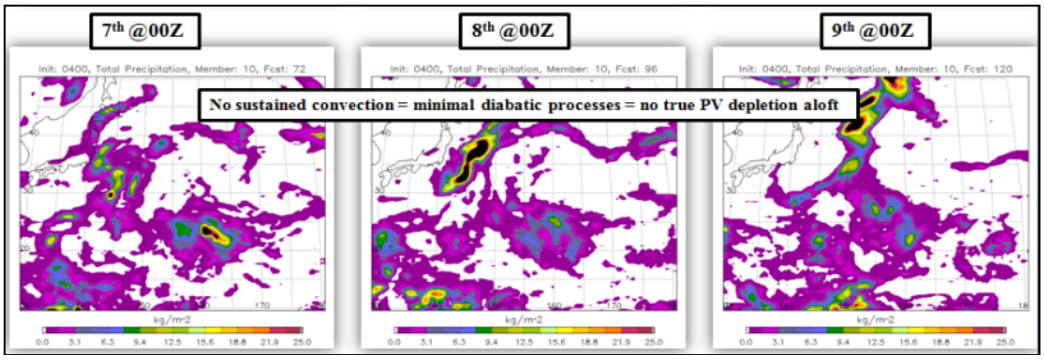

Figure 70. Ensemble member 10 six-hour total precipitation (mm) 72, 96 and 120-hour forecasts initialized 0000 UTC 4 September valid for 0000 UTC 7, 8 and 9 September.

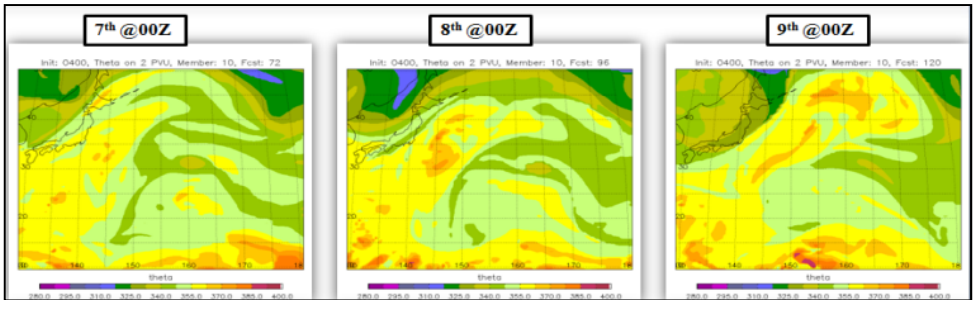

Figure 71. Ensemble member 10 potential Temperature on the 2 PVU surface initialized 0000 UTC 4 September valid0000 UTC 7, 8, and 9 September.

THIS PAGE INTENTIONALLY LEFT BLANK

V. CONCLUSIONS AND FUTURE WORK

A. CONCLUSIONS

Davis and Bosart (2004) coined the term tropical transition (TT) to describe the avenue to tropical cyclogenesis that involves an extratropical precursor. Resent work in the Atlantic basin has illustrated that: i) a significant fraction of Atlantic tropical cyclones (TCs) exhibit an extratropical precursor, ii) the vast majority of these TT cases involve a breaking wave along the dynamic tropopause, and iii) diabatic processes appear to be of primary importance. With the exception of Sadler in the 1970s, there is a paucity of research regarding TT in the western North Pacific (WNP). The overarching goal of this work is, therefore, to re-examine TT research in the WNP.

More specifically, we hope to investigate the relevance of TT in the WNP in terms of a two-stage evolutionary process. During stage 1, upper-level forcing in the form of tropopause-level potential vorticity (PV) anomaly results in near-continuous deep convection. This is conducive to tropical cyclogenesis in that mid-level moistening and the formation of a low-level vorticity feature can occur. However, deleterious to tropical cyclogenesis, a robust tropopause-level PV anomaly is associated with significant values of vertical wind shear. During stage 2, continued diabatic processes serve to rearrange the upper-level PV structure in such a way as to reduce the vertical wind shear, thereby resulting in an environment that is conducive to tropical cyclogenesis.

To address the relevance of TT and the two-stage evolution in the WNP, a subjective analysis of all TT events during the years 2002–2008 was conducted. The methodology entailed the identification of the incipient low-level vorticity feature that subsequently intensified to at least tropical storm strength. If the emergence of this feature was deemed to be directly associated with a feature of extratropical origin (i.e., a tropopause-level PV anomaly emanating for the extratropical waveguide), the event in question was termed a TT. If no such extratropical feature was identified, the storm was termed a non-TT event.

TT cases accounted for approximately 14% of all TC events from 2002–2008. TT events predominately occurred during the late summer / early fall. The maximum in time appears to represent a "sweet spot" for TT occurrence, when there is a collocation between enhanced wave breaking and conducive local environmental conditions. TT events tended to form farther to the north in comparison to non-TT events (typically forming between 15 and 35^{o}N). TT events tended to be relatively weak and short-lived when compared to non-TT cases. This particular result is consistent with observations from the Atlantic basin.

In addition to the subjective climatology, a case-study of a particular TT event was conducted. TCS-037 / TS 16W occurred in September 2008 during Tropical Cyclone Structure (TCS-08) field program (Elsberry and Harr 2008). For this case, Schönenberger (2010) illustrated that a PV streamer was able to initiate near-continuous deep convection. A closed low-level circulation was identified by research aircraft. This circulation feature was unable to attain coherence, likely in response to significant vertical wind shear in the environment surrounding the PV streamer. In response to continued cloud diabatic processes, a significant rearrangement of tropopause-level PV was observed. A "channel" of reduced upper-level PV and a concomitant reduction of vertical shear resulted in the formation and intensification of a coherent low-level vortex that could tracked going forward in time. It is this incipient disturbance that became TS 16W, as diagnosed by JTWC.

For this study, ensemble prediction data from the ECMWF were obtained to examine the dynamics and predictability of the event. Data for four initialization times were examined (0000 UTC on 4–7 September 2008). An automatic tracking algorithm was designed to identify and determine the path of the low-level vorticity maximum at 925 hPa (as a proxy for the storm center position). For all tracked low-level vorticies, both maximum vorticity and the area-average, deep (200–850 hPa) vertical wind shear were catalogued.

A specific focus was placed on the investigation of ensemble members initialized at 0000 UTC 4 September. The ensemble data predicted significant spread in the qualitative and quantitative nature of the dynamical evolution. Five subjective categories were identified, largely based on the strength and location of the low-level vorticity feature. These categories represented different dynamical evolutions that, upon further study, could shed light on the two-stage hypothesis outlined above. Using six-hourly precipitation accumulation as a proxy for diabatic processes and dynamic tropopause maps to represent upper-level forcing, each category was investigated in detail.

For the two categories that exhibited a low-level vortex of similar magnitude to that observed, it was determined that the two-stage hypothesis was indeed valid (i.e., sustained convection associated with upper-level forcing resulted in near-continuous deep convection and that, over time, diabatic processes altered the tropopause-level structure in such a way as to reduce vertical wind shear). The primary difference between the two categories was the ultimate track of the resulting vortex. The track deviation was attributed to the strength of the mid-level ridge (steering flow).

Two additional categories were diagnosed as "weak vortex" cases, wherein a low-level vorticity feature was identified, but it failed to remain coherent and / or attain the observed magnitude. For these cases, the evolution along the dynamic tropopause exhibited significant differences than observed. As with the previous two categories, there existed a similar track deviation with these weak vortex cases.

A final category was comprised of members where no low-level vortex could be identified. It was determined that, due to differences along the dynamic tropopause, sustained deep convection was not observed.

B. FUTURE WORK

There are a number of avenues via which this work can be expanded. At present, the 2002–2008 climatology represents a fairly limited amount of data. For example, the inclusion of the 2009 TC season would likely have had a significant effect on the overall

results (as it, similarly to the 2008 season but in contrast to the 2002–2007 seasons, exhibited a relative high frequency of TT events). In addition, it would be useful to refine the methodology in such a way as to make it more objective in nature. This could be accomplished by establishing threshold values of relevant dynamical fields (similar to the approach of McTaggart-Cowen et. al. 2008)

Expanding the scope of the use of ensemble prediction data would also be useful. This can be accomplished by looking at a number of cases (rather than one particular example). It would also be interesting, from a predictability standpoint, to examine ensemble prediction data for a number of operational centers. Regarding the study of dynamical processes using ensemble prediction data, it would be useful to conduct empirical orthogonal functions to identify the categories describing different dynamical pathways predicted in the forecast data. This would remove the subjective nature of the analysis and provide important statistical information.

Finally, the use of idealized numerical modeling of the TT process would be incredibly insightful. The myriad of model fields available would provide significantly more information than is available via observational data. In addition, one can manipulate the environment in such a model setting to ascertain the sensitivity of the TT process to the structure of the relevant feature (e.g., PV streamer, local environmental characteristics).

APPENDIX. TT CLIMATOLOGY

#	Name	TT	M	D	Lat	Lon	Dur	Int
2008								
1	TS 01W	N	1	12	12.5	118.0	3	40
2	T Neoguri	N	4	14	8.0	121.0	6	100
3	T Rammasun	N	5	7	8.0	133.0	5	135
4	TS Matmo	N	5	14	16.2	124.0	2	40
5	T Halong	N	5	15	12.0	116.0	5	75
6	T Nakri	N	5	27	12.0	138.0	6	125
7	T Fengshen	N	6	18	8.0	133.0	7	110
8	T Kalmaegi	Y	7	14	20.0	128.0	4	90
9	T Fung-Wong	N	7	24	21.5	133.0	4	95
10	TS Kammuri	Y	8	4	20.0	120.0	3	50
12	TS 11W	N	8	13	28.0	127.5	2	35
13	TS Vongfong	Y	8	14	25.0	133.0	2	55
14	T Nuri	N	8	16	14.5	142.0	5	100
15	TS 14	N	8	26	15.0	128.0	3	35
16	T Sinlaku	N	9	8	16.0	127.0	12	125
17	TS 16W	Y	9	10	30.5	147.0	2	35
18	TS 17W	Y	9	14	34.0	148.0	0	35
19	T Hagupit	Y	9	17	17.0	143.0	6	125
20	T Jangmi	N	9	23	12.0	139.0	7	140
22	TS Mekkhala	N	9	28	15.5	112.8	2	55
24	TS Higos	N	9	29	8.0	133.0	5	40
25	TS 22W	N	10	14	18.8	108.2	1	35
26	TS Bavi	Y	10	18	22.0	152.0	1	45
28	TS Maysak	N	11	7	13.0	118.0	3	55
29	TS Haishen	Y	11	15	23.5	146.8	1	40
30	TS Noul	N	11	16	10.3	116.0	1	40
32	T Doliphin	Y	12	10	12.0	154.0	9	85
	Total TT:	**9**						
	Total Storms:	27						

Subjective classifications for 2008 tropical cyclones in the western Pacific. The green column contains the classifications (Y=TT or N = non-TT). Column 1 is storm number. Column 2 is the storm name. Column 3 is the subjective classification (Y=TT or N = non-TT). Column 4 is the month. Column 5 is the day. Columns 6 and 7 are latitude/longitude, respectively, corresponding to the storm's center at the given date/time. Column 8 is the storms duration in days. Column 9 is the max intensity (kts).

2007								
1	T Kong-Rey	N	3	31	7.0	157.5	6	100
2	ST Yutu	N	5	16	5.5	150.0	6	130
3	TD Toraji	N	7	4	18.0	10.5	1	35
4	T Man-Yi	N	7	7	4.5	148.0	8	125
5	T Usagi	Y	7	28	18.0	152.0	6	120
6	TD 6W	N	8	2	12.5	113.0	5	30
7	T Pabuk	N	8	5	19.0	136.2	4	70
8	TS Wutip	N	8	7	16.8	129.8	2	30
10	ST Sepat	N	8	12	17.7	135.5	7	140
12	T Fitow	N	8	28	20.0	155.0	10	80
13	TS Danas	Y	9	7	25.8	157.5	4	65
14	T Nari	N	9	12	20.0	127.0	4	125
15	ST Wipha	N	9	15	18.4	133.8	4	135
16	TD 14W	N	9	20	11.4	137.5	1	30
17	TS Francisco	N	9	23	19.7	115.7	2	45
18	T Lekima	N	9	30	15.0	115.6	4	70
19	ST Krosa	N	10	1	17.0	131.5	7	130
20	TS Lingling	N	10	12	19.0	179.0	2	40
21	T Kaijiki	N	10	19	18.3	148.0	2	115
22	TS Faxai	N	10	26	22.4	131.0	1	40
23	T Peipah	Y	11	3	18.2	129.5	6	75
24	TS Tapah	N	11	11	19.7	140.3	1	35
26	T Hagibis	N	11	18	8.6	128.1	9	80
25	T Mitag	N	11	20	11.9	138.2	8	95
26	TD 25W	N	11	26	14.5	133.0	1	25
27	TD 26W		11	28	20.0	137.0	1	25
	TS Haiyan		10	4	27.0	172.0	2	50
	Total TT:	**3**						
	Total Storms:	27						

2006								
1	TS 01W	N	3	4	5.7	138.4	3	35
2	T Chanchu	N	5	8	9.0	138.0	10	125
3	TS Jelawat	N	6	26	13.5	119.0	3	45
4	ST Ewiniar	N	6	29	6.0	141.0	12	130
6	TS Bilis	N	7	8	12.0	142.0	6	50
8	T Kaemi	N	7	18	9.2	146.0	7	75
9	T Prapiroon	N	7	31	15.8	123.0	4	70
10	ST Saomai	N	8	4	7.0	151.5	6	140
11	TS Maria	Y	8	5	25.0	147.0	4	60
12	TS Bopha	N	8	6	22.0	132.0	4	55
13	TS Wukong	N	8	12	20.5	141.5	7	55
14	TS Sonamu	N	8	13	17.0	126.5	3	45
15	TD 13W	N	8	24	19.0	122.8	1	30
17	T Shanshan	**Y**	9	10	15.0	136.0	8	120
18	TD 15W	N	9	12	18.0	115.5	1	30
19	ST Yagi	N	9	17	20.0	157.0	7	140
20	TD 17W	N	9	23	13.0	112.5	2	30
21	T Xangsane	N	9	25	12.0	128.0	6	125
22	TS Bebinca	N	10	1	17.0	133.0	5	35
23	TD Rumbia	N	10	4	20.0	154.0	2	30
24	T Soulik	N	10	9	13.0	157.5	6	90
25	ST Cimaron	N	10	26	12.4	137.5	9	140
27	T Chebi	N	11	9	16.0	137.5	5	125
28	ST Durian	N	11	25	9.5	144.0	11	135
29	T Utor	N	12	7	8.5	137.0	7	100
30	TD Trami	N	12	17	11.0	141.5	1	30
	Total TT:	**2**						
	Total Storms:	26						

2005								
1	T Kulap	N	1	13	5.0	153.0	5	65
2	T Roke	N	3	13	7.5	148.0	4	80
3	T Sonca	N	4	20	8.0	142.0	6	115
4	ST Nesat	N	5	30	9.0	147.0	11	125
5	ST Haitang	Y	7	11	22.0	154.0	8	140
6	TS Nalgae	Y	7	20	24.0	164.0	3	55
7	TS Banyan	N	7	21	14.0	137.0	6	60
8	TS Washi	N	7	28	18.0	113.0	3	45
9	T Matsa	N	7	31	10.5	136.0	7	90
10	T Sanvu	N	8	10	14.0	131.0	3	65
11	T Mawar	N	8	19	21.0	142.0	8	125
12	T Guchol	Y	8	19	22.5	153.0	6	65
13	ST Talim	N	8	26	12.5	144.0	6	130
14	ST Nabi	N	8	29	15.0	154.0	9	140
15	T Khanun	N	9	6	10.5	138.0	5	115
16	TS Vicente	N	9	16	14.0	115.0	2	50
18	T Damrey	N	9	20	15.0	125.0	7	90
17	T Saola	N	9	20	21.0	153.0	6	100
19	T Longwang	N	9	25	18.5	146.0	7	125
21	TD 20W	N	10	7	17.0	111.0	0.5	30
22	T Kirogi	N	10	10	23.0	134.0	4	115
23	T Kai-Tak	N	10	28	13.0	117.0	5	85
24	TS Tembin	N	11	7	10.0	138.0	4	45
25	T Bolaven	N	11	13	7.0	132.0	7	70
26	TS 25W	N	12	18	8.0	115.0	2	45
	Total TT:	**3**						
	Total Storms:	25						

2004								
1	TS 01W	N	2	11	10.4	144.0	5	40
2	TS 02W	N	3	16	5.9	137.1	6	45
3	ST Sudal	N	4	4	6.4	150.3	11	130
4	ST Nida	N	5	13	7.8	132.2	8	140
5	TD 05W	N	5	15	9.5	110.4	2	35
6	T Omasis	N	5	15	6.1	143.6	6	60
7	T Conson	N	6	4	15.3	116.2	11	100
8	T Chanthu	N	6	9	10.6	125.4	4	75
9	T Dianmu	N	6	13	8.1	136.9	8	155
10	T Mindulle	N	6	23	16.2	143.5	11	125
11	T Tingting	N	6	25	11.6	152.3	9	80
12	TS Kompasu	N	7	13	20.9	129.2	3	45
13	T Namtheun	N	7	25	22.1	150.3	7	90
15	T Meranti	Y	8	3	19.4	166.2	5	90
14	TD Malou	N	8	4	30.1	137.9	1	30
16	T Rananim	N	8	7	16.7	130.1	6	90
17	TS Malakus	Y	8	10	25.5	156.8	2	35
18	T Megi	N	8	14	15.3	142.9	5	65
19	ST Chaba	N	8	18	12.0	163.0	13	155
20	T Aere	N	8	19	12.1	136.2	7	85
21	TS 21W	N	8	26	13.5	151.9	2	30
22	ST Songda	N	8	27	10.9	166.6	11	125
23	TS Sarika	N	9	4	16.8	150.1	3	60
24	TD Haima	Y	9	12	26.7	121.9	1	35
25	T Maeri	N	9	20	16.6	134.6	9	125
26	ST Ma-on	N	10	4	16.6	134.6	5	140
27	T Tokage	N	10	12	13.6	147.5	8	125
29	T Nock-ten	N	10	15	9.2	162.4	12	110
30	T Muifa	N	11	14	11.1	131.8	12	115
31	T Nanmadol	N	11	28	6.0	149.2	3	130
32	TS Talas	?	12	10	7.7	171.5	9	50
33	TS Noru	N	12	17	13.2	152.0	4	55
	Total TT:	**3**						
	Total Storms:	32						

2003								
1	TS Yan-Ysn	N	1	15	3.1	175.1	5	50
2	ST Kujira	N	4	9	3.7	160.2	13	135
3	TD 3W	N	5	17	7.8	130.4	4	34
4	T Chan-Hom	N	5	19	6.3	149.3	8	115
5	TS Linfa	N	5	25	16.5	118.6	5	60
6	TS Nangka	N	5	31	17.2	117.0	4	40
7	T Soudelor	N	6	11	9.4	137.2	7	115
10	T Koni	N	7	15	10.0	132.1	7	65
9	ST Imbudo	N	7	16	6.6	143.2	8	130
11	T Morakot	N	8	1	16.9	125.9	4	65
12	T Etau	N	8	2	12.4	139.9	7	110
14	T Krovanh	N	8	15	9.6	150.7	11	90
13	TS Vacmo	Y	8	19	20.8	125.4	1	35
15	T Dujuan	Y	8	28	17.6	137.5	6	125
16	ST Maemi	Y	9	5	14.1	143.3	8	150
17	T Choi-Wan	N	9	17	20.7	129.2	5	95
19	T Koppu	N	9	24	15.9	137.1	7	90
20	TD 18W	N	10	6	18.0	116.2	4	25
21	TD 19W	Y	10	12	30.3	129.8	1	30
22	T Ketsana	N	10	18	14.9	130.2	8	125
23	T Parma	N	10	20	20.5	142.8	11	130
24	TD 22W	N	10	22	11.8	114.9	2	30
25	TS 23W	N	10	23	10.4	101.0	4	35
26	T Melor	N	10	30	13.0	128.7	5	70
28	T Nepartak	N	11	12	12.0	134.0	7	75
29	ST Lupit	N	11	20	9.1	162.0	11	145
30	TS 27W	N	12	24	13.3	135.8	3	35
	Total TT:	**4**						
	Total Storms:	27						

2002								
1	TS Tapah		1	10	9.2	135.0	4	50
2	ST Mitag	N	2	26	6.0	157.0	10	140
	TD 3W	N	3	19	5.0	137.0	6	30
3	TD 4W	N	4	5	11.5	155.2	2	30
4	ST Hagibis	N	5	15	7.0	149.0	6	140
5	TD 06W	N	5	28	19.5	116.0	1	25
6	T Noguri	N	6	6	20.0	115.0	5	85
8	ST Chataan	N	6	28	5.0	154.0	13	150
9	T Rammasun	N	6	28	10.0	136.0	8	110
10	ST Halong	N	7	7	9.2	158.0	8	135
11	TS Nakri	N	7	8	22.0	118.0	5	40
12	ST Fengshen	N	7	14	12.0	170.0	13	145
13	TS 13W	N	7	18	8.0	128.0	4	35
15	T Fung-Wong	?	7	20	24.0	144.0	7	65
14	TD Kalmaegi	Y	7	20	15.5	-178.0	1	30
16	TS Kammuri	N	8	2	19.0	119.0	3	50
17	TD 17W	Y	8	5	34.0	149.0	0.5	25
18	TD 18W	N	8	10	11.0	131.0	3	35
19	ST Phanfone	N	8	11	10.0	160.0	9	135
20	TS Vongfong	N	8	15	14.5	115.0	5	55
21	T Rusa	N	8	22	14.0	164.0	9	115
22	T Sinlaku	N	8	28	16.0	156.0	10	110
25	TS Hagupit	N	9	10	20.0	118.0	2	45
26	TS Mekkhala	N	9	23	14.0	113.0	4	55
27	ST Higos	Y	9	26	16.0	157.0	6	135
28	T Bavi	N	10	9	13.0	155.0	5	70
29	TD 27W	N	10	17	18.0	154.0	2	30
30	TD 28W	N	10	18	14.0	176.0	1	30
36	TS Maysak	N	10	26	19.0	166.0	3	60
38	T Haishen	N	11	20	10.0	148.0	4	95
39	ST Pongsona	N	12	2	6.0	165.0	8	130
	Total TT:	**3**						
	Total Storms:	31						

THIS PAGE INTENTIONALLY LEFT BLANK

LIST OF REFERENCES

Davis, C. A. and L. F. Bosart. 2003: Baroclinically Induced Tropical Cylcogenesis. *Monthly Weather Review*, **131**, 2730–2747.

Davis, C. A. and L. F. Bosart. 2004: The TT Problem. *Bulletin of the American Meteorological Society*, **85**, 1657–1662.

Davis, C. A. and L. F. Bosart. 2006: The formation of hurricane Humberto (2001): The importance of extra-tropical precursors. *Quarterly Journal of the Royal Meteorological Society*, **132**, 2055–2085.

DeMaria, M. et al. 2001: A Tropical Cyclone Genesis Parameter for the Tropical Atlantic. *Weather and Forecasting*, **16**, 219–233.

Elsberry, R. L., and P.A. Harr. 2008: Tropical Cyclone Structure (TCS08) Field Experiment – Scientific Basis, Observational Platforms, and Strategy. *Asia-Pacific Journal of Atmospheric Sciences*, **44**, 1–23.

Emanuel, K. 2003: Tropical Cyclones. *Ann. Rev. Earth Planet. Sci*. **31,** 75–104.

Emanuel, K. 2005: *Divine Wind: The History and Science of Hurricanes*. Oxford University Press.

Ertel, H. Ein neuer hydrodynamischer Wirbelsatz. *Meorologishe Zeitschrift*. **59**, 277–281.

Funatsu, B. M. and D. W. Waugh. 2008: Connection between Potential Vorticity Intrusions and Convection in the Eastern Tropical Pacific. *Journal of the Atmospheric Sciences*, **65**, 987–1002.

Hacker, J. 2011: Advanced Numerical Weather Prediction. Naval Postgraduate School, lecture notes for MR4324.

Hulme, A. L. and J. E. Martin. 2009: Synoptic- and Frontal-Scale Influence on Tropical Transition Events in the Atlantic Basin. Part I: A Six-Case Survey. *Monthly Weather Review*, **137**, 3605–3625.

Hulme, A. L. and J. E. Martin. 2009: Synoptic- and Frontal-Scale Influence on Tropical Transition Events in the Atlantic Basin. Part II: Tropical Transition of Hurricane Karen. *Monthly Weather Review*, **137**, 3626–3650.

Kiladis, G. N., and K. M. Weickmann. 1992: Extratropical Forcing of Tropical Pacific Convection during Northern Winter. *Monthly Weather Review*. **120**, 1924–1939.

Martin, J.E. 2006: *Mid-Latitude Atmospheric Dynamics – A First Course*. Wiley.

Martius, O. et al. 2007: Breaking Waves at the Tropopause in the Wintertime Northern Hemisphere: Climatological Analysis of the Orientation and the Theoretical LC1/2 Classification. *Journal of Atmospheric Sciences*, **64**, 2576–2592.

McTaggart-Cowan, R. et. al. 2008: Climatology of Tropical Cyclogenesis in the North Atlantic (1948–2004). *Monthly Weather Review*, **136**, 1284–1304.

Musgrave, K.D. et. al. 2008: Numerical Simulations of the Formation of Hurricane Gabrielle (2001). *Monthly Weather Review*, **136**, 3151–3167.

Sadler, James C. 1976: A role of the Tropical Upper Tropospheric Trough in Early Season Typhoon Development. *Monthly Weather Review*, **104**, 1266–1278.

Sadler, James C. 1978: Mid-Season Typhoon Development and Intensity Changes and the Tropical Upper Tropospheric Trough. *Monthly Weather Review*, **106**, 1137-1152.

Schönenberger, Fabian. Tropical Transition in the Western Pacific. 2010: Master's of Science Thesis, Institute for Atmospheric and Climate Science ETH-Zürich.

Stehrenberger, Eva. 2010: Forecasting the Tropical Transition of a Cyclone: TIGGIE Forecast Analysis of the Precursor to Typhoon Dolphin in the West Pacific. Institute for Atmospheric and Climate Science ETH-Zurich.

Stone, R. 2011: Air/Ocean Numerical Modeling. Naval Postgraduate School, lecture notes for MR4323.

TIGGE, cited 2012: WWRP-THORPEX TIGGE. [Available online at http://tigge.ecmwf.int/documents/additional/TIGGE_leaflet_2010.pdf]

Waugh, D. W., and L.M. Polvani, 2000: Climatology of Intrusions into the Tropical Upper Troposphere. *Geophysical Research Letters*, **27**, 3857–3860.

Wernli, H. and H.C. Davies. 1997: A Lagrangian-based Analysis of Extratropical Cyclones. I: The Method and Some Applications. *Quarterly Journal of the Royal Meteorological Society,* **123**, 467–489.

INITIAL DISTRIBUTION LIST

1. Defense Technical Information Center
   Ft. Belvoir, Virginia

2. Dudley Knox Library
   Naval Postgraduate School
   Monterey, California

3. Professor Richard Moore
   Naval Postgraduate School
   Monterey, California

4. Professor Patrick Harr
   Naval Postgraduate School
   Monterey, California

5. Professor Michael Montgomery
   Naval Postgraduate School
   Monterey, California

6. Air Force Weather Technical Library
   Asheville, North Carolina

7. Captain Edward J. Rozak
   Detachment 5
   Kaena Point Solar Observatory, Hawaii